LOAN DOCUMENT

PHOTOGRAPH THIS SHEET

DTIC ACCESSION NUMBER

LEVEL

INVENTORY

D

EPA-600/R-97-038

DOCUMENT IDENTIFICATION

Apr 97

DISTRIBUTION STATEMENT A
Approved for Public Release
Distribution Unlimited

DISTRIBUTION STATEMENT

HANDLE WITH CARE

ACCESSION FOR
NTIS GRA&I ☒
DTIC TRAC ☐
UNANNOUNCED ☐
JUSTIFICATION

BY

DISTRIBUTION/

AVAILABILITY CODES

DISTRIBUTION	AVAILABILITY AND/OR SPECIAL	
A-1		

DISTRIBUTION STAMP

DATE ACCESSIONED

DATE RETURNED

19990609 037

DATE RECEIVED IN DTIC

REGISTERED OR CERTIFIED NUMBER

PHOTOGRAPH THIS SHEET AND RETURN TO DTIC-FDAC

DTIC FORM 70A JUN 90

DOCUMENT PROCESSING SHEET

PREVIOUS EDITIONS MAY BE USED UNTIL STOCK IS EXHAUSTED.

LOAN DOCUMENT

United States
Environmental Protection
Agency

EPA-600/R-97-038

April 1997

PP 309

Research and Development

A MODELING AND DESIGN STUDY USING HFC-236ea AS AN ALTERNATIVE REFRIGERANT IN A CENTRIFUGAL COMPRESSOR

Prepared for

Strategic Environmental Research and Development Program

Prepared by

National Risk Management
Research Laboratory
Research Triangle Park, NC 27711

FOREWORD

The U.S. Environmental Protection Agency is charged by Congress with protecting the Nation's land, air, and water resources. Under a mandate of national environmental laws, the Agency strives to formulate and implement actions leading to a compatible balance between human activities and the ability of natural systems to support and nurture life. To meet this mandate, EPA's research program is providing data and technical support for solving environmental problems today and building a science knowledge base necessary to manage our ecological resources wisely, understand how pollutants affect our health, and prevent or reduce environmental risks in the future.

The National Risk Management Research Laboratory is the Agency's center for investigation of technological and management approaches for reducing risks from threats to human health and the environment. The focus of the Laboratory's research program is on methods for the prevention and control of pollution to air, land, water, and subsurface resources; protection of water quality in public water systems; remediation of contaminated sites and groundwater; and prevention and control of indoor air pollution. The goal of this research effort is to catalyze development and implementation of innovative, cost-effective environmental technologies; develop scientific and engineering information needed by EPA to support regulatory and policy decisions; and provide technical support and information transfer to ensure effective implementation of environmental regulations and strategies.

This publication has been produced as part of the Laboratory's strategic long-term research plan. It is published and made available by EPA's Office of Research and Development to assist the user community and to link researchers with their clients.

E. Timothy Oppelt, Director
National Risk Management Research Laboratory

EPA REVIEW NOTICE

EPA-600/R-97-038
April 1997

A MODELING AND DESIGN STUDY USING HFC-236ea AS AN ALTERNATIVE REFRIGERANT IN A CENTRIFUGAL COMPRESSOR

by

Predrag Popovic
Howard N. Shapiro
Iowa State University
Ames, IA 50011

EPA Cooperative Agreement No. CR 820755-01-4

Project Officer:

Theodore G. Brna
U.S. Environmental Protection Agency
National Risk Management Research Laboratory
Air Pollution Prevention and Control Division
Research Triangle Park, NC 27711

Prepared for:

U.S. ENVIRONMENTAL PROTECTION AGENCY
OFFICE OF RESEARCH AND DEVELOPMENT
WASHINGTON, DC 20460

ABSTRACT

A centrifugal compressor which is a part of a CFC-114 chiller installation was investigated operating with the new refrigerant HFC-236ea, a proposed alternative to CFC-114. A large set of HFC-236ea operating data, as well as a limited number of CFC-114 data were available for this study. It was determined that the compressor performance can be successfully described by a relatively simple analytical compressor model. Two compressor models, the first of which was obtained from the literature, were developed on the basis of thermodynamics analysis and by utilizing the data base. Two empirical relations were required to predict mass flow rate and the refrigerant state at the compressor exit for each model. The second model is based on empirical relations derived directly from the data base rather than the general empirical relations used in the first model. The literature model had to be optimized for two parameters and corrected for the influence of the inlet guide vanes to yield results comparable to the newly developed model. Both models were based on the HFC-236ea data, and they exhibited systematic errors when used with CFC-114, which indicated the models' dependence on the refrigerant. Both models modeled refrigerant state at the compressor outlet excellently (± 5 F), while the mass flow rate was modeled with larger differences to the data (± 20 %). In addition to being quantitatively superior, the new model has more physical relevance; thus, it was used for the compressor design analysis. In the design analysis, the compressor geometric parameters were varied for constant operating conditions seeking trends in compressor performance. It appeared that the compressor geometric parameters were appropriately chosen in the compressor design. Also, the model indicated a valid physical behavior since all of the trends in the compressor performance were readily explainable.

This report was submitted in fulfillment of CR820755-01-4 by Iowa State University under the sponsorship of the U.S. Environmental Protection Agency. This report covers a period from January 1994 to September 1995.

CONTENTS

FIGURES

TABLES

ABBREVIATIONS AND SYMBOLS

ABBREVIATIONS

a ---------- speed of sound

A_2, A_3 ---------- impeller and diffuser discharge areas respectively.

$\hat{A}$ ----------diffuser width parameter appearing in Equations 3-18 and 3-21

b_2, b_3 ---------- impeller and diffuser exit axial dimensions respectively

b_D ----------diffuser axial width

b_{exp} ----------axial dimension at the diffuser inlet

B ---------- ratio of the diffuser inlet depth to the impeller flow passage depth

C_1, C_2, C_3, C_4 ------ curve-fitted coefficients in Equation 5-7

ca_0, ca_1, ca_2 --------- curve-fitted coefficients in Equation 5-28

$\hat{c}_f$ ----------friction factor in Equation 3-21

cos ---------- cosine of angle

cot---------- cotangent of angle

C_P ----------static pressure coefficient defined in Equation 3-17

d; D ---------- diameter

F----------degrees Fahrenheit

h---------- enthalpy

H----------head

IGV ----------inlet guide vane

k_B ----------blockage factor

$\dot{m}$ ----------mass flow rate

M---------- compressor Mach number

n---------- polytropic exponent

p ---------- pressure

Q ---------- volumetric flow rate

R ---------- ratio of diffuser outlet to inlet radii

RPM ---------- shaft speed (revolutions per minute)

s ---------- entropy

sin ---------- sine of angle

t ---------- temperature

tan ---------- tangent of angle

U ---------- impeller peripheral velocity

V ---------- refrigerant absolute velocity

V_a ----------axial velocity component

V_r ----------radial velocity component

V_u ----------tangential velocity component

w ---------- work per unit mass

W ---------- relative velocity of refrigerant

$\dot{W}$ ----------power

Z ---------- number of blades

GREEK SYMBOLS

α ---------- incidence angle

β ---------- blade tip angle

ε ---------- jet-to-wake area ratio

ϕ ---------- flow coefficient defined in Equation 3-5

γ ---------- angular momentum ratio defined by Equation 3-18

η ---------- efficiency

κ ---------- specific heat ratio

λ ---------- swirl coefficient defined by Equation 3-19

μ ---------- work (head) coefficient defined in Equation 3-7

π ---------- pi, constant = 3.14159

Θ ---------- flow coefficient used for compressor performance map (Equation 3-25)

ρ ---------- density

σ ---------- slip factor

τ ---------- torque

Ω ---------- work coefficient used for performance map (Equation 3-25)

ω ---------- angular velocity

ξ ---------- pressure loss coefficient

ψ ---------- head coefficient defined by Equation 3-20

SUBSCRIPTS

1 ----------referring to the compressor inlet

2 ----------referring to the impeller exit and the diffuser inlet

3 ----------referring to the compressor exit which coincide with the diffuser exit

corr ---------- corrected

D ---------- diffuser

dim ---------- dimensionless

fric ---------- friction

id ---------- ideal

im ---------- impeller

is ---------- isentropic

meas ---------- measured

mix ---------- mixing

mod ---------- modeled

p, pol ---------- polytropic

ref ---------- reference

th ---------- theoretical

ACKNOWLEDGMENTS

This work was sponsored by the Environmental Protection Agency (EPA) in cooperation with the United States Navy as EPA Cooperative Agreement CR820755-01-4. EPA's funding for this work was provided by the DoD's (Department of Defense's) SERDP (Strategic Environmental Research and Development Program) and SERDP's support is gratefully acknowledged.

The authors would like to express their appreciation to EPA's project officer, Theodore G. Brna, for his guidance and support in completing this work. Also, the authors would like to express appreciation to Jim Hanrahan and Tom Cavallaro with the Naval Surface Warfare Research Center in Annapolis, Maryland who were very helpful and always available in providing data and other information about the Navy's experimental chiller installation. In addition, the authors would like to thank the chiller manufacturer, York International Inc., for providing the design specifications of the investigated compressor.

CHAPTER 1

INTRODUCTION

Centrifugal compressors are commonly used in refrigeration installations. Their most versatile applications are in medium to large refrigeration systems in which the relatively high initial cost of the compressors is offset by their more efficient operation. Chillers are refrigeration systems of medium to large size, often providing chilled water to be used for air-conditioning. They are very commonly built with centrifugal compressors. As in every refrigeration installation, the compressor has the vital function in characterizing the chiller performance. The chiller installation investigated in this project, used on board Navy ships, is built with a single stage centrifugal compressor.

In recent years, negative effects of CFC (chloroflourocarbon) refrigerants on the stratospheric ozone layer have been recognized, and a significant campaign has been raised in search of alternative refrigerants that are less harmful to the ozone layer. The Montreal Protocol, enacted in 1987, has set in motion a major effort worldwide to phaseout CFC production and use. The new refrigerants have been sought among hydrofluorocarbons (HFCs), in which the chlorine atom is omitted from their structure. The CFC phase-out is thought to be the most cost effective if a new refrigerant would be effectively utilized in old refrigeration installations with minimal alterations in the installations. Therefore, the majority of new HFC refrigerants were investigated as drop-in replacements.

U.S. Navy surface ships and submarines are equipped with air-conditioning installations that have centrifugal chillers operating with CFC-114 refrigerant. The Environmental Protection Agency (EPA) in cooperation with the Navy has been seeking a CFC-114 drop-in replacement. Therefore, EPA sponsored a number of research projects related to the CFC-114 replacement in the mentioned chillers. One alternative HFC refrigerant which appears to satisfy all physical and chemical characteristics for the Navy fleet was found to be HFC-236ea refrigerant. In addition, HFC-236ea has very similar thermodynamic characteristics to CFC-114, so it was presumed that the performance of the Navy chiller operating with this refrigerant would not change significantly. Hence, this project represents a part of the investigation directed to evaluate this CFC-114 alternative refrigerant as a possible drop-in replacement in Navy chillers.

The Navy set up an experimental chiller test facility in Annapolis at the Naval Surface Warfare Research Center. This typical chiller installation, which has been used to test the Navy fleet air-conditioning installations, is well instrumented and set up to generate experimental data corresponding to different chiller operating conditions. The data have been gathered over several years with several different refrigerants. From this large data base, the entire data set of HFC-236ea and several CFC-114 operating points were accessible to be investigated in this project.

The data were already taken before this phase of the project started. Therefore, the authors had no influence in setting up the experimental installation, nor any insight as to the quality of the data. Also, the uncertainty of the results presented in this report is highly dependent on the data uncertainty, so the lack of information about data uncertainty prevented any reasonable uncertainty analysis of the results in this project.

The results in this project are presented in the English unit system rather than in the SI unit system. It is still common engineering practice in U.S. to use the English unit system, and the data recorded by the Navy were in English units. Conversion factors from English units to the corresponding SI units are included in Appendix B.

1.1 OBJECTIVE

The objective of this study was to conduct a thorough literature review regarding centrifugal compressors and then, on the basis of the information gathered, build an accurate but simple compressor model utilizing the available compressor experimental data. Further, the developed compressor model would be used to suggest eventual design adjustments to enhance compressor performance with the alternative HFC-236ea refrigerant.

Literature Review

A centrifugal compressor represents a very complex dynamic machine, commonly regarded by authors as the most complex fluid flow encountered in practice. There are a large number of different parameters affecting compressor performance, so the first goal of this project was to address and understand phenomena important in centrifugal compressor performance. Also, already developed analytical centrifugal compressor models were sought for eventual use as the starting point of the compressor model development. Further, if a model were found to be fully applicable to the investigated compressor, it would be reproduced and used for the design analysis.

Compressor Model

The ultimate goal of every modeling process is to achieve a completely general model which would account for all of the effects of the modeled system. The ultimate goal for refrigeration compressor modeling would be development of a model which would be invariant to the refrigerant type, the compressor geometric characteristics, and the specific compressor operating conditions. However, this is very arduous to accomplish because of refrigeration compressor complexity.

Another aspect of compressor modeling is its analytical complexity. Complexity of a compressor model commonly improves its accuracy, although a reasonable balance between accuracy and complexity must be sought. Some complex models are developed by solving the exact fluid flow field through the compressor utilizing the complex fluid flow equations, while on the other hand simpler models are developed by defining compressor performance by its end states and some characteristic overall performance parameters. The complex models are laborious to develop and they should be utilized in compressor design development. The simpler models, which usually consist of several analytical equations, are feasible for compressor (chiller) simulation programs.

The trade-off between model complexity and accuracy should be addressed in compressor model development to suit the purpose for which the investigation is being performed. The emphasis in the modeling procedure will be put on developing a simple, accurate model based on the available data.

Design Analysis

A drop-in refrigerant replacement in a particular refrigeration installation commonly tends to reduce compressor performance efficiency. A particular compressor is especially designed to operate with a certain refrigerant, and therefore performance of that compressor with any other fluid is usually less efficient. The development of an accurate compressor model may indicate certain design adjustments which may result in compressor performance enhancement.

This goal, which is another objective in this study, can be achieved by analysis of geometric parameters incorporated in the compressor model. Nevertheless, one has to be very careful with such an analysis because of the complexity of the compressor performance. Also, this kind of design analysis should be only an indicator of the generic trends in the compressor performance rather than specific design suggestions.

1.2 APPROACH TO COMPRESSOR MODEL DEVELOPMENT

A centrifugal compressor consists of a rotor (impeller), discharge volute (diffuser), and its casing. The impeller and the diffuser are modeled differently, since they represent completely separate entities of the compressor in which energy transfer occurs. However, their interaction in the compressor assembly adds to the complexity of the compressor performance description.

Fluid Mechanics Approach - Exact Solution

The fluid flow through a centrifugal compressor is one of the most complex analytical problems. This flow exhibits a strong three-dimensional nature requiring solution of the complete set of the fundamental fluid dynamic equations (Navier-Stokes equations).

In addition, a property function is used to determine required refrigerant properties. The only apparent simplification to this fluid flow problem is that the model should be postulated as a steady state or time invariant. The steady state set of the fundamental fluid dynamics equations are partial differential equations, and they can be solved only by numerical methods, if no further simplifications are applied. The numerical solution of the problem requires the development of a mesh on which a finite difference method is applied. The mesh most likely has to be very fine to account for complex compressor geometry. The solution is then obtained by simultaneous solution of a large number of equations corresponding to the set grid points. Setting the grid scheme and actual solving of the obtained system of equations are very onerous processes.

Thermodynamics Approach - Approximate Solution

Knowledge of the detailed fluid flow field is not necessary to characterize performance of the compressor. The compressor, or its components, can be modeled by the control volume approach by evaluating overall energy transfer (or losses) across appropriate control volumes. Compressor performance can also be described by correlating its end states, for instance by the polytropic compression exponent which is common practice in refrigeration compressor modeling.

This approach does not give the exact prediction of the compressor performance because it is impossible to account for all effects causing losses in the energy transfer within the compressor. However, the compressor performance can be evaluated by this method with reasonable accuracy. In order to improve a compressor

model's accuracy, experimental data for that particular compressor may be utilized. Popovic and Shapiro (1995) developed a reciprocating compressor model using this approach, and they reported very good results.

It was decided to use this approach to model the Navy compressor. The impeller and the diffuser were assumed to be separate control volumes; hence, the refrigerant state at their interface had to be established.

The standard form of the compressor model (Popovic and Shapiro, 1995) has the following inputs:

- inlet refrigerant state,
- shaft speed, and
- outlet state pressure,

while the model has to predict:

- mass flow rate,
- a refrigerant property at the compressor exit state, and
- compressor energy consumption.

This model form allows the compressor model to be readily incorporated in a simple refrigeration installation, allowing the simulation of that particular refrigeration installation. Therefore, development of the centrifugal compressor model in this form would allow its inclusion in the entire Navy chiller simulation.

CHAPTER 2

CONCLUSIONS AND RECOMMENDATIONS

The purpose of this study was to investigate the performance of an CFC-114 centrifugal chiller using HFC-236ea as an alternative refrigerant. This Navy chiller is a well instrumented experimental installation on which experimental operating points were generated for use in this study. Most of the data available for this study were for HFC-236ea; hence, all the modeling work was based on this refrigerant data set. The centrifugal compressor, which is the main component of the chiller, was described with analytical models which were further quantitatively compared in this study. The best of the models was further analyzed for the effects of the compressor geometric parameters, suggesting eventual design modifications to the compressor.

2.1. CHILLER (COMPRESSOR) PERFORMANCE

The centrifugal compressor which was investigated in this study is an open type. It has a single stage, one impeller, and a vaneless diffuser. Control of the compressor performance is achieved by the following means:

- variable gear box (compressor shaft speed),
- inlet guide vanes utilized for the fine refrigerant flow rate control and for an extension of the stable compressor operating range, and
- compressor by-pass loop used to crudely control the flow rate through the installation (the chiller capacity).

In studying the chiller operating points, it was concluded that the available data provides a good basis for a compressor model. As an example, the chiller capacity was varied between 20 and 140 percent of the design capacity, while the inlet guide vane settings were altered between 10 and 90 degrees.

Compressor Energy Model

The losses occurring in the energy transfer from the compressor shaft to the refrigerant are approximately constant. Quantitatively, these losses are around one percent of the total power delivered to the compressor shaft. Since the energy losses are constant, the compressor shaft power is modeled in Section 4.4 as a linear function of the energy transferred to the refrigerant. Thus, the compressor shaft power can be very successfully estimated by knowing the compressor refrigerant mass flow rate and the enthalpy difference across the compressor.

Most of the data available for this study did not have the total compressor energy input recorded; hence, the modeling of the total energy input in the compressor was abandoned. Also, the CFC-114 data points indicated lower energy losses within the compressor than the HFC-236ea operating points. Thus, the HFC-236ea compressor performance line correlating the compressor shaft power with the rate of energy transferred to the refrigerant in the impeller is different than the CFC-114 performance line. This was the first indication that compressor modeling depends on the operating refrigerant.

Compressor Performance Map

A standard form performance map for the investigated compressor was provided by the compressor manufacturer, although the performance map was constructed for the compressor operating with a refrigerant different than the refrigerants examined in this study. A feasible relation between the performance map and the actual compressor operating points was impossible to find. The experimental data points, when plotted in the form of the compressor performance map in Section 4.5, vaguely resembled a compressor map. Therefore, it was inferred that the modeling of the compressor performance should be sought in some other way.

2.2. COMPRESSOR MODELING

Based on a thorough literature review, it was decided to describe the compressor performance thermodynamically by regarding the compressor as a control volume. This modeling approach considers overall compressor performance characteristics rather than exact flow field information within the compressor. Further, a centrifugal compressor must be divided in two entities: the impeller and the diffuser. These compressor parts are treated as separate control volumes. Therefore, the refrigerant state between the impeller and the diffuser must be determined.

Existing Model

A centrifugal compressor model was extracted from the Braun et al. (1987) chiller simulation, and the model is presented in Section 5.2. The model complied with the desired model input/output format defined in Section 1.2, and it was built on two generic empirical relations which were based on an extensive data base for similar centrifugal compressors. However, these empirical relations were based on the compressors without the inlet guide vanes.

As initially developed, the model greatly overestimated the refrigerant flow rate; therefore, the model was subjected to an optimization procedure. The differences between measured and modeled flow rates were minimized for two compressor parameters (blockage factor and reference polytropic efficiency) using the HFC-236ea data. When the optimized parameters were incorporated, the flow rate was estimated within a relative difference margin of ± 40 percent. One of the optimized parameters, the blockage factor, was found to be physically unreasonable. In addition to the doubtful physical validity of the model, another shortcoming of the existing model was the requirement to input the compressor polytropic exponent.

Further, the modeled flow rate was corrected for the influence of the inlet guide vane angles utilizing the available data. The flow rate was modeled within ± 20 percent relative difference, while the exit state temperature was modeled within ± 10 F for the most of the HFC-236ea data points. The CFC-114 data indicated the presence of a systematic error, implying that the compressor model depended on the particular refrigerant.

New Model

The main difference between the new model (Section 5.3) and the existing model is that the available experimental data were utilized to generate empirical relations rather than using the general empirical relations. In addition, the inlet guide vane settings and the slip factor were incorporated in the compressor model.

It was determined that the empirical relations which had the least error were those matching the following model parameters:

- the impeller isentropic efficiency as a function of the inlet guide vane position, and
- the dimensionless enthalpy as a function of the flow coefficient.

HFC-236ea data were used to generate these two empirical relations. The first empirical relation had larger variance than the second relation, and also the errors generated in deriving the empirical relation are proportional to the model output prediction errors.

The by-pass operation mode flow rate is successfully correlated to the measured flow rate for the known percentage of the by-pass valve opening; hence, the new model is feasible for this operating mode.

A systematic error occurred in the model estimate for the CFC-114 data points; hence, the model is a function of the refrigerant type. A different set of empirical relations should be developed for CFC-114, which requires a larger experimental data base.

The blockage factor was optimized to improve the physical validity of the new model, and the optimized value has more physical relevance than the blockage factor determined for the existing model.

Quantitative Comparison Between Two Models

Table 2.1. Quantitative comparison between two compressor models.

Comparison between measured and modeled compressor parameters	HFC-236ea data used to build empirical relations		HFC-236ea additional data points.		CFC-114 data points	
	Average *	Max. †	Average	Max.	Average	Max.
The Existing Model						
Flow rate w/o IGV cor.[%] ‡	13.96	36.81	22.27	49.71	30.67	76.25
Flow rate IGV corrected[%] ‡	6.33	21.85	7.66	15.57	19.22	31.01
Exit state temperature [F] §	1.22	3.43	3.49	9.07	13.97	47.31
Shaft power [%]	15.67	21.04	20.27	39.40	33.04	52.99
The New Model						
Flow rate prediction [%] ‡	4.45	19.51	12.57	19.84	22.84	55.08
Exit state temperature [F] §	0.89	2.21	2.13	6.11	6.21	17.81
Shaft power [%] ‡	3.13	13.38	9.26	17.22	20.54	42.61

* The mean value for a set of absolute differences between measured and modeled particular compressor parameters for the data set in question.

† The maximum absolute difference between measured and modeled particular compressor parameters for the data set in question.

‡ The comparison results are presented in terms of the absolute relative difference between measured and modeled particular compressor parameter, X, given as percentage: $\text{Difference}[\%] = \left|(X_{meas} - X_{mod})/X_{meas}\right| 100$

§ The comparison between measured and modeled compressor exit state temperatures is given in terms of absolute difference between measured and modeled temperatures in degrees Fahrenheit for the particular data set:

$$\text{Difference}[F] = \left|t_{3,meas}[F] - t_{3,mod}[F]\right|$$

IGV - Inlet Guide Vane

From the comparison results presented in Table 2.1, it can be inferred that the new model estimates the compressor performance parameters better than the existing model. In addition to the increased physical validity of the new model, this improvement in the parameter estimation definitely classifies the new model as the better of the two.

The new model is dependent on the refrigerant type. The model represented here is developed for HFC-236ea data: hence, a different set of empirical relations should be developed for a different refrigerant operating in the same compressor. There were not enough CFC-114 data points available in this study to develop a CFC-114 model.

The new HFC-236ea model can estimate the flow rate within ± 20 percent relative difference between the measured and modeled flow rates, exit state temperature within ± 3 F, and the compressor shaft power within ± 14 percent relative difference.

In addition to being a quantitatively superior model, the new model also has more physical validity than the existing model for the following reasons:

- The blockage factor in the new model was derived to be 0.9, while the existing model blockage factor was optimized to the value of 0.24. The existing model blockage factor must have accounted for some other compressor performance effects, diminishing the model's physical relevance.
- The existing model required the polytropic exponent and the reference polytropic efficiency to be estimated as input.
- The existing model inlet guide vane setting is introduced in the model through the flow rate correction formula, while in the new model the inlet guide vane angle was a fundamental factor upon which the model was developed.

Refined Model

A more detailed centrifugal compressor model was built on the new model and is outlined in Appendix A. This refined model needed two empirical relations, and the best relations appeared to be relations correlating the same pairs of parameters as in the new model The refined model contains the following improvements:

- the variable slip factor, and
- a more detailed diffuser model.

The set of equations of the refined model never yielded a reasonable solution. Errors generated in the model output solution were found to be functions of the sequence in which the equations were solved. However, the source of such a spurious behavior of the system of equations was never identified. The authors still believe that the system might be solvable with good equation-solver software.

2.3 DESIGN ANALYSIS

Three representative experimental HFC-236ea data points were kept constant in the analysis as the compressor operating input. The compressor design parameters which were used in the new model were varied to investigate their effects on the compressor performance. Each design parameter was varied independently, keeping the other compressor design parameters and the compressor operating input constant.

The results obtained in the design analysis (Chapter 6) are found to be physically reasonable. All the trends observed were readily explainable with the centrifugal compressor theory given in Chapter 3.

Although the compressor model indicated reasonable physical behavior, the design analysis should be interpreted qualitatively. The intent of the design analysis was to indicate trends in the compressor performance with the design input variations rather then to suggest specific changes in the compressor design. Since the compressor model was found to be sensitive to the refrigerant type, it is reasonable to assume that the model is sensitive to the compressor design modifications. Also, the assumption of constant operating input with design input variations should be regarded with some reservations because of the indicated sensitivity of the compressor model.

The effects of the design parameters on the compressor model results are summarized in the following bulleted section:

- The number of impeller blades is directly related to the slip factor. As reported in Chapter 3, impeller performance as a function of the slip factor has a positive gradient, while the flow rate as a function of the slip factor is negatively sloped. These trends were observed in the design analysis, and it appears that the number of blades were chosen appropriately. Increasing the number of blades by about 10 percent might improve compressor performance, but would result in a pressure drop of approximately 15 percent.
- The blade tip angle is inversely related to the slip factor but directly related to the compressor performance. The trends observed in the blade tip angle design analysis were very similar to the trends encountered in number of impeller blades design analysis. The blade tip angle appears to be well chosen. Enlarging tip angle by about 5 percent might improve the work coefficient by roughly 10 percent and reduce the flow rate by about 20 percent, with an increase of 1 to 2 psi in impeller exit pressure.
- Increasing the impeller inlet diameter improves compressor performance and reduces the mass flow rate. The flow rate variations are more significant than the variation in the work coefficient, which is the primary quantitative measure of impeller performance. The pressure at the impeller exit and the compressor exit enthalpy are not affected by this design parameter. The influence of inlet diameter on compressor performance rapidly diminishes as the flow is throttled with guide vanes. For these reasons, the inlet diameter should be excluded from the eventual impeller design modification.

- The impeller exit diameter greatly affects the magnitude of the flow rate, indicating a large gradient as the flow rate is varied with the size of the impeller. The compressor performance (work coefficient) is a negatively sloped function of the exit impeller diameter. The exit diameter changes should be very limited, since a 10 percent increase in the impeller exit diameter roughly doubles the mass flow rate.
- The impeller discharge area is directly related to the impeller axial width, so it affects the flow rate considerably. Impeller performance as a function of the impeller axial width has a small negative gradient, while there is no significant change observed in the impeller exit state pressure. The impeller exit axial width may be altered to change flow rate if necessary for a relatively small change in the compressor performance.

2.4. RECOMMENDATIONS

Based on this study, the following recommendations are offered:

1. The refrigerant flow rate was not measured on the chiller installation, but rather estimated from the condenser and the evaporator energy balances. Since the flow rate was found to be an extremely sensitive value in the compressor models, the flow rate should be **verified** on the experimental installation. As the vital value in any refrigeration compressor modeling procedure, the flow rate should be verified by even several flowmeters on a single experimental refrigeration installation. At the very least, measurements of the flow rates through the chiller and the compressor by-pass loop should be obtained.
2. The total compressor power consumption should always be measured and reported. The total compressor power consumption is an important parameter to include in the modeling in order to be able to predict compressor energy requirements for different compressor operating conditions.
3. The compressor in the Navy chiller has a vaneless diffuser. However, vaned diffusers are also widely used in centrifugal compressors. Their advantages over the vaneless diffusers are in providing a broader stable compressor operating range and in reducing the fluid expansion losses at the diffuser inlet. However, this type of diffuser has greater friction losses than the vaneless diffuser. The use of a vaned diffuser should be considered.
4. Both models were dependent on the refrigerant type. The models presented here were developed based on HFC-236ea data; hence, a different set of empirical relations should be developed for a different refrigerant operating in the same compressor. This should give insight into the dependence of the model on the refrigerant type.
5. A better compressor performance map than the one provided by the compressor manufacturer should be developed, which may require a wider range of the operating conditions, especially compressor Mach numbers. Such a performance map might be a better tool with which to model the compressor performance.

6. Further attempts should be made to solve the refined model outlined in Appendix A. It is anticipated that the refined model, if a solution to its set of the equations were found, would improve the accuracy of the new model.
7. Increasing the number of blades by about 10 percent might improve compressor performance, but would result in a pressure drop of approximately 15 percent.
8. Enlarging the tip angle by about 5 percent might improve the work coefficient by roughly 10 percent and reduce the flow rate by about 20 percent, with an increase of 1 to 2 psi in the impeller exit pressure.
9. The inlet diameter should be excluded from the eventual impeller design modification.
10. One has to be very careful modifying the impeller diameter, since it strongly influences compressor performance.
11. The compressor exit axial width may be enlarged to increase flow rate, if necessary, for a relatively small deterioration in the compressor performance.

CHAPTER 3

CENTRIFUGAL COMPRESSOR THEORY

A centrifugal compressor can be classified in a broad group of dynamic machines called turbomachines. A typical centrifugal compressor schematic is shown in Figure 3.1. The centrifugal compressor consists of a rotor (impeller), rotor casing, and discharge volute (diffuser). A fluid flowing through such a compressor is greatly accelerated in the compressor rotor (dynamic head increase). Then the dynamic head is converted to static head (pressure rise) in the diffuser. It is a common practice to design multiple impeller compressors, referred to in the literature as multistage centrifugal compressors.

A centrifugal compressor represents a highly complicated system to model analytically. Fluid flow through the compressor is three-dimensional in nature. The impeller and diffuser are modeled separately as they represent compressor entities in which energy transfers occur. In addition, the compressor assembly exhibits some phenomena which represent complex interactions between the compressor parts.

The literature survey presented here includes most of the phenomena encountered in centrifugal compressor performance. However, less emphasis is placed on fluid flow modeling by means of computational fluid mechanics, which is the subject of most recent publications treating this type of compressor. The objective of this project, as stated in Chapter 1, was to obtain a relatively simple analytical model by concentrating on predicting the compressor performance based on knowledge of the end states of each compressor component.

It should be recognized that in the following text there are three distinct refrigerant states considered within the compressor. The refrigerant state at compressor inlet state coincides with the impeller inlet state, and it is denoted as state 1. Refrigerant state 2 corresponds to the impeller exit state, the diffuser inlet state, and also is sometimes referred to as the compressor mid state. Refrigerant state 3 denotes the sate at diffuser exit, which is the same as the compressor exit.

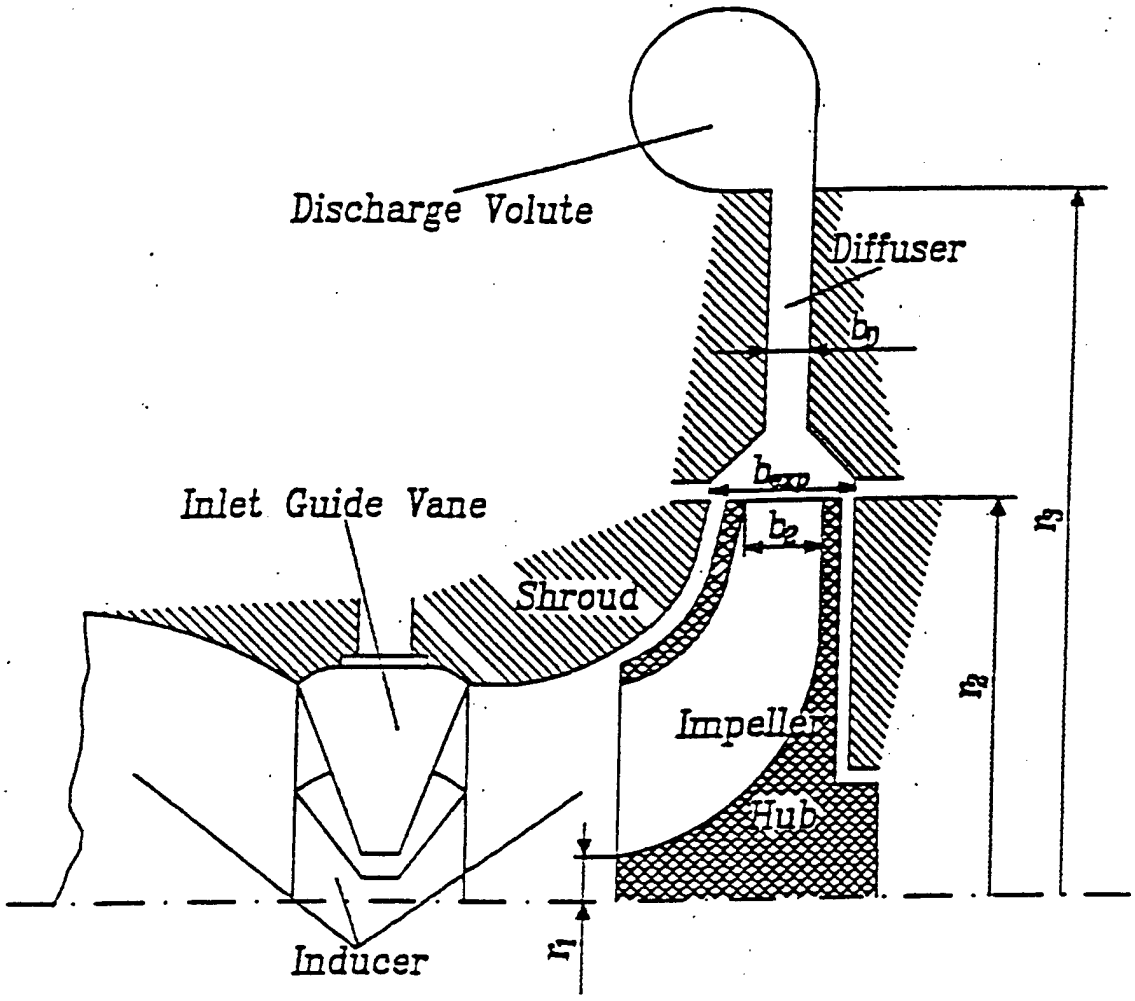

Figure 3.1. A typical centrifugal compressor.

3.1 IMPELLER

The impeller is the rotor in a centrifugal compressor in which an incoming refrigerant is accelerated in passing from the inlet to the outlet diameter. The compressor shaft energy brought into the impeller is converted mainly into the increase of the refrigerant dynamic head.

Fluid flow through an impeller is three-dimensional in nature. The complex flow field within an impeller was reported by Farge and Johnson (1992) who measured flow field parameters in five planes within a specially designed backswept compressor impeller. There are few developed complex computational models to solve for the exact flow field within impeller, one being presented by Hathway et al. (1993). Solving for the exact fluid field within an impeller control volume is beyond the scope of this project; consequently, the literature survey about impeller modeling was directed toward publications in which the impeller performance was characterized by its end states.

3.1.1 EULER EQUATION

The general equation applicable for any turbomachinery rotor results from Newton's Second Law of Motion being applied to fluid traversing the rotor. A generic diagram of the rotor with velocity diagrams is represented in Figure 3.2.

The absolute fluid velocity is decomposed in three mutually perpendicular velocity components. States 1 and 2 denote the impeller inlet and the exit states, respectively. The axial component of velocity, V_a, change relates to the axial load imposed on the thrust bearing in the impeller casing. The radial velocity component, V_r, yields a journal load. Neither of these velocities affects the angular motion of the impeller, but rather the amount of friction produced in the impeller bearings (Shepherd, 1956). The change in magnitude of tangential velocity, V_u, cause a change in the angular momentum (moment of momentum).

Assuming steady state flow and conservation of mass across the impeller, the net torque is given by the following form of Newton's Second Law of Motion:

$$\tau = \dot{m}\left(r_1 V_{u1} - r_2 V_{u2}\right) \tag{3-1}$$

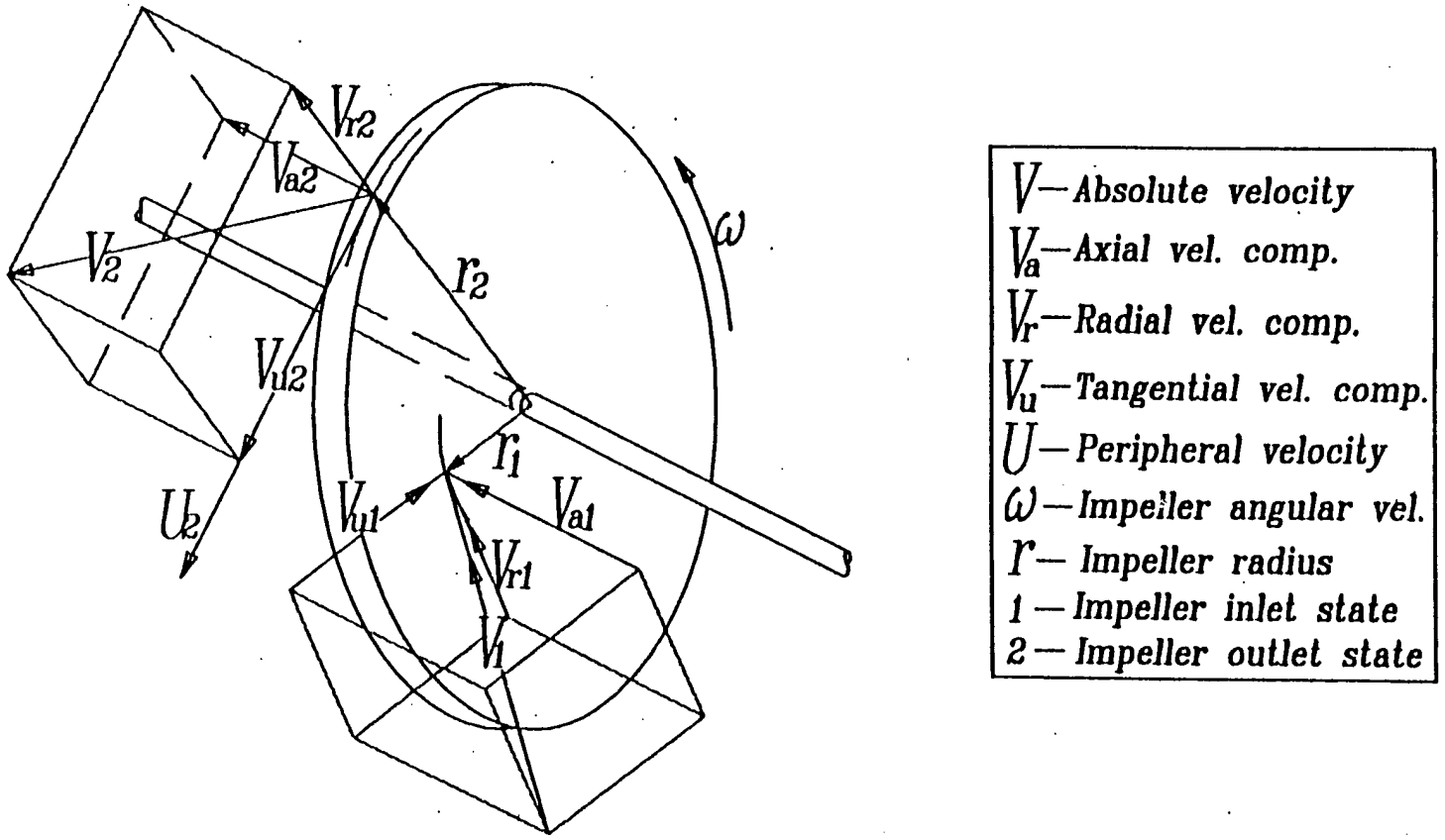

V — *Absolute velocity*
V_a — *Axial vel. comp.*
V_r — *Radial vel. comp.*
V_u — *Tangential vel. comp.*
U — *Peripheral velocity*
ω — *Impeller angular vel.*
r — *Impeller radius*
1 — *Impeller inlet state*
2 — *Impeller outlet state*

Figure 3.2. Impeller velocity diagrams.

The energy transfer rate between the fluid and the rotor, $\dot{W}$, is the product of the net torque and the angular velocity of the rotor; ω. Multiplication of Equation 3-1 by the angular velocity and noting that $\omega = U/r$ yields

$$\dot{W} = \tau\omega = \dot{m}H = \dot{m}(U_1 V_{u1} - U_2 V_{u2}) \tag{3-2}$$

where H denotes the compressor head (energy transferred to fluid per unit mass) and U represents the impeller linear velocity. The total work rate (power), $\dot{W}$, of the compressor is negative ($U_1 V_{u1} < U_2 V_{u2}$), which is in agreement with the normal thermodynamics sign convention signifying the power input to the fluid.

This is the Euler equation, which is the fundamental energy equation representing conservation of the angular momentum across the impeller. The Euler equation is applicable to all types of turbomachines.

The effects of the absolute fluid velocity axial components at the impeller end states do not enter into the analysis of the Euler equation. The reason is that the Euler equation involves angular momentum only in the radial plane, due to moments about the rotational axis of the shaft, and therefore has no axial component. Therefore, the fluid absolute velocity can be decomposed into two velocity components, $\bar{V} = \bar{V}_r + \bar{V}_u$, in the impeller radial plane presented in Figure 3.3.

The fluid absolute velocity, $\bar{V}$, results from the impeller rotational motion and motion of the fluid relative to the impeller. Hence the absolute velocity is the sum of the impeller linear velocity, $\bar{U}$, and the fluid relative velocity, $\bar{W}$, $\bar{V} = \bar{U} + \bar{W}$.

These two definitions of the fluid velocity are included in the velocity triangles in Figure 3.3. The velocity triangles are represented in the radial plane of the impeller, since the axial velocity component was neglected.

Using the inlet and the outlet velocity diagrams from Figure 3.3, the Euler equation can be modified as follows (Shepherd, 1956):

$$H = \frac{1}{2}[(V_1^2 - V_2^2) + (U_1^2 - U_2^2) + (W_2^2 - W_1^2)] \tag{3-3}$$

The first term in Equation 3-3 accounts for the change of absolute kinetic energy, or dynamic head, occurring in the impeller. The second term in the modified Euler equation represents the change in energy due to the movement from one radius of rotation to another. Shepherd (1956) refers to this term as centrifugal energy. The change of linear rotor velocity contributes to a change in the static pressure. The third term in Equation 3-3 represents the change of kinetic energy due to change in relative fluid velocity. The change in the relative velocity results in a change of the static head (pressure).

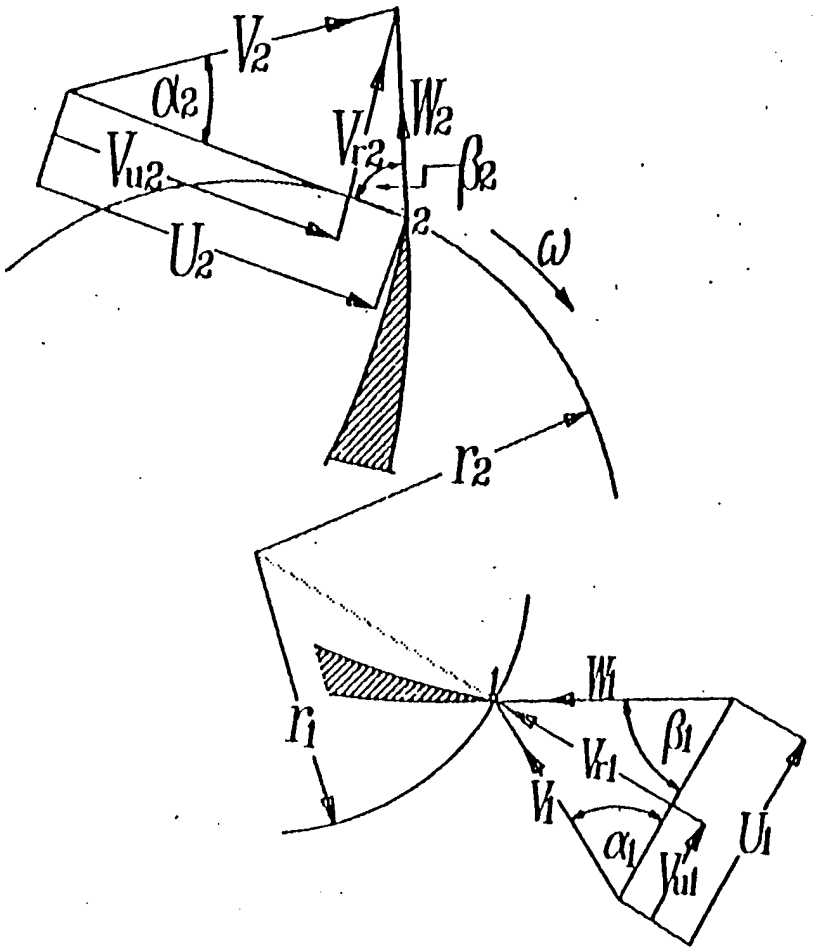

V	Absolute velocity
W	Relative velocity
V_r	Radial veocity component
V_u	Tangential velocity component
U	Peripheral velocity
α	Incidence angle
β	Blade tip angle
ω	Impeller angular velocity
1	Impeller inlet state
2	Impeller outlet state

Figure 3.3. Impeller velocity triangles in radial plane.

The ratio of energy transfer in the rotor associated with static pressure to the total energy transfer into impeller is defined by Equation 3-4, as the degree of reaction or simply reaction, R (Shepherd, 1956):

$$R = \frac{\frac{1}{2}\left[(U_1^2 - U_2^2) + (W_2^2 - W_1^2)\right]}{H} \tag{3-4}$$

Reaction can be positive, negative, or zero. Zero reaction (no pressure rise across the impeller) defines the impulse type of turbomachines.

3.1.2 FLUID VELOCITY ANGLES

Various angles in Figure 3.3 should be distinguished. Two important geometric parameters are the impeller inlet and outlet blade tip angles, which are denoted respectively by β_1 and β_2 . In addition, the angles that the absolute velocity vectors make relative to the tangential direction are called incidence angles, and they are denoted by α_1 and α_2, respectively.

The blade tip angle represents an important compressor performance parameter. For ideal impeller performance, the blade tip angle equals the angle at which the refrigerant enters and departs impeller. The actual angle of refrigerant departure is always less than the blade tip angle due to an occurrence known as fluid slippage. These angles are important tools in correlating velocity components.

3.1.3 IMPELLER PERFORMANCE PARAMETERS

There are several dimensionless parameters important in the investigation of centrifugal compressor operation (Sheets, 1950). The ratio of the radial velocity component to the impeller linear velocity is defined as the flow coefficient, ϕ, or:

$$\phi_2 = \frac{V_{r2}}{U_2} \tag{3-5}$$

Here, the flow coefficient is given for the refrigerant state at the impeller exit (compressor mid state), since this dimensionless parameter is usually investigated there. The flow coefficient can be thought as being directly related to the refrigerant flow rate.

Typical values of the flow coefficient are between 0.1 and 0.4. The impeller exit radial velocity component is usually taken to be the mean velocity of the flow leaving the impeller. This velocity is determined by using the volumetric flow rate of the fluid leaving the impeller:

$$V_{r2} = \frac{Q_2}{A_2 k_B} = \frac{(\dot{m}/\rho_2)}{A_2 k_B} \tag{3-6}$$

A_2 represents the nominal discharge area at the impeller exit, while the blockage factor k_B accounts for the definite impeller blade thickness reducing the discharge area. The blockage factor is an empirical parameter that can be determined from experimental data. If the blockage factor is calculated from experimental data, it may also take into account effects of the uneven fluid profile leaving the impeller or other factors affecting impeller performance.

The second dimensionless parameter which is related to compression work is the compressor work coefficient. The work coefficient, μ, is the ratio of the tangential component of velocity to the impeller linear velocity:

$$\mu_2 = \frac{V_{u2}}{U_2} \tag{3-7}$$

The most important work coefficient, as shown in Equation 3-7, is the one corresponding to the impeller exit state. At this state, the dynamic head is at its largest value, which corresponds to the largest velocity magnitudes. The velocities at the impeller inlet and at the diffuser outlet states are significantly smaller; therefore, the work coefficients corresponding to those states are less important in characterizing compressor performance. Large work coefficients suggest better impeller performance, with the ideal impeller having a work coefficient of unity. Thus, the work coefficient may be regarded as a measure of the impeller performance.

$$\sigma = 1 - slip/U_2$$

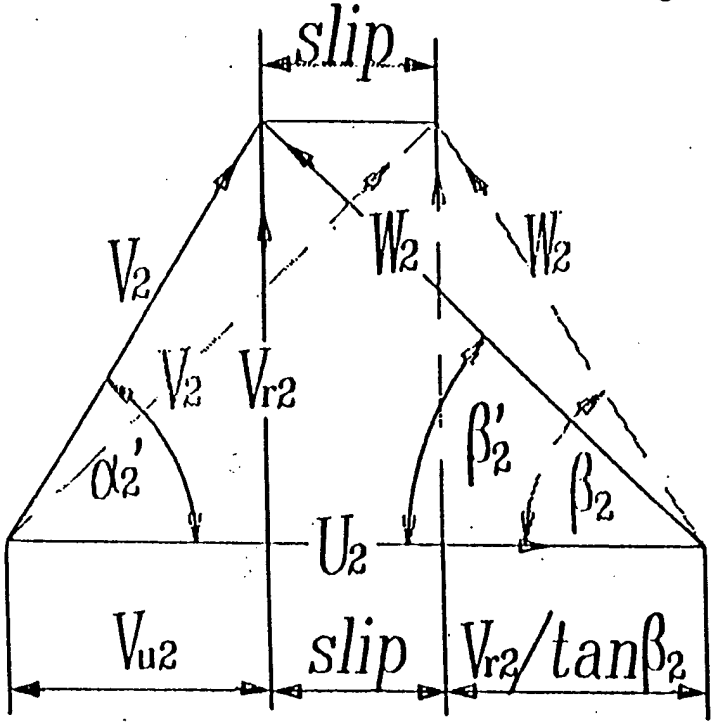

V	Absolute velocity
W	Relative velocity
V_r	Radial veocity component
V_u	Tangential velocity component
U	Peripheral velocity
α	Incidence angle
α'	Actual incidence angle
β	Blade tip angle
β'	Fluid departure angle
σ	Slip factor
2	Impeller outlet state

Figure 3.4. Impeller slippage phenomena

3.1.4 SLIP PHENOMENA

The deviation of the exit fluid flow direction from the blade angle is mainly due to vorticity of the refrigerant flow and viscous effects (Van den Braembusse, 1985). This deviation, known as fluid slip, is shown on the impeller exit velocity triangle in Figure 3.4. The ideal velocity triangle is represented with the lighter dashed lines, and the fluid in that case departs from the impeller at the blade tip angle β_2. However, due to the fluid slip, the fluid is actually discharged at the angle β_2', which corresponds to the real velocity triangle drawn in darker continuous lines in Figure 3.4. The reduction of the impeller discharge angle causes a decrease in the tangential velocity component, therefore reducing the compressor work coefficient. The amount of the tangential velocity component reduction is the fluid slip. Quantitatively the fluid slip is expressed in dimensonless form as the slip factor. There are two definitions of the slip factor found in literature. The Wiesner (1967) definition was selected in this project: $\sigma = 1 - \frac{slip}{U_2} = 1 - \frac{U_2 - (V_{u2} + V_{r2}/\tan\beta_2)}{U_2}$.

Using the velocity triangles in Figure 3.4, the above definition of the slip factor, and the definitions of the compressor performance parameters given in Equations 3-5 and 3-7 the slip factor, σ, can be expressed as;

$$\sigma = 1 - 1 + \frac{V_{u2}}{U_2} + \frac{V_{r2}/\tan\beta_2}{U_2} = \mu_2 + \frac{\phi_2}{\tan\beta_2} \tag{3-8}$$

which is the sum of the work coefficient and the flow coefficient divided by the tangent of the impeller blade tip angle.

Wiesner (1967) investigated different empirical expressions for the slip factor calculation. He concluded that among a number of proposed analytical expressions available in the literature, Busemann (1928) gave the best correlation for the slip factor. Wiesner (1967) approximated a relatively complex Busemann (1928) slip factor formula with the following empirical expression in which Z denotes the number of impeller blades:

$$\sigma = 1 - \frac{\sqrt{\sin\beta_2}}{Z^{0.7}} \tag{3-9}$$

Sheets (1950) proposed the solidity limit, which he based on the Wisclenius (1965) calculation procedure. Wiesner (1967) adopted and confirmed that this expression, given in Equation 3-10, is applicable to the Busemann (1928) slip factor relation:

$$sol_{lim} = \left(\frac{r_2}{r_1}\right)_{max} \equiv EXP\left(\frac{8.16 \sin\beta_2}{Z}\right) \tag{3-10}$$

The solidity limit represents the maximum impeller radius ratio allowed for the given number of impeller blades. If the impeller radius ratio is less than the solidity limit, Wiesner (1967) derived a corrected empirical slip factor relation. In other words, Wiesner (1967) introduced a correction factor to the relation given in Equation 3-9, which is the best fit to the Busemann (1928) slip factor estimate:

$$\sigma = 1 - \frac{\sqrt{\sin\beta_2}}{Z^{0.7}}\left[1 - \left(\frac{r_1/r_2 - 1/sol_{lim}}{1 - 1/sol_{lim}}\right)\right] \tag{3-11}$$

The empirical relations Equations 3-9 through 3-11 estimating the slip factor were confirmed for a large number of pump and compressor impellers investigated by Wiesner (1967). The slip factor cannot be regarded as a constant value for all operating conditions, as argued in the discussion part of the Wiesner (1967) paper. For example, the slip factor increases for decreasing flow rate, hence there is less deviation from the exit blade tip angle (Shepherd, 1956).

Dean and Senoo (1960) developed a two-dimensional model of the flow leaving the impeller which includes two distinguishable flow regions: jet and wake. The jet region is on the leading edge, while the wake region occurs on the trailing edge. They treated these flow regions separately. According to the postulated theory, as the flow rate is reduced, more separation occurs; hence enlarging the wake region of the flow leaving the impeller. As the jet region is reduced, the flow deviation from the blade angle is decreased. Apparently as the flow rate decreases, the slip factor tends to unity.

Johnston and Dean (1966) further developed the jet-wake model analytically, introducing a parameter ε which represents the jet to wake flow region area ratio. Eckert and Schnell (1980) developed a correction, μ_{cor}, for the work coefficient, μ, affected by the presence of the wake flow region at the impeller exit:

$$\mu_{cor} = \frac{1}{1 + (1-\varepsilon)(1/\mu - 1)} \tag{3-12}$$

Combination of Equations 3-7 and 3-11 yields a correction expression for the slip factor to account for the presence of the wake flow region. The corrected slip factor, Equation 3-13, becomes a function of the flow coefficient; therefore the slip factor becomes dependent on the compressor operating conditions:

$$\sigma_{cor} = \frac{1}{1+(1-\varepsilon)\left[1/(\sigma-\phi_2/\tan\beta_2)-1\right]} + \frac{\phi_2}{\tan\beta_2} \qquad (3\text{-}13)$$

By accounting for slip factor effects in the Euler energy equation, Equation 3-2, the so-called ideal compressor head is obtained. The ideal head represents the maximum obtainable energy transfer to the fluid across the impeller, and it is less than the Euler head. The frictional losses and turbulent flow losses account for the real head being less than the ideal head generated in the impeller.

3.1.5 OTHER IMPELLER PARAMETERS

There are several factors affecting actual impeller performance by reducing the ideal compressor head. Some of these factors are functions of the impeller and casing design, their assembly, etc. These effects are hard to account for analytically. In addition, the geometry of the impeller blades, the number of blades, the clearance between the shroud and impeller, and the impeller axial exit width are some of the performance factors which can be readily found in technical publications related to centrifugal compressors.

An example of how difficult it is to quantitatively account for some factors affecting impeller performance is found by considering the type of impeller. Shepherd (1956) distinguished between open and shrouded impellers. An open impeller, according to Shepherd (1956), has a single shroud formed by the disc itself, while a shrouded impeller has a second bounding surface joining the front edges of the vanes (double- or fully shrouded). In the open impeller there is a flow loss due to fluid passing over the stationary casing, while in the shrouded impeller there is power loss due to the scrubbing action of the fluid and the rotating shroud (Shepherd, 1956).

3.2 COMPRESSOR INDUCING SECTION

The inducer represents the inlet section of the compressor preceding the impeller. The compressor inlet channel, the guide vanes, and the actual impeller inlet (hub and shroud design at the joint with the inlet channel) define the inducer which is shown in Figure 3.1. The inducer has an important role in controlling overall compressor performance. Van den Braembusse (1985) reports two basic purposes in designing the compressor inducer:

- extension of the compressor operating range between surging and choking and
- avoiding refrigerant inlet relative speeds that approach the speed of sound.

The parameters influencing these design aspects are:

- inlet blade tip angle,

- impeller shroud diameter,
- impeller hub diameter, and
- inlet guide vanes.

The inlet blade tip angle reportedly has a significant influence on the limiting choking flow which is addressed in Section 3.4.3.

The impeller shroud diameter should be considered because it determines the highest inlet velocity, and hence the fluid achieves the speed of sound at the compressor shroud diameter. An increase in the shroud diameter shifts the compressor choking flow, which is defined in Section 2.4, to the region of the lower flow rates. Also, increasing the shroud diameter reduces energy transfer in the impeller (Van den Braembusse, 1985).

In order to keep the inlet refrigerant Mach number low and to reduce friction losses generated in the impeller, the hub-to-shroud radius ratio should be considered. Usually, in order to avoid large shroud diameters, the hub diameter is kept as small as mechanical design allows. Van den Braembusse (1985) provided a formula for estimating the minimum hub radius. Also Van den Braembusse (1985) reported that for a smaller hub-to-shroud radius ratio, the minimal relative inlet Mach numbers occur for the smaller values of the hub diameter.

The impeller inducing section sometimes contains guide vanes which can throttle the flow if necessary. The fluid flow is throttled by guide vanes to control flow rate through the compressor and to extend the feasible compressor operating range, as described in Section 3.4.

The inlet guide vane settings may be incorporated in the model through the inlet velocity magnitudes, assuming that the guide vane gives direction to the absolute fluid velocity vector.

The compressor inlet velocity diagram is shown in Figure 3.5. The incoming refrigerant relative velocity, W_1, is assumed to have an identical angle to the inlet blade tip angle, β_1. Although there are deviations of fluid angles from the angles assumed, they are commonly neglected in compressor modeling (Turton, 1995).

It was already assumed that direction of the guide vanes coincide with the refrigerant absolute velocity vector direction. The inlet guide vane angle was measured from the completely closed position (zero degrees) to the fully open position of 90 degrees. Hence, looking at the inlet velocity triangle, it can be inferred that the inlet guide vane angle coincides with the incidence angle, α_1. In case of the inlet guide vanes being completely open ($\alpha_1 = 90^\circ$) there is no flow throttling; therefore, the absolute velocity is in radial direction, Figure 3.5.

From the inlet velocity diagram geometry in Figure 3.5, the following relations can be derived for the inlet absolute velocity and its tangential component, respectively:

$$V_1 = \frac{U_1 \tan\beta_1}{\sin\alpha_1 + \tan\beta_1 \cos\alpha_1} \tag{3-14}$$

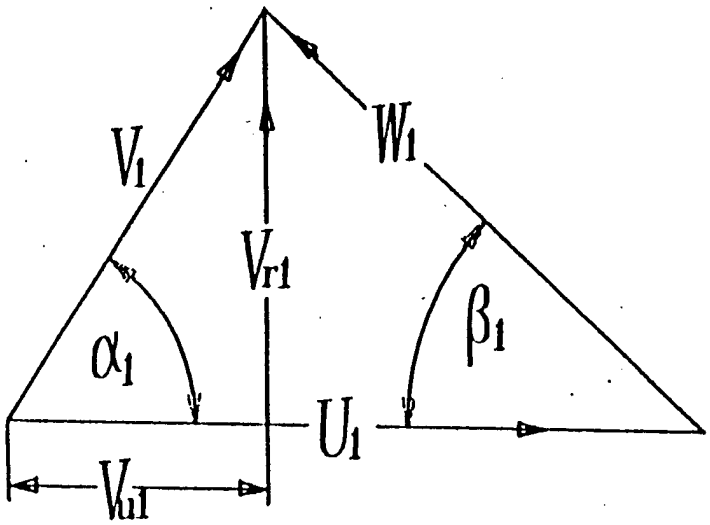

V — *Absolute velocity*
W — *Relative velocity*
V_r — *Radial vel. comp.*
V_u — *Tangential vel. comp.*
U — *Peripheral velocity*
α — *Incidence angle*
β — *Blade tip angle*

Figure 3.5. Impeller inlet velocity triangle.

$$V_{u1} = V_1 \cos\alpha_1 \tag{3-15}$$

3.3 DIFFUSER

The diffuser is a spiral volute in which the refrigerant dynamic head is converted into static head. Diffusers are classified as vaneless or vaned, and these two types of diffusers are modeled differently. Basically, vaned diffusers reduce losses occurring in diffusion of the non-uniform fluid flow entering the diffuser.

The flow leaving the impeller is highly non-uniform in the tangential and axial directions, as explained by Van den Braembusse (1985), which is due to boundary layer development along the diffuser walls, secondary flow, and flow separation. Turton (1995) states that in general the diffusers have strongly three-dimensional fluid flow and very uncertain flow regimes. Ayder et al. (1993) measured the actual flow field in a vaneless diffuser and proposed a computational method to solve for the flow field in a diffuser. Their measurements confirmed the highly three-dimensional flow field in a diffuser.

3.3.1 VANELESS DIFFUSERS

Emphasis in this literature review will be given to the vaneless type of diffuser because a vaneless diffuser is a part of the centrifugal compressor investigated in this project.

The simplest flow model through a diffuser is a one-dimensional model, which was outlined by Van den Braembusse (1985) after development by Stanitz (1952). The flow is assumed to be uniform in the axial and tangential directions, varying only in the radial direction.

Accounting for circumferential non-uniformity in the diffuser flow field, as postulated in the jet-wake model (Section 3.1.4), in conjunction with the one-dimensional model represents a two-dimensional flow model through a vaneless diffuser. The jet-wake theory of the flow leaving the impeller developed by Dean and Senoo (1960) can be applied for two-dimensional refrigerant flow through the diffuser. The model introduces circumferential distortion into the one-dimensional model flow. Johnston and Dean(1966) developed an incompressible flow diffuser model which accounts for two types of pressure losses in vaneless diffusers: friction and sudden expansion losses:

The friction losses are given by:

$$\xi_{fric} = 1 - C_P - \frac{1}{R^2}\left[(\gamma_2\lambda_2)^2 + \left(\frac{b_3}{b_2}\right)^2\right] \Big/ \left(\lambda_2^2 + 1\right) \tag{3-16}$$

where C_P represents the static pressure coefficient:

$$C_P = \frac{p_3 - p_2}{1/2\ \rho_2\ V_2^2} \tag{3-17}$$

The solution of the two-dimensional problem is given in terms of the dimensionless parameter, γ_2,

$$\gamma_2 = \frac{1}{1+\lambda_2^2\ \hat{A}(R-1)} \tag{3-18}$$

which was defined by Johnston and Dean (1966) as the angular momentum ratio. Explanations of the parameters in Equation 3-18 follow.

The inlet swirl parameter, λ_2, which appears in the expression for the calculation of the angular momentum ratio is defined by:

$$\lambda_2 = 2\pi\left(\frac{b_2}{r_2}\right)\frac{\psi_2}{\phi_2} \tag{3-19}$$

The impeller (diffuser inlet) head coefficient, ψ_2,

$$\psi_2 = \frac{p_2 - p_1}{1/2\rho_2 U_2^2} \tag{3-20}$$

takes into account the calculation of the inlet swirl coefficient. The head coefficient is adopted from Johnston and Dean (1966).

The diffuser width parameter, $\hat{A}$, which appears in Equation 3-18 is given in Equation 3-21. The friction factor, $\hat{c}_f$, in Equation 3-21 was estimated by Johnston and Dean (1966) to be between 0.005 and 0.01. The diffuser exit radius, r_3, and the diffuser exit axial width, b_3, are geometric parameters which are labeled on Figure 3.1:

$$\hat{A} = \frac{\hat{c}_f\ r_3}{b_3} \tag{3-21}$$

The geometric parameter R, which appears Equation. 3-18, is defined as the ratio of the diffuser exit radius, r_3, and the diffuser inlet (impeller outlet) radius, r_2.

The sudden expansion pressure losses, ξ_{mix}, are due to mixing of the jet and the wake flow regions. Johnston and Dean (1966) assumed that at the inlet of the diffuser there is a substantial pressure drop due to the blending of the two streams. The mixing is completed in the inlet section of the diffuser; hence, the flow becomes uniform shortly after entering the diffuser. The sudden expansion losses are estimated by:

$$\xi_{mix} = \frac{1}{1+\lambda_2^2}\left[\frac{(1-\varepsilon)-B}{(1-\varepsilon)}\right]^2 \tag{3-22}$$

The wake-to-jet flow area ratio, ε, is the same parameter appearing in the corrected slip factor expression, Equation 3-13, correlating the diffuser model with the impeller model. The geometric parameter B is the ratio of the diffuser inlet depth to the impeller flow passage depth.

The ideal diffuser performance may be defined as the ideal compressible diffusion from the diffuser inlet to the diffuser outlet state. This maximum pressure conversion is denoted as the ideal pressure at state 3, $p_{3,id}$.

The diffuser efficiency, η_D, can be defined as the ratio of the actual pressure conversion to the ideal pressure conversion in the particular diffuser:

$$\eta_D = \frac{p_3 - p_2}{p_{3,id} - p_2} \tag{3-23}$$

The pressure rise in the diffuser is balanced with the pressure losses; thus:

$$\eta_D + \xi_{fric} + \xi_{mix} = 1 \tag{3-24}$$

The two-dimensional diffuser model presented here combined with the variable slip factor was found to be suitable to implement into a compressor model. The compressor model, called the refined model, is described in Section 5.4.

Van den Braembusse (1985) reports that axial non-uniformity of the refrigerant flow in the diffuser is due to the skewness of the absolute refrigerant flow. This axial distortion, which can cause back flow in the diffuser and hence diffuser stall, is not accounted for in the presented two-dimensional diffuser model.

A three-dimensional model of the flow through diffusers was postulated by Senoo et al. (1977). They based the model on the Jansen (1964) work, in which he outlined the behavior of a realistic flow through a vaneless diffuser. The Senoo et al. (1977) model is based on asymmetric flow between the diffuser walls. The authors solved the Navier-Stokes equations and reported good agreement with their experimental data as well as some data from the literature. This type of model is too complicated to be implemented in this project, requiring a development of the detailed fluid flow field solution.

3.3.2 VANED DIFFUSERS

Van den Braembusse (1985) outlined the flow behavior in vaned diffusers and classified them as curved vane or channel diffusers. In general the main advantage of the vaned diffusers is an extension of the operating range between surge and choke as reported by Senoo et al. (1983). Vaned diffusers have lower losses due to a less sudden diffusion of the fluid leaving the impeller.

Detailed measurements of the fluid flow were conducted on a several vaned diffusers by Stein and Rutenberg (1988). They proposed a computational procedure to model the flow field in a vaned diffuser. Further consideration of vaned diffusers is beyond the scope of the present study.

3.4 OVERALL COMPRESSOR PERFORMANCE

Compressor performance is usually given on a compressor performance map. A typical, hypothetical map is drawn in Figure 3.6.

The compressor performance is described in terms of head and flow rate by coefficients which have been widely accepted in industry. These important coefficients were recognized by Sheets (1950), who defined them as the head coefficient and the flow coefficient. They are given, respectively, by:

$$\Omega = g w_P / a_1^2 \tag{3-25}$$

where w_P is compressor polytropic work; g is gravitational constant; and a_1 is the speed of sound of the refrigerant at the compressor inlet state; and

$$\Theta = Q_1 / a_1 D_1^2 \tag{3-26}$$

where Q_1 is volumetric flow rate at the impeller inlet, and D_1 is the impeller inlet diameter.

It should be noted that these coefficients are different from the head and the flow coefficients defined from the fluid velocity triangles in Section 3.1.3. The flow coefficient, Θ (Equation 3-26), is based only on the compressor inlet geometry and the refrigerant flow rate. By contrast, the flow coefficient, ϕ (Equation 3-5), is defined at the compressor mid state (at the impeller exit) as the velocity ratio. Also apparent is the difference between the head coefficients, Ω and μ, given respectively in Equations 3-25 and 3-7. The head and flow coefficients used to construct the performance map are utilized to analyze compressor performance by treating it as a single overall control volume. On the other hand, the head and flow coefficients defined from the velocity triangles are used to analyze compressor performance in more depth by defining separate control volumes for the impeller and diffuser.

Compressor performance lines are plotted for different compressor Mach numbers (speeds) in Figure 3.6. The compressor Mach number is commonly defined as the ratio of the impeller exit linear velocity to the speed of sound of the refrigerant entering the impeller:

$$M = \frac{U_2}{a_1} \tag{3-27}$$

Lines of constant efficiency, η, are also plotted on Figure 3.6. It must be recognized that actual compressor performance is limited by phenomena known as surge and choke, as indicated on Figure 3.6. The typical performance chart indicates that the usable operating range is restricted at the higher compressor Mach numbers.

Centrifugal compressors usually have guide vanes at the compressor inlet to control overall compressor performance. The guide vanes control the flow rate, influence the compressor operating range, and their setting introduces another variable into an already complex fluid machine. The compressor performance at the same speed differs for different settings of the vane angles. Common practice is to obtain compressor performance maps for constant rotational speed and different inlet vane angle positions (ASHRAE, 1992).

The system behavior phenomena of surge, stall, and choking are discussed in the following sections.

3.4.1 SURGE

Referring again to Figure 3.6, surge occurs at the lower flow rates, causing unstable compressor operation. As the flow rate is decreased from the maximum head point along the positively sloped operating curves, lower pressures are produced by the machine. Instantaneously, back pressure is higher than the delivered pressure, and flow ceases, since delivery cannot be maintained against a reversed pressure gradient. The compressor operating point would move to the characteristic curve point corresponding to zero flow. Then, the fluid in the delivery system has cleared, the back pressure has been lowered, and the machine can start delivery.

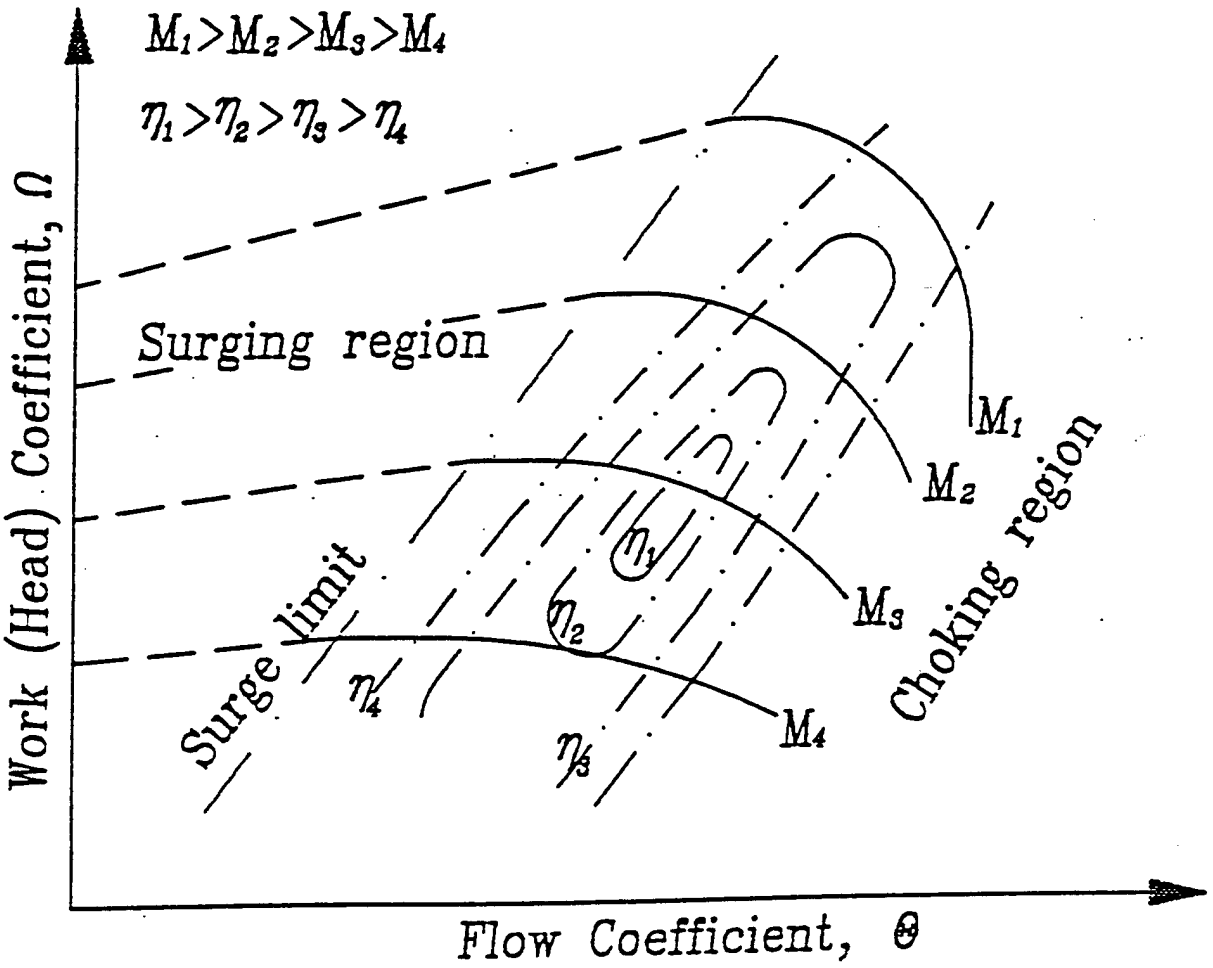

Figure 3.6. Typical compressor performance map.

Surging may be eliminated by designing compressors with totally negatively sloped ideal characteristic curves (Shepherd, 1956). However this implies using a very small angle for backward curved vanes, which reduces the energy transfer in the impeller.

Surge occurs when the slope of the overall pressure rise exceeds a certain positive value (Van den Braembusse, 1985), and the surge limiting value is due to compressor geometry and throttling characteristics. For instance, a throttled flow at the impeller inlet tends to shift the surging limit point to the left, increasing the available operating range for the given operating speed. Most commonly, the surge point coincides with the point of maximum overall pressure rise.

Surging is characterized by noise and vibration, and it can be easily distinguished by oscillatory loading and unloading of the compressor driver. The compressor impeller speeds up and slows down in such an operating mode (ASHRAE, 1992).

3.4.2 STALL

Slightly to the left of the surge envelope is the compressor operating region in which so-called compressor stall may occur. It is sometimes called incipient surge (ASHRAE, 1992). Compressor stall is a local instability in the diffuser depending on local flow conditions, and it is distinguished from the compressor surge. Van den Braembusse (1985) defined the stall phenomena as zones of low energy fluid which rotate in the diffuser at subsychronous speed. Jansen (1965) conducted a detailed analysis of the rotating stall phenomenon.

Rotating stall as a local compressor instability generates tremendous noise, but it does not adversely affect the overall compressor performance as much as compressor surge. Rotating stall may generate forces which can induce vibration of the entire compressor.

3.4.3 CHOKED FLOW

Choked flow occurs due to fluid compressibility as the refrigerant velocity approaches the sonic velocity. When choking occurs, the flow rate stays fixed regardless of the pressure ratio, and the compressor characteristic almost becomes vertical. Choked flow is sometimes referred to as stonewalling (ASHRAE, 1992).

The limiting mass flow rate can be increased (Van den Braembusse, 1985) by increasing the impeller shroud radius, which increases the compressor Mach number, and hence shifts the compressor operating curve to the left. However, it was already observed that operation at higher Mach numbers diminishes the compressor operating ranges between the surging and choking limits. Rodgers (1962) suggested that inlet blade tip angle has a

considerable effect on choking. Decreasing inlet blade tip angle shifts the value of the choking flow to the left on a compressor performance map.

3.4.4. SPECIFIC SPEED

Specific speed, N_S, given in Equation 3-28 is a significant compressor parameter. Many attempts have been made to correlate the specific speed with compressor performance. However, compressor performance depends on more parameters than used in the definition of specific speed. The specific speed, which has been derived from dimensional analysis (Shepherd, 1956), can be related only approximately to compressor performance;

$$N_S = \frac{\omega Q^{0.5}}{H^{0.75}} \tag{3-28}$$

Shepherd (1956) reported that similar turbomachines have peak overall efficiencies in a very limited range of specific speeds. Van den Braembusse (1985) gave a curve relating impeller performance deterioration as a function of the specific speed. He also suggested that the specific speed should be investigated only relative to impeller performance. Rodgers (1980) investigated the relation of specific speed and impeller efficiency in detail. Impellers with backward curved vanes have optimum performance at higher values of specific speed than impellers with radial blades (Van den Braembusse, 1985). It was even reported in ASHRAE (1992) that the best centrifugal compressor efficiencies are attainable at specific speeds between 600 and 850.

3.4.5 COMPRESSOR REYNOLDS NUMBER

Wiesner (1979) conducted a thorough study of the effects of compressor Reynolds number on centrifugal compressor performance. Wiesner (1979) adopted the ASME definition of the compressor Reynolds number, which takes impeller exit tip speed, impeller exit axial width, and refrigerant properties at the compressor inlet as the characteristic values. Wiesner (1979) reported that there are significant changes in compressor performance, especially in the range of low Reynolds numbers. He provided correction equations for all compressor performance parameters at operating conditions different from the design condition.

The effects of the Reynolds number are more noticeable for multistage compressor operation. Slightly different correction equations for the performance parameters due to effects of the Reynolds number were developed by Casey (1985), who suggested to account for the compressor friction losses with a simple empirical

relation. An improvement to the correction expressions for the effects of the compressor Reynolds number given by Casey (1985) was developed by Straub et al. (1987). A standardized test procedure for investigating Reynolds number effects was also proposed (Straub et al., 1987).

3.5 SUMMARY

Most of the phenomena affecting compressor performance are addressed in this chapter. It can be inferred that compressor performance is complex and can only be exactly depicted by solving three-dimensional flow fields within the impeller and the diffuser. However, the emphasis in this project is the evaluation of compressor performance from the standpoint of treating the compressor as a control volume.

It must be emphasized that the compressor models are built on separate impeller and diffuser models, since they represent the compressor components in which energy conversion occurs. Also, the standard overall compressor performance can be described by the experimentally developed performance map which is also utilized in model development. In summary, the following compressor characteristics might be useful in the further model development:

- In the impeller energy is transferred to the refrigerant, and in the ideal case the amount is given by the Euler equation. Fluid slip at the impeller exit reduces the Euler head. Several equations were provided to estimate the quantitative measure of the fluid slip, the slip factor.
- The compressor in the Navy chiller has a vaneless diffuser. The vaneless diffuser pressure losses were estimated by the solution of a two-dimensional fluid flow model. Vaned diffusers are also widely used in centrifugal compressors. They have the advantage over vaneless diffusers in broadening the stable compressor operating range and reducing the fluid expansion losses at the diffuser inlet. However, this type of diffuser has greater friction losses than the vaneless diffuser
- The guide vanes are used to control compressor operation by throttling the refrigerant flow into the compressor. The inlet guide vane setting was related to the compressor inlet velocity diagram.
- The standard compressor performance map is a powerful tool in depicting compressor operation because it defines the stable compressor operating range. All phenomena occurring in compressor operation are addressed and important parameters are defined.

CHAPTER 4

CENTRIFUGAL COMPRESSOR: DESCRIPTION, TEST FACILITY, DATA, AND PERFORMANCE CHARACTERISTICS

4.1. CENTRIFUGAL COMPRESSOR CHILLER DESCRIPTION

The centrifugal compressor analyzed in this project is part of a 125-ton air conditioning chiller. The chiller installation was designed to operate with refrigerant CFC-114. The alternative refrigerant HFC-236ea was investigated in the chiller as an eventual drop-in replacement. Figure 4.1 shows the basic schematic of the chiller plant.

The chiller capacity is controlled to maintain a desired chilled water temperature and to prevent compressor motor overloading. Capacity control is achieved by adjusting the compressor inlet guide vanes and by a compressor by-pass loop.

Fine control of chiller capacity control is achieved with inlet guide vane angle adjustments. The inlet guide vanes are moved by a pneumatic operator which automatically responds to the chilled water thermostat. The guide vanes induce refrigerant prerotation, and therefore throttle the refrigerant flow, which has a negative effect on the compressor performance. Although inlet guide vanes reduce compressor efficiency by throttling effects, they extend the stable compressor operating range.

Rough chiller capacity control is accomplished by the compressor by-pass loop. The compressor by-pass operating mode is activated by opening the by-pass valve which allows a certain fraction of refrigerant flow to be recirculated through the compressor, therefore reducing the refrigerant mass flow rate in the rest of the chiller. The by-passed refrigerant, which is at the state corresponding to the compressor exit state, is mixed with the refrigerant leaving the evaporator, and then the mixture is brought to the compressor. This operating mode is utilized for extreme off-design chiller operating conditions.

The centrifugal compressor is an open type, single stage with a vaneless diffuser. The compressor shaft speed can be varied through an adjustable gear box. A specially designed oil system lubricates the compressor bearings. A part of the oil system is a water-cooled oil cooler, which is indicated in Figure 4.1 as an internal part of the compressor assembly.

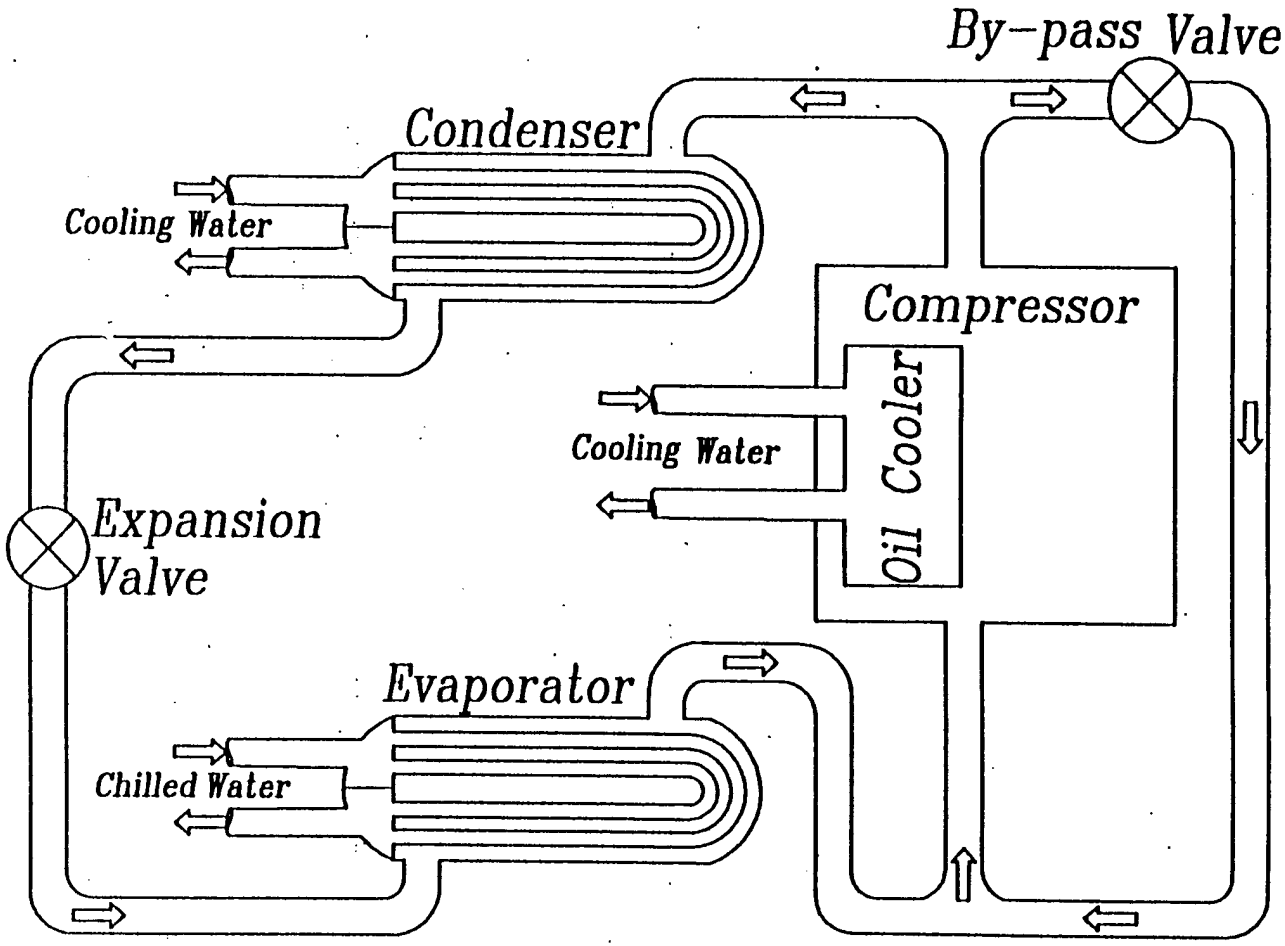

Figure 4.1. Centrifugal compressor chiller plant diagram.

The evaporator and condenser chiller heat exchangers are shell and tube type with two passes on the water side. Two-phase refrigerant flows over copper finned-tube bundles inside these heat exchangers.

4.2. CENTRIFUGAL CHILLER EXPERIMENTAL FACILITY

The experimental chiller installation was set up in the Naval Surface Warfare Research Center in Annapolis, Maryland. A data acquisition system was used to monitor measuring devices mounted throughout the experimental chiller plant. A schematic of the instrumentation is given in Figure 4.2.

The following measuring devices were installed in the chiller test facility:

- Thermocouples were located at the inlets and the exits of the compressor, evaporator, and condenser on the refrigerant side. Also, all the inlet/outlet water-side heat exchanger locations were instrumented with temperature gauges.
- Pressure transducers were installed on the refrigerant side of the chiller at the inlets and outlets of the compressor, evaporator and the condenser.
- Compressor shaft speed was recorded by a tachometer.
- A torquemeter mounted on the compressor shaft was set up to measure the compressor shaft torque. Using the measured torque and speed, the compressor shaft power could be determined.
- A watt transducer was used to record the total power consumption of the chiller plant. Measurements of the compressor total power consumption and the energy delivered to the compressor shaft allow an estimate of the compressor motor efficiency.
- Flowmeters were installed in each heat exchanger's water loop to record the respective water volumetric flow rates.

The position of the inlet guide vanes and the percentage of by-pass valve opening were also recorded during data taking.

The refrigerant mass flow rate, which was not measured directly on the Navy chiller installation, was calculated as the average value from the evaporator and the compressor energy balances. Since the refrigerant flow rate was not measured, the flow rate through the compressor in the by-pass operation mode is larger than the flow rate reported as the average value based on the heat exchanger energy balances. Thus, the experimental data points with the by-pass valve open have to be regarded cautiously in development of a compressor model.

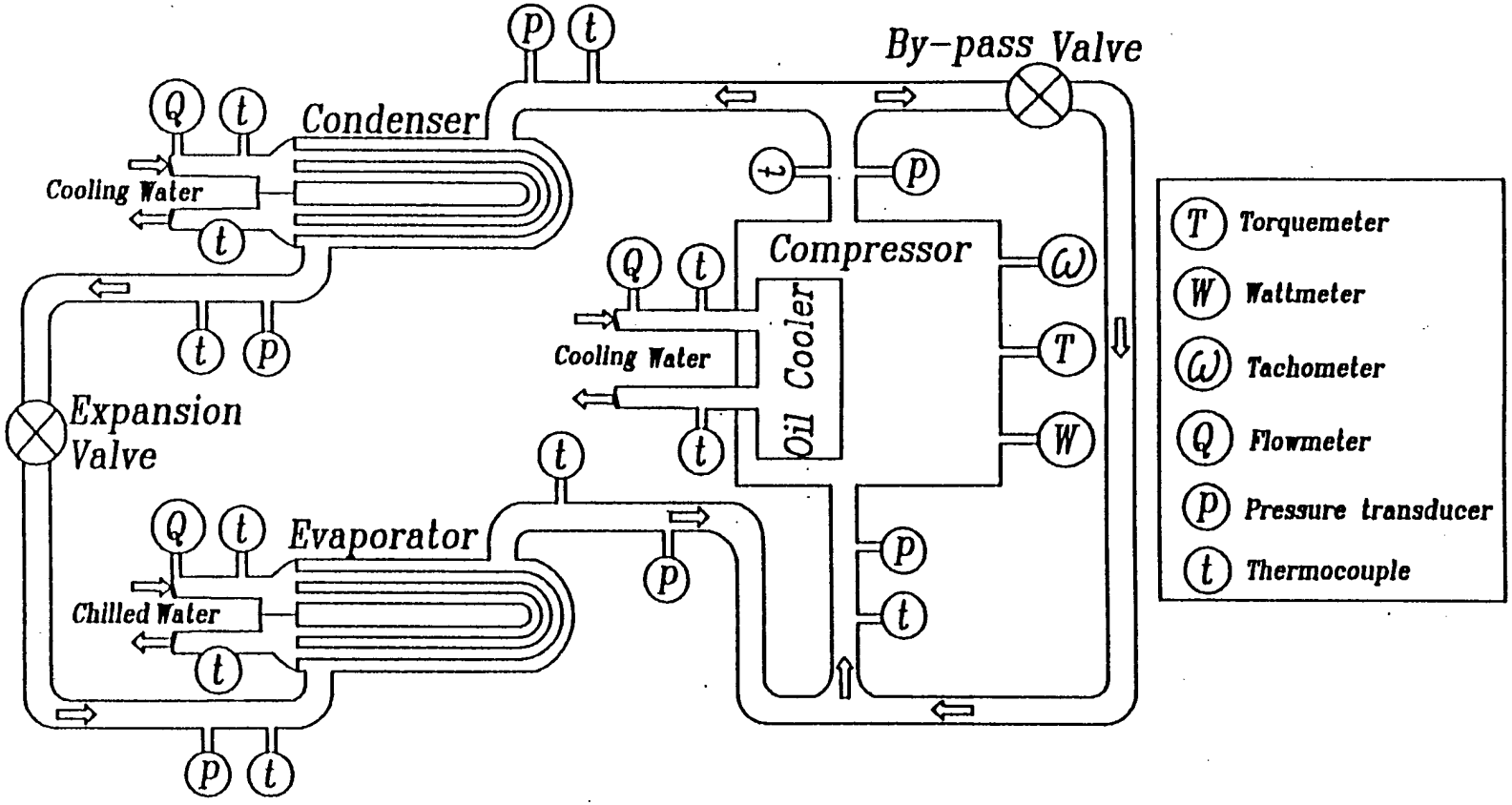

Figure 4.2. Chiller plant instrumentation scheme.

Table 4.1. Operating range for experimental values on the chiller plant.

Some Chiller Installation Measured Values	Unit *	HFC-236ea		CFC-114	
		Max	Min	Max	Min
Compressor Mach Number		1.71	1.54	1.72	1.55
Suction Pressure	psi	17.0	11.1	14.5	10.7
Discharge Pressure	psi	55.4	39.8	47.2	24.5
Compression Ratio		4.52	2.68	3.46	1.83
Suction Temperature	F	62	36	58	38
Discharge Temperature	F	128	99	133	99
Condenser Inlet Temperature	F	89	60	88	65
Oil Cooler Water Inlet Temperature	F	68	60	No data	No data
Inlet Guide Vane Position	degrees open	88	20	88	8
Percentage Of Design Capacity	percent	138	30	102	19
Compressor Shaft Power	hp	194	119	151	47.5
Mass Flow Rate	lbm/min	637	150	598	98.9

* SI Unit system was not used in this project since the Naval Surface Warfare Research Center conducted the experimental points having measured chiller performance characteristics in English units: therefore, it was anticipated that analysis of the data would be more useful (understandable) if performed in English Units. However, the conversion factors to corresponding SI units of every English unit used in this project are given in Appendix B.

Ranges of experimental operating conditions for both refrigerants are shown in Table 4.1. The evaporator outlet temperature was set for the majority of operating conditions to be 44 degrees Fahrenheit, as a very common design chilled water temperature for air-conditioning applications. The compressor shaft speed was varied to achieve compressor Mach numbers between 1.5 and 1.7, and the chiller capacity was varied from 140 percent to 20 percent of the compressor design point capacity. The experimental compressor operating range presented in Table 4.1 is comparable for both refrigerants, indicating that both data sets were generated by subjecting the compressor to similar operating conditions. The only noticeable difference between these experimental data sets might be the range of chiller capacity.

The data were taken over a broad range of chiller (compressor) operating points; therefore the data appear to be a good base for the further analysis.

4.3. CENTRIFUGAL COMPRESSOR EXPERIMENTAL DATA

The Naval Surface Warfare Research Center initially supplied HFC-236ea data for 97 operating points which formed the basis for the compressor model. Fourteen CFC-114 experimental data points were obtained in the course of the project.

The HFC-236ea data points were divided into two groups. The first group of data points were designated to be used as the basis for compressor model development. The chiller by-pass mode operating points were excluded from this group of data points because the mass flow rate through the compressor was unknown. It was observed that several HFC-236ea data points at the compressor inlet were in the two-phase region. This was determined on the basis of the reported temperatures and pressures at the compressor inlet by using the refrigerant property program REFPROP 4.01 (1994). The pressures and temperatures were not thermodynamically consistent. Since two-phase conditions are inadequately described by pressure and temperature alone, the suspicious data points were assumed to be saturated vapors at the reported compressor inlet pressures. The data points which are in the by-pass compressor operating mode and the data points for which measured refrigerant at the compressor inlet state appeared to be in the two-phase region are denoted as additional HFC-236ea data points. These data points were regarded with less significance in further analysis since some systematic errors might have been introduced.

There were just 14 CFC-114 data points provided by the Naval Surface Warfare Research Center, of which six were in the by-pass mode. This rather small number of operating data points was considered to be insufficient for development of a compressor model; hence, these data points were used to check the versatility of HFC-236ea model for this different refrigerant.

These three experimental data susbsets are represented separately throughout this report using the nomenclature shown in Table 4.2. This nomenclature is used consistently whenever the effects of different data subsets are either analyzed or compared.

Table 4.2. Experimental Data Points Subset Information

Data Points Subset	Total number of data points	By-pass mode number of points	Data subset labels in figures
HFC-236ea base data set	80	0	*
Additional HFC-236ea data points	17	6	o
CFC-114 data points	14	6	+

The readings of the watt transducer were not recorded during the HFC-236ea data taking. Therefore, modeling of the total compressor power consumption was not possible. Also, the amount of by-pass valve opening was not recorded for the CFC-114 data points limiting eventual development of a by-pass mode model.

4.4. INITIAL EXPERIMENTAL DATA ANALYSIS

Data from the experimental chiller plant were investigated to observe the overall chiller behavior under different operating conditions. In this section, a preliminary analysis of data is performed to understand chiller plant behavior and to investigate the necessity of compressor model development.

The preliminary analysis of the experimental data revealed that the measured shaft power can be successfully related to the amount of energy transferred to the refrigerant by a linear function (see Figure 4.3). The by-pass operating mode data points were excluded because the reported mass flow rate was always less than the actual mass flow rate through the compressor. The relation shows that losses occurring in the energy transfer from the compressor shaft to the refrigerant are constant, i.e., invariant to the compressor operating conditions. Quantitatively, these losses are approximately 330 Btu/min (7.8 hp), and the largest portion is due to the rate of energy rejection in the oil cooler. Studying the data points, it was found that this heat transfer rate was constant value at roughly 240 Btu/min. Therefore, the remaining losses, which consist of shaft friction, heat flow out of the compressor control volume other than the heat rejected in the oil cooler, and losses due to imperfect flow through the compressor, amount to approximately 90 Btu/min (2.1 hp). When this value is compared with the values of the compressor shaft power in Table 4.1., it can be concluded that the compressor performs quite efficiently from the standpoint of energy transfer from the compressor shaft to the refrigerant.

The best-fit linear equation obtained by fitting the HFC-236ea experimental data is,

$$\text{Shaft Power}[\text{Btu / min}] = 327.78 + 1.1547 * [\dot{m}(h_3 - h_1)] \qquad (4\text{-}1)$$

which has a mean standard deviation of the fit of 7.7 Btu/min. This equation can not be applied for the CFC-114 data points since these points on Figure 4.3 are slightly shifted to the right, indicating a necessity for a different curve-fitted line. Also, it can be inferred that the chiller performance is better with CFC-114 than with HFC-236ea refrigerant, since the vertical axis intercept of the line fitted through the CFC-114 data would be smaller than the similar intercept of the HFC-236ea line, indicating less energy loss from the shaft. Therefore, based on the data points in Figure 4.3, the compressor appears to perform better with CFC-114 refrigerant in terms of efficiency. This may also indicate that a model based on the HFC-236ea base data set may not be applicable to the CFC-114 refrigerant.

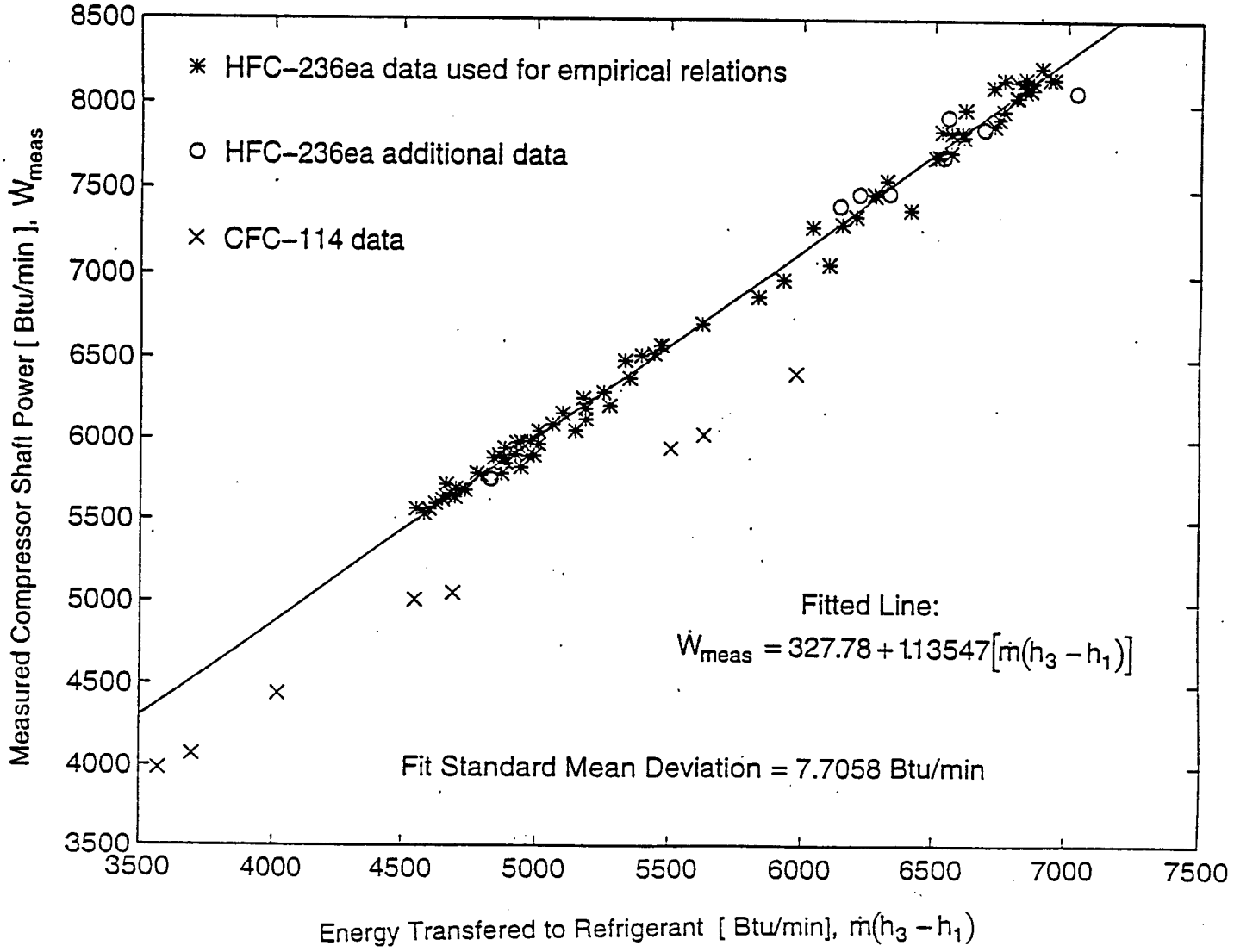

Figure 4.3. Compressor shaft power as a function of the energy delivered to refrigerant.

Refrigerant throttling at the compressor inlet cannot be directly modeled as a function of refrigerant mass flow rate. All the data points for which the by-pass valve was closed are plotted in Figure 4.4 and show that the refrigerant flow rate has considerable scatter when plotted as a function of the inlet guide vane angle. Therefore, the inlet guide vane throttling of the refrigerant flow cannot be simply accounted for by the changes in mass flow rate, but rather a more complex analytical model is required. Apparently, the refrigerant induced prerotation not only affects mass flow rate, but also influences overall compressor performance.

The compressor pressure ratio plotted versus the refrigerant flow rate in Figure 4.5 verifies that there is no simple relation between these two parameters. The pressure ratio is not an unique function of the flow rate, as a generic theoretical compressor performance map might postulate (pressure rise versus flow rate). This is an indicator that the compressor performance cannot be depicted just by the parameters plotted in Figure 4.5, but a more complex model is necessary

4.5. COMPRESSOR PERFORMANCE MAP

The compressor manufacturer provided a performance map for the compressor operating with a refrigerant other than the two refrigerants investigated in this study. The possibility to eventually adjust the given performance map to the refrigerants investigated in order to predict the compressor performance seemed appealing.

A generic centrifugal compressor performance map was described in Section 3.4. The map is constructed by plotting the work versus the flow coefficient. The coefficients were defined in Equations 3-25 and 3-26 respectively. The performance map supplied by the manufacturer was constructed in the same way as the generic compressor performance map.

The entire HFC-236ea base data set was divided into four data subsets corresponding to different compressor Mach numbers (defined by Equation 3-27 in Section 3.4.). The sorted data were plotted in Figure 4.6 following the idea of the generic compressor performance map. The data points in Figure 4.6 appear to be quite scattered, and it is not possible to identify compressor performance lines for particular compressor Mach numbers. In general, the work and the flow coefficient are related in a similar fashion as in the generic performance map. That is, there is a positive gradient for low values of the flow coefficient until a maximum is reached after which the gradient becomes generally negative. This behavior is most clearly shown for the data points corresponding to a Mach number of about 1.6, which vaguely resembles a compressor performance line for a particular compressor Mach number.

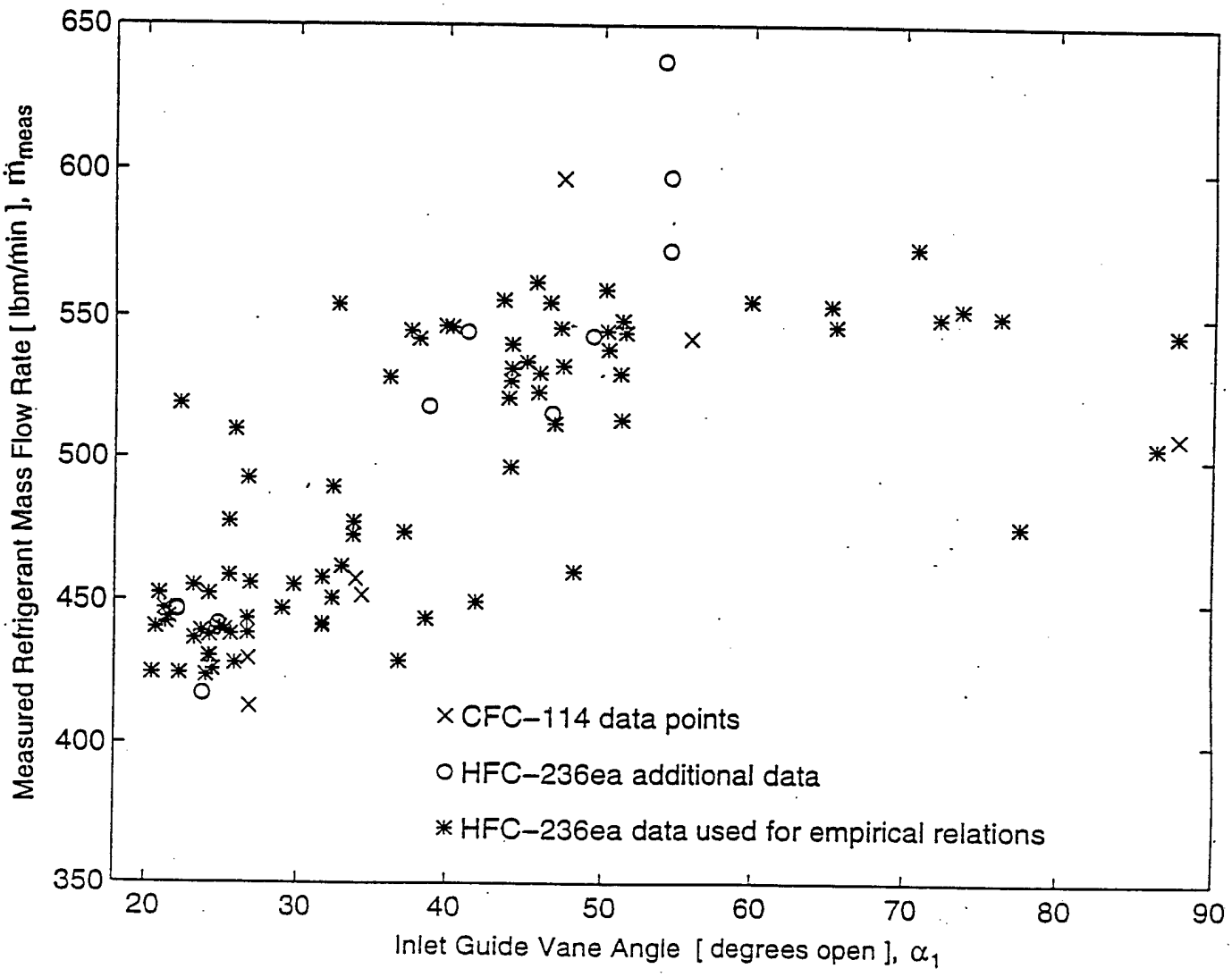

Figure 4.4. Dependence of refrigerant flow rate on inlet guide vane angle position.

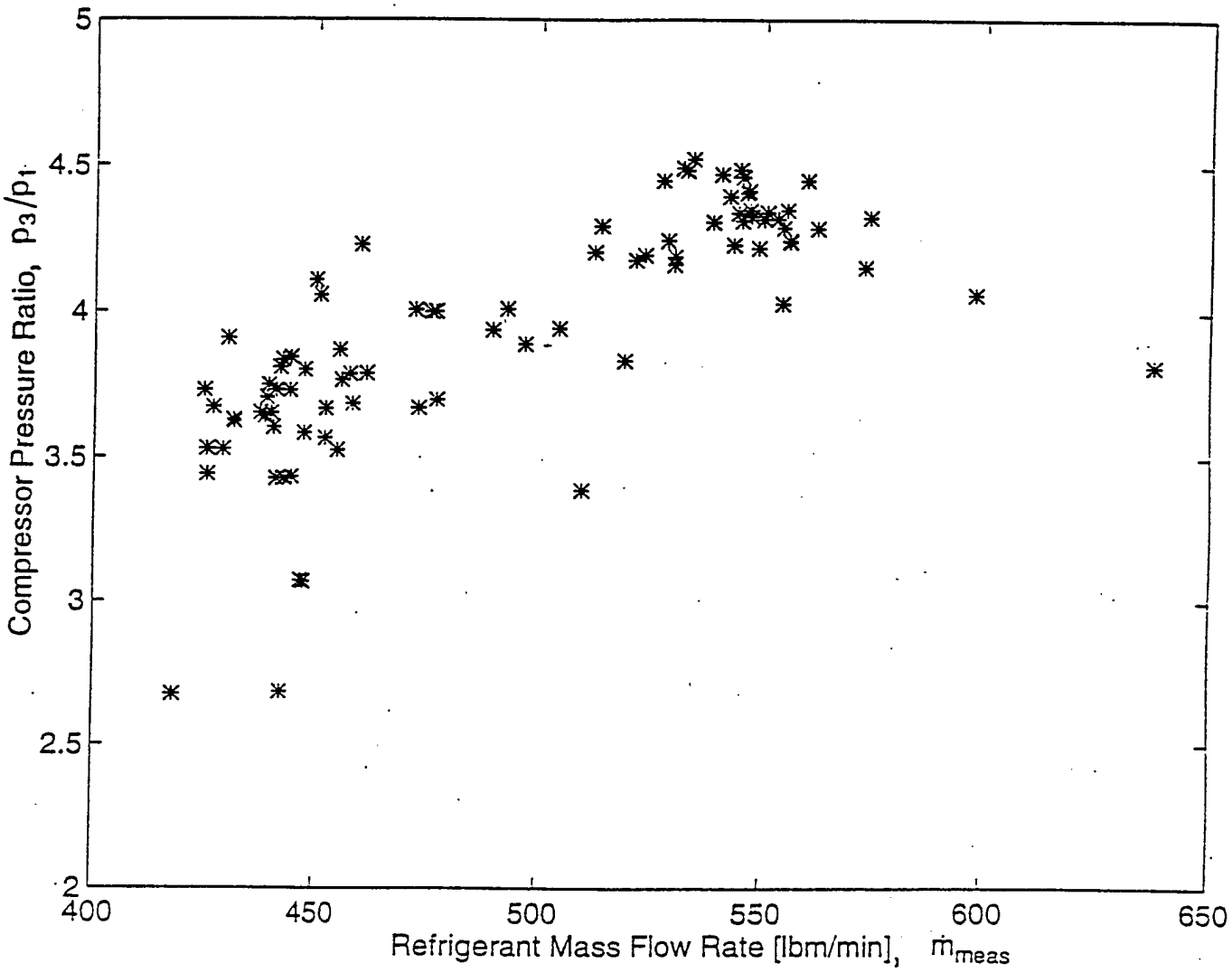

Figure 4.5. Dependence of refrigerant flow rate on pressure ratio for HFC-236ea data points.

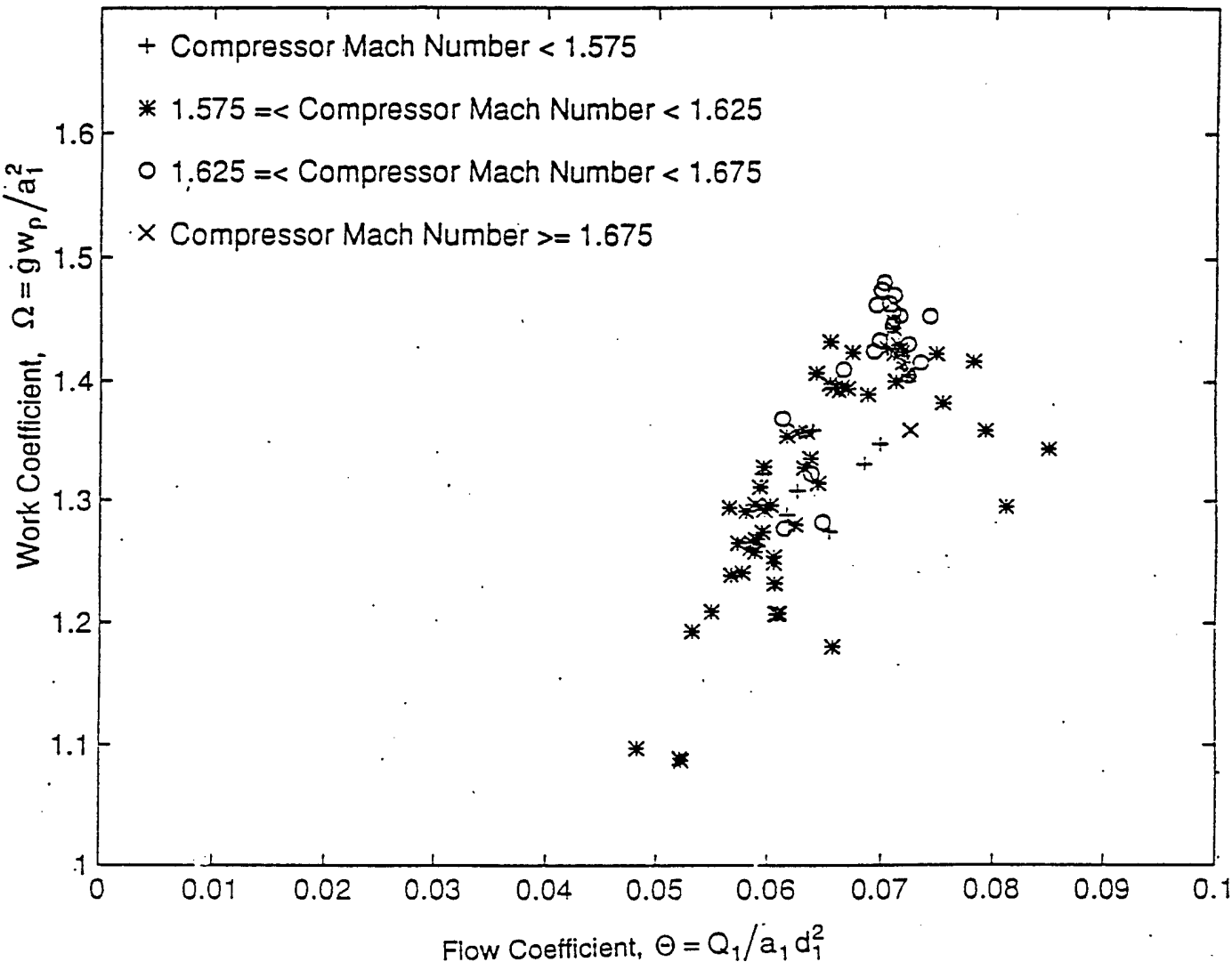

Figure 4.6. Compressor performance map for different compressor Mach numbers.

The data set corresponding to the compressor Mach number of 1.6 was compared with the performance line for the same Mach number reproduced from the manufacturer's compressor map. As can be seen on Figure 4.7, the HFC-236ea data are scattered, but the general trend resembles the superimposed performance line. Also, the HFC-236ea data points indicate a steeper gradient than the superimposed performance line. No satisfactory relation was found between the given performance line and the HFC-236ea data, so it was concluded that different inlet guide vane angle settings must be causing the apparent data scatter. It is significant to notice that the manufacturer provided different surge points along the performance line in Figure 4.7, corresponding to different inlet guide vane settings. This verifies that the compressor operating range can be extended with induced prerotation of the refrigerant.

The HFC-236ea data points characterized by the compressor Mach number of 1.6 were further divided into four groups corresponding to different inlet guide vane (IGV) angle settings. The points on Figure 4.8 appear to be quite clearly grouped around different IGV angle values. For the lowest IGV setting, the data points are significantly dispersed, appearing not to correspond to a single performance line. The IGV setting corresponding to approximately 50 degrees open shows that those data points can be well modeled with a single continuous (performance) line. Other IGV settings did not have enough experimental data points to be conclusive about the eventual dependence among the investigated parameters.

In conclusion, the use of the compressor performance map was found to be unfeasible since the data did not behave completely in the customary fashion. The data appeared to be quite scattered, not always exhibiting definite trends on the figures presented in this section. In addition, the performance map for the given refrigerant differs from the HFC-236ea experimental data, and no relations were found between the performance map and the experimental data. Because of the reasons mentioned above, the idea of modeling the compressor using a performance map was abandoned in this project.

Although a compressor performance map bears important information about the particular compressor operating characteristics (surge line and choked flow for a particular compressor Mach number), the data presented here did not follow the manufacturer's performance map well. One inference is the significant dependence on the particular refrigerant. In addition, the accuracy of the data points and propagation of measurement error could not be determined. A feasible adjustment for the manufacturer performance map which would correlate the map and the measured data points was not found. Therefore it was anticipated that some other form of more detailed compressor modeling was needed in order to analyze the experimental data.

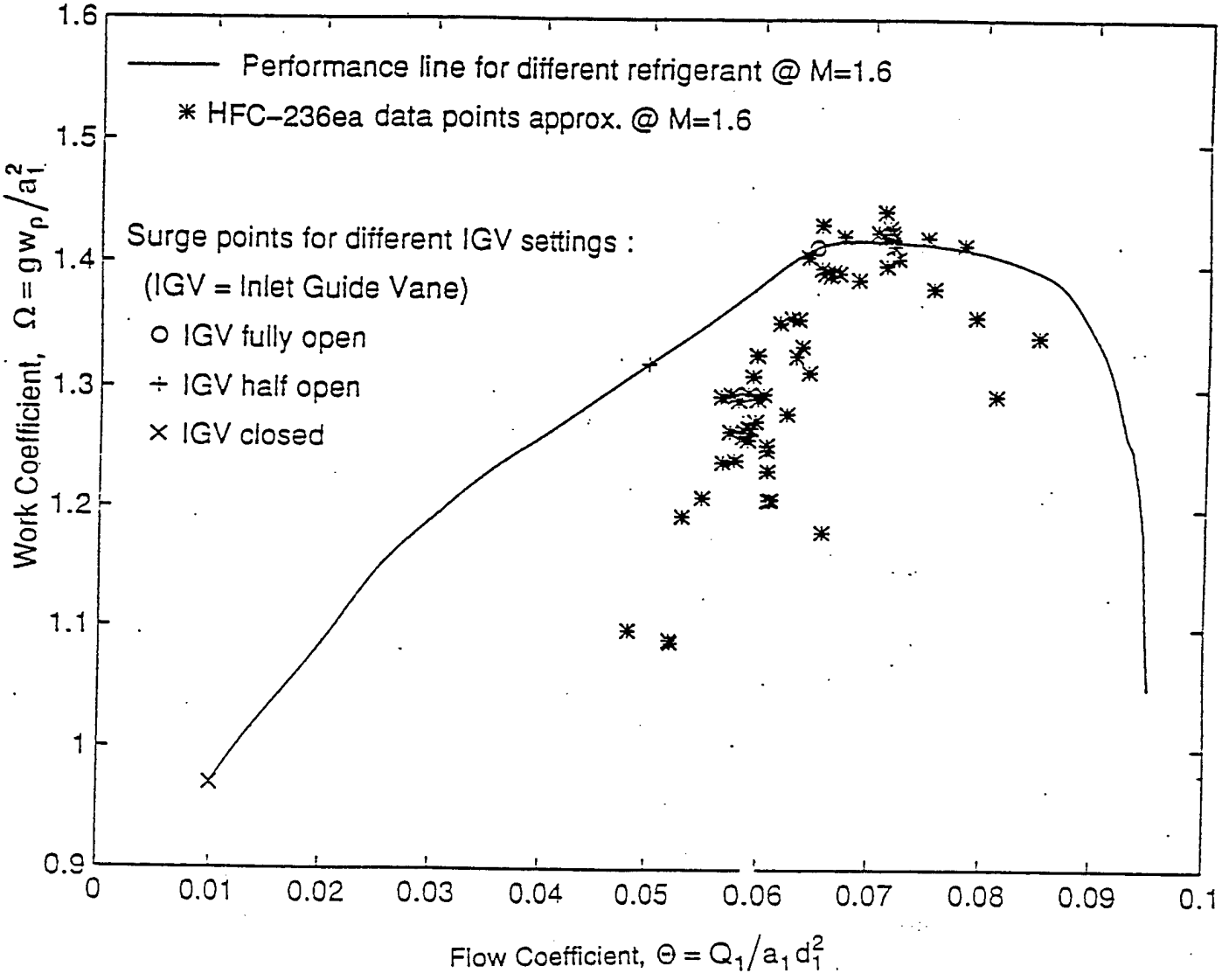

Figure 4.7. Comparison between manufacturer performance map and HFC-236ea experimental data at compressor Mach number of 1.6.

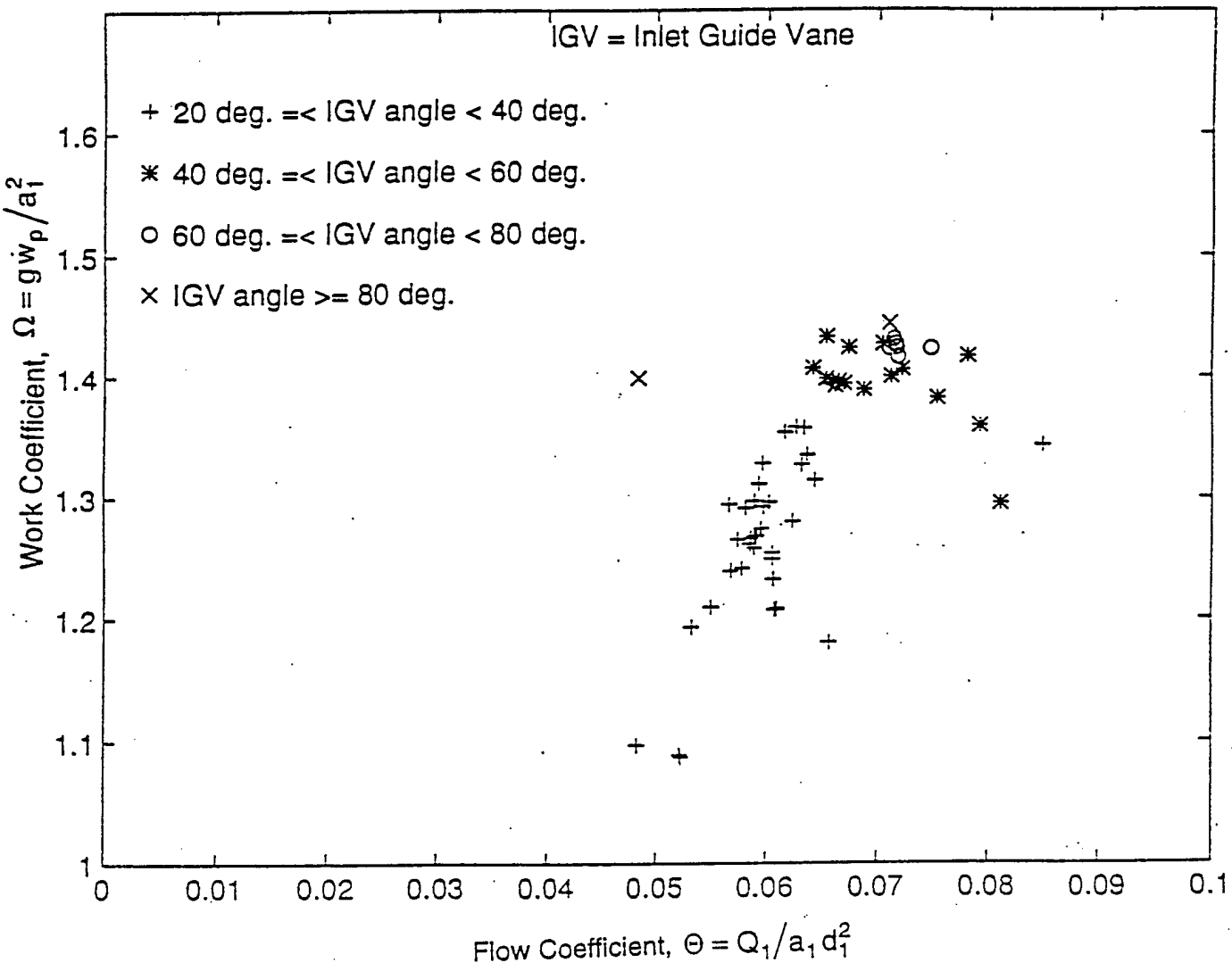

Figure 4.8.: Compressor performance map for different inlet guide vane settings at compressor Mach number of 1.6.

CHAPTER 5

COMPRESSOR MODELING

5.1 INTRODUCTION

A centrifugal compressor is a complex dynamic machine to depict analytically. There are a number of parameters affecting compressor performance as summarized in Chapter 3. Based on the literature survey in Chapter 3, the following goals were set for the compressor model development:

- the impeller and the diffuser should be modeled separately,
- the refrigerant state between these two components should be estimated,
- the performance of each compressor component must be characterized by the refrigerant inlet and exit states,
- experimental data might be used to develop additional relations for the model, if necessary, and
- the inlet guide vane setting should be incorporated in the model.

As stated above, the objective of this project was to develop a simple compressor model which would characterize accurately compressor performance. By incorporating the goals listed in the previous paragraph, such a model would be an integral part of the entire refrigeration system model which describes the Navy chiller in this study. The compressor represents the most complex part in any refrigeration system, whereas other components are readily simulated more easily with acceptable accuracy. Hence, a simple and accurate compressor model would be quite valuable in the refrigeration system simulation.

If the developed model indicates a reasonable predictive accuracy, it can be used for limited design analysis. This analysis is limited because such a complex turbomachine is approximated with a simple model which does not encompass all of the parameters relevant to the compressor performance. Also, empirical relations developed using particular data points are likely to be of limited accuracy at operating conditions far from where they were developed. Compressor geometric parameters introduced in the model may be varied in order to investigate their influence on the compressor model behavior, therefore suggesting how compressor behavior would be affected by design modifications.

Keeping in mind that the compressor model would be incorporated in the refrigeration system simulation, a standard compressor model format was adopted which was discussed in detail in Chapter 1. A good compressor model of the desired form was extracted from the literature, and two new models were developed.

5.2. APPLICATION OF EXISTING MODEL

An existing chiller simulation developed by Braun et al. (1987) has a relatively simple compressor model of the form desired in this project. This compressor model was extracted from the existing chiller model and then modified for the Navy chiller.

The model was developed on the following assumptions:

- the compressor impeller and diffuser are modeled separately,
- the refrigerant state between the two compressor components is estimated,
- the performance of each compressor component is characterized by its refrigerant end states,
- two empirical relations were developed from the experimental study by Wiesner and Caswell (1959),
- the inlet guide vane setting is not incorporated in the model,
- the compressor inlet and outlet velocities are neglected, and
- the impeller performance is characterized as isentropic.

5.2.1 MODEL DEVELOPMENT

The impeller exit linear speed, U_2, which is an important parameter in the characterization of compressor performance is the product of the impeller exit circumference and the compressor shaft speed, RPM;

$$U_2 = \pi d_2 \, RPM \tag{5-1}$$

The compressor performance parameters which were defined in Section 3.1.3. are utilized in this model. The flow coefficient, ϕ_2, at the impeller exit;

$$\phi_2 = \frac{V_{r2}}{U_2} = \frac{\dot{m}}{A_2 \, k_B \, U_2 \, \rho_2} \tag{5-2}$$

is defined as the ratio of the impeller discharge radial velocity to the impeller tip velocity. The radial velocity can be determined from the fluid flow rate, $V_{r2} = (\dot{m}/\rho_2)/(A_2 k_B)$, using the continuity equation. The impeller discharge area, $A_2 = \pi d_2 b_2$, is equal to the product of the impeller outer circumference and the impeller axial width, b_2. The blockage factor, k_B, in Equation 5-2 accounts for the blade thickness and a deviation from the uniform velocity distribution at the impeller exit, and it is usually determined experimentally.

The second important dimensionless parameter depicting the compressor performance is the work coefficient;

$$\mu_2 = \frac{V_{u2}}{U_2} = \frac{V_{u2} U_2}{U_2^2} = \frac{w}{U_2^2} \tag{5-3}$$

which is defined as the ratio of the tangential velocity component V_{u2} to the impeller exit linear velocity. If the ratio defining the work coefficient is multiplied and divided by the magnitude of the impeller tip velocity, the expression following the second equality sign in Equation 5-3 is obtained. Further on, the authors neglected the influence of the entering refrigerant velocity and simplified the Euler equation given by Equation 3-2, $w = U_2 V_{u2}$, by expressing the compressor work per unit mass w only in terms of the impeller exit velocities. Incorporating this modified Euler equation into the expanded work coefficient definition, the final expression which follows the last equality sign in Equation 5-3 for the work coefficient was derived.

The polytropic compression work per unit mass is calculated between the actual inlet and outlet compressor states:

$$w_{pol} = \frac{n}{n-1} \frac{p_1}{\rho_1} \left(\left(\frac{p_3}{p_1} \right)^{\frac{n-1}{n}} - 1 \right) \tag{5-4}$$

The polytropic exponent, n, has to be estimated. An average value of polytropic exponent was determined for each refrigerant using the actual inlet and exit state data. The fact that the polytropic exponent must be approximated is a limitation of the model.

The ratio of the polytropic compression work to the compressor work transferred by the Euler work (total compression work converted in the compressor impeller) is known as the polytropic efficiency:

$$\eta_{pol} = \frac{w_{pol}}{w} \tag{5-5}$$

The compressor Mach number in Equation 5-6 is defined as the ratio of the impeller linear velocity, defined in Equation 5-1, to the refrigerant speed of sound at the compressor inlet state, a_1:

$$M = \frac{U_2}{a_1} \tag{5-6}$$

Wiesner and Caswell (1959) related the performance of a number of centrifugal compressors with vaneless diffusers. They showed that the polytropic efficiency can be expressed in terms of the flow coefficient and the compressor Mach number. The relative polytropic efficiency was normalized by taking the average of absolute peak efficiencies for four compressors having the reference compressor Mach number of 1.1. All other efficiencies are represented in terms of this nominal efficiency The nominal polytropic efficiency or the reference efficiency can be taken as the peak efficiency from the compressor performance chart. The reference efficiency should be in the vicinity of 80 percent (Wiesner and Caswell, 1959).

Braun et al. (1987) curve-fitted this performance chart obtaining the first empirical relations for their compressor model. Their curve-fitted compressor empirical relation correlates the polytropic efficiency to the compressor Mach number and the impeller tip flow coefficients

$$\frac{\eta_{pol}}{\eta_{ref}} = \left[1 + C_1(1.1 - M)\right]\left[1 - \exp\left(\phi_2(C_2\phi_2^2 + C_3\phi_2 + C_4)\right)\right] \tag{5-7}$$

in which the authors reported the following curve-fitting coefficients:

$$C_1 = 0.109 \qquad C_2 = 58.5 \qquad C_3 = -6 \qquad C_4 = -18.8$$

The relative compressor efficiency (Equation 5-7) is plotted for several compressor Mach numbers, M's, when varying the flow coefficient, ϕ_2.

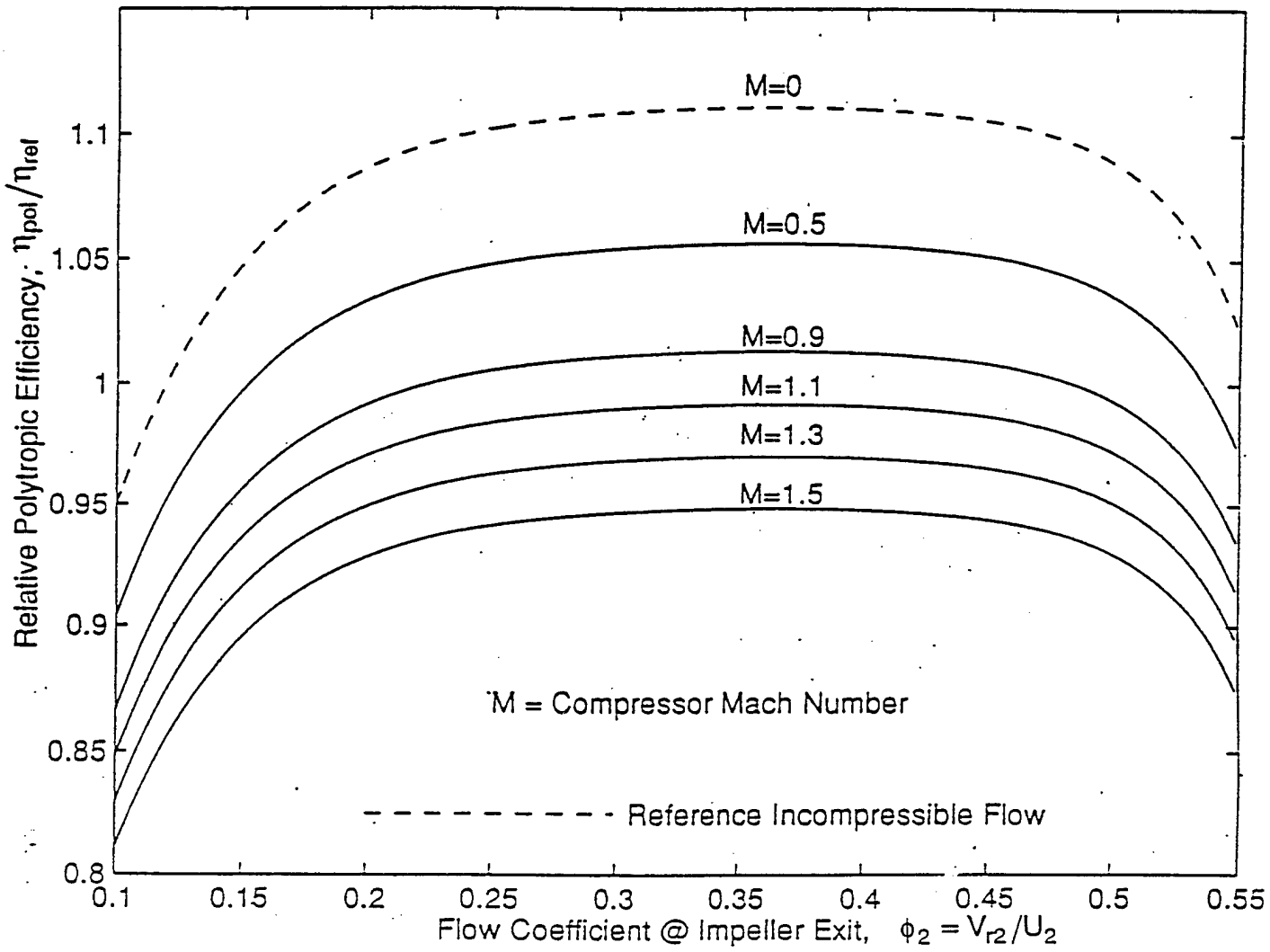

Figure 5.1. Relative polytropic efficiency as a function of compressor Mach number and flow coefficient, reproduced from Equation 5-7.

In their experimental study, Wiesner and Caswell (1959) took the reference polytropic efficiency to be an averaged peak polytropic efficiency for four different compressors taken from their performance charts. For practical purposes, the authors suggested that the peak efficiency for the particular compressor should be taken as the reference polytropic efficiency.

The polytropic head coefficient, μ_{pol}, drawing the parallel to the work coefficient expression in Equation 5-3, is defined as the ratio of the polytropic work per unit mass to the squared peripheral impeller tip velocity:

$$\mu_{pol} = \frac{w_{pol}}{U_2^2} \tag{5-8}$$

Contrary to the polytropic head coefficient, the theoretical work coefficient can be expressed in terms of the exit nominal blade angle from the ideal velocity triangle. The theoretical head coefficient, $\mu_{2,th}$, is derived from the theoretical velocity diagram given in Section 3.1.1. in Figure 3.3. The real head coefficient is always smaller than the theoretical head coefficient due to fluid slip, non-uniform velocity profiles, etc.:

$$\mu_{2,th} = \frac{U_2 - V_{r2}\cot\beta_2}{U_2} = 1 - \phi_2 \cot\beta_2 \tag{5-9}$$

The polytropic head coefficient is plotted as a function of the flow coefficient and the impeller outlet nominal blade angle in Figure 5.2 which is directly expanded from Equation 5-10. The functional dependence between the polytropic work coefficient and the flow coefficient appears as a series of straight lines for every nominal outlet impeller tip angle in Figure 5.2. The largest polytropic head coefficient is for a radial blade compressor converting 69 percent of the theoretical work coefficient. Braun et al. (1987) curve-fitted the data presented by Wiesner and Caswell (1959) to obtain the following empirical expression

$$\mu_{pol} = 0.69(1 - \phi_2 \cot\beta_2) = 0.69\mu_{2,th} \tag{5-10}$$

The absolute velocity of the refrigerant vapor leaving the impeller can be determined from the impeller exit velocity triangle (Figure 3.3) in terms of the radial and tangential velocity components. Combining the expression from the velocity diagram and the definitions of the performance parameters in Equations 5-2 and 5-3 yields an expression for the square of refrigerant absolute velocity leaving the impeller:

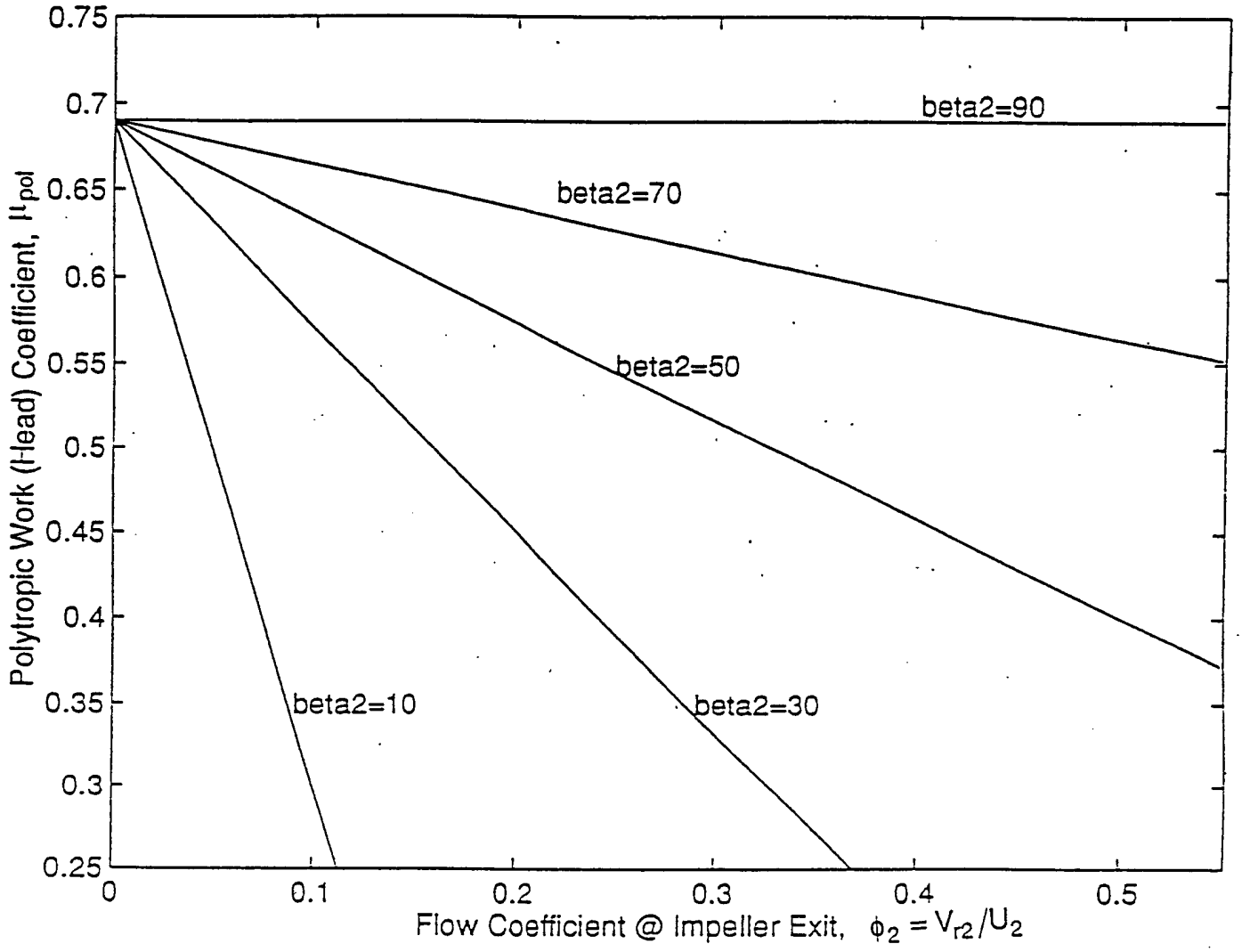

Figure 5.2. Compressor performance chart relating the polytropic work coefficient to the flow coefficient for different blade tip angles constructed from Equation 5-10.

$$V_2^2 = V_{r2}^2 + V_{u2}^2 = U_2^2(\phi_2^2 + \mu_2^2) \qquad (5\text{-}11)$$

in terms of the flow and the work coefficients.

Applying the energy balance to the compressor impeller gives,

$$h_2 - h_1 = w - 0.5V_2^2 = U_2\, V_{u2} - 0.5V_2^2 \qquad (5\text{-}12)$$

where the work per unit mass w is determined by the simplified Euler equation. By neglecting the impeller inlet velocities,which was explained for Equation 5-3, the authors obtained the simplified Euler equation, $w = U_2\, V_{u2}$.

In order to fix the refrigerant state at the impeller exit, Braun et al. (1987) assumed the process through the impeller to be isentropic. The entropies of refrigerant entering and leaving impeller are set equal, enabling the mid-compressor refrigerant state to be defined. Hence, the density of the refrigerant leaving the impeller can be calculated by a property relation for a refrigerant in question:

$$\rho_2 = f(h_2, s_1) \qquad (5\text{-}13)$$

Braun et al. (1987) assumed in their model that the kinetic energy, $V_2^2 / 2$ of refrigerant entering the diffuser is completely converted to useful energy. The velocity of the refrigerant leaving the diffuser is, in other words, negligible compared to the velocity of the refrigerant entering the diffuser. State 3 represents the state of the refrigerant vapor leaving the diffuser.

$$h_3 - h_2 = \frac{V_2^2}{2}, \qquad \text{where} \quad V_3 << V_2 \qquad (5\text{-}14)$$

Equation 5-14 is derived from the diffuser energy balance, neglecting the refrigerant velocity, V_3, leaving the diffuser of the compressor.

The compressor model input and output parameters are summarized in Table 5.1.

Table 5.1. Braun et al. (1987) compressor model input/output information.

INPUT		OUTPUT
RPM Compressor shaft speed.	1.	U_2 Impeller peripheral velocity.
d_2 Impeller outer diameter	2.	ϕ_2 Flow coefficient.
A_2 Impeller exit flow area.	3.	ρ_2 Mid-compressor state density.
K_B Blockage factor.	4.	μ_2 Work (head) coefficient.
p_1 Inlet state pressure.	5.	w Euler work.
ρ_1 Inlet state density.	6.	w_{pol} Compression polytropic work.
p_3 Exit state pressure.	7.	η_{pol} Polytropic efficiency.
n Compressor polytropic exponent.	8.	M Impeller Mach number.
a_1 Inlet state speed of sound.	9.	μ_{pol} Polytropic work coefficient.
η_{ref} Compressor reference efficiency.	10.	$\mu_{2,th}$ Theoretical work coefficient.
β_2 Impeller blade exit tip angle.	11.	V_2 Impeller exit absolute velocity.
h_1 Inlet state enthalpy.	12.	h_2 Impeller exit state enthalpy.
s_1 Inlet state entropy.	13.	h_3 Compressor exit state enthalpy.
b_2 Impeller exit axial width.	14.	$\dot{m}$ Compressor mass flow rate.

5.2.2. SOLUTION OF THE MODEL

There are 14 equations, Equations 5-1 through 5-14, and 14 unknowns depicting the compressor. The blockage factor was originally taken to be 1 (no effects of blade thickness), and the reference polytropic efficiency was taken to be the maximum efficiency noted on the compressor performance chart which was obtained from the compressor manufacturer.

The polytropic exponents were taken as average values of the polytropic exponents between the compressor end states for the entire data set for each refrigerant. The average polytropic exponent for HFC-236ea was 1.046, while for CFC-114 it was determined to be 1.094.

The system of 14 equations was solved simultaneously using a solver based on the Newton method for simultaneous solution of a system of equations. The solution was very sensitive to the initial values chosen. The property function given by Equation 5-14, which was provided by REFPROP 4.01(1994), was found to be particularly sensitive.

Taking a good initial guess, the system of equations was solvable. The two output values were directly compared to the experimentally measured values of refrigerant mass flow rate and outlet state temperature. The modeled refrigerant mass flow rate was greatly overestimated, having values approximately five times larger than those measured on the installation. Therefore, the Braun et al. (1987) model was found to be inadequate, and the solutions are not presented. The outlet state prediction was within a reasonable margin of a error, ± 15 percent.

In order to improve the refrigerant mass flow rate estimates, an optimization procedure was performed for two parameters in the existing model.

5.2.3 MODEL OPTIMIZATION

As found in a number of technical papers related to modeling of the centrifugal compressor, the blockage factor has to be taken into consideration. The blockage factor can account for the thickness of the blades and a non-symmetric velocity profile leaving the impeller. Since there is no general rule regarding this parameter's value, a way to determine the blockage factor is an optimization procedure which minimizes prediction errors of parameters of interest.

The reference polytropic efficiency is taken to be the second optimization variable. The manufacturer performance chart was constructed for the same impeller performing with a refrigerant different from CFC-114; therefore, it can be presumed that the peak efficiency for the other refrigerant has a different value.

A constrained optimization routine was developed to minimize the flow rate prediction errors for 80 HFC-236ea data points, which were identified as the points to be used for generating the empirical relation. The blockage factor can take the maximum value of one in the ideal case, and the minimum was picked to be 0.2, as this is an approximate numerical limit for obtaining a set of reasonable solutions. The minimum reference polytropic efficiency value was taken to be 50 percent, as it was presumed that a compressor should not be designed with the maximum efficiency lower than 50 percent. The upper value for the reference polytropic efficiency was set to be the ideal efficiency of 100 percent.

The constrained optimization routine consisted of three optimization methods. The Newton method, the Steepest Descent method, and the ordinary search method. The methods were applied in the order listed above. The Newton method was always used to check if the objective function was showing convergence toward a minimum in a step. In the case that the Newton routine would diverge, the Steepest Descent method was employed. The plain search method was used only in the case that both methods were diverging from the minimum in the particular step.

The optimization procedure converged to the following solution:

- The blockage factor was $k_B = 0.235$.

- The reference efficiency was $\eta_{ref} = 0.823$.

The blockage factor appears to be rather small since it accounts for a reduction of the flow rate in the proximity of 75 percent. This represents a very unreasonable value for the effects of the impeller blade thickness and non-uniform velocity profile. The value of the blockage factor must have been affected by some other model errors. On the contrary, the reference polytropic efficiency seems to be a reasonable value, although it is larger than the peak efficiency reported on the impeller performance map.

5.2.4. ANALYSIS OF THE OPTIMIZED MODEL

The solutions of the optimized system of equations were obtained by consecutive substitution of variables, since it was observed that this is a more stable procedure to yield a solution when compared to the Newton's method of simultaneous equation solving. The block diagram of the solving order for the optimized model is shown in Figure 5.3. As observed from the solution flow diagram in Figure 5.3, the solution of the model is very simple since there are no iteration loops.

The model was solved for the entire set of data points. The refrigerant flow rate comparison between the modeled and the measured values is given in Figure 5.4, excluding data points for which the chiller capacity was controlled by the by-pass valve. The form in which modeled and measured flow rates in Figure 5.4 were compared will be maintained throughout the remaining text to compare particular measured and modeled compressor parameters. The continuous (solid) line in Figure 5.4. represents the line on which all the data would lie in the case of the perfect model; therefore as the data is more grouped around the solid line, the modeling is more successful.

Other means of comparison between measured and modeled parameters should be defined at this point. Relative difference between a particular measured and modeled compressor parameter, e.g. X, is the absolute difference between the magnitude of the measured parameter, X_{mes} ,and the magnitude of the modeled parameter, X_{mod} , divided by the X_{mes} ; $\text{Relative Difference} = \frac{X_{mes} - X_{mod}}{X_{mes}}$. Also, the absolute value of the relative difference (absolute relative difference) is found convenient to be used for comparison between measured and modeled compressor parameters; $\text{Absolute Relative Difference} = \left| \frac{X_{mes} - X_{mod}}{X_{mes}} \right|$.

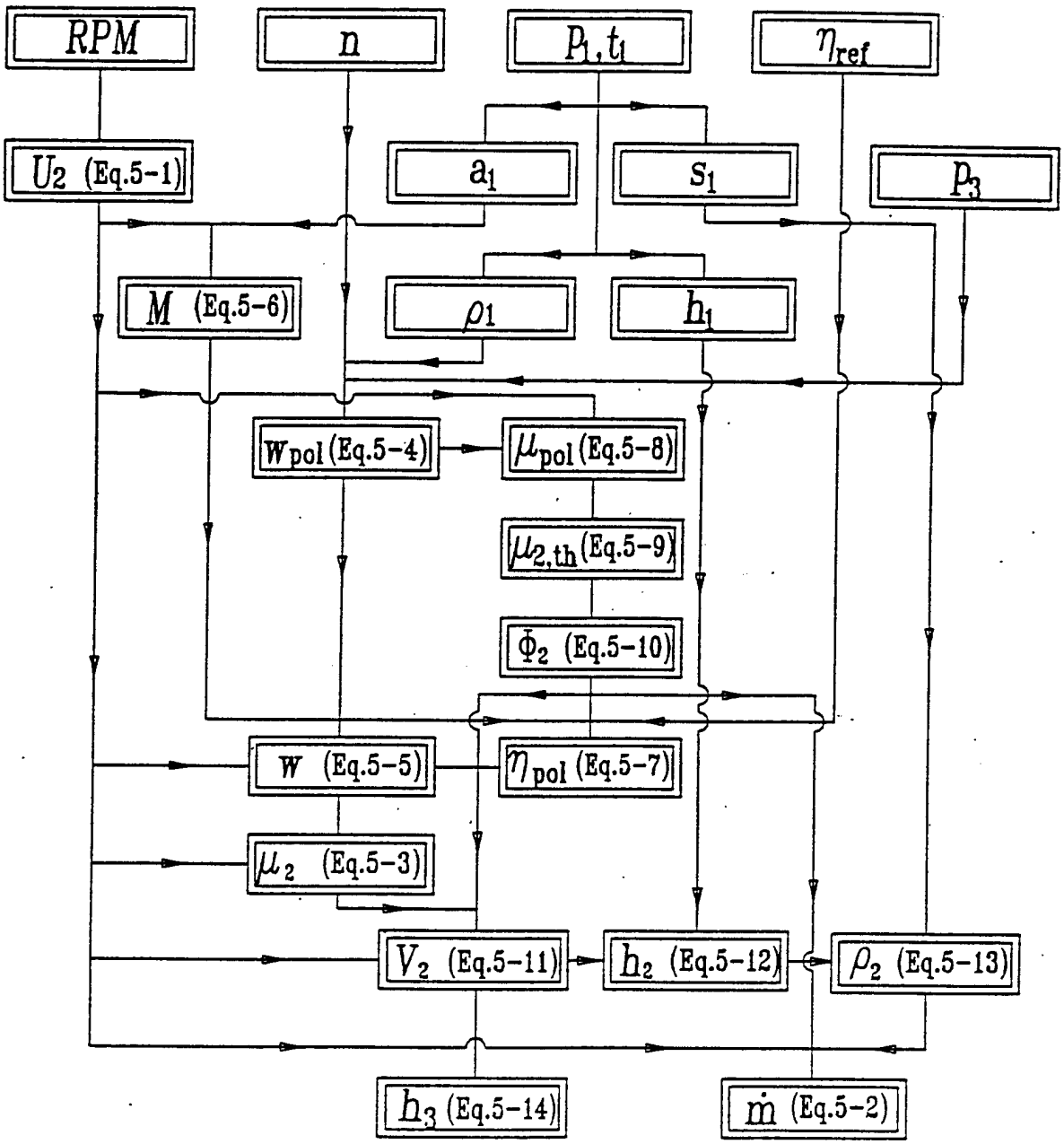

Figure 5.3. Optimized model solution flow diagram.

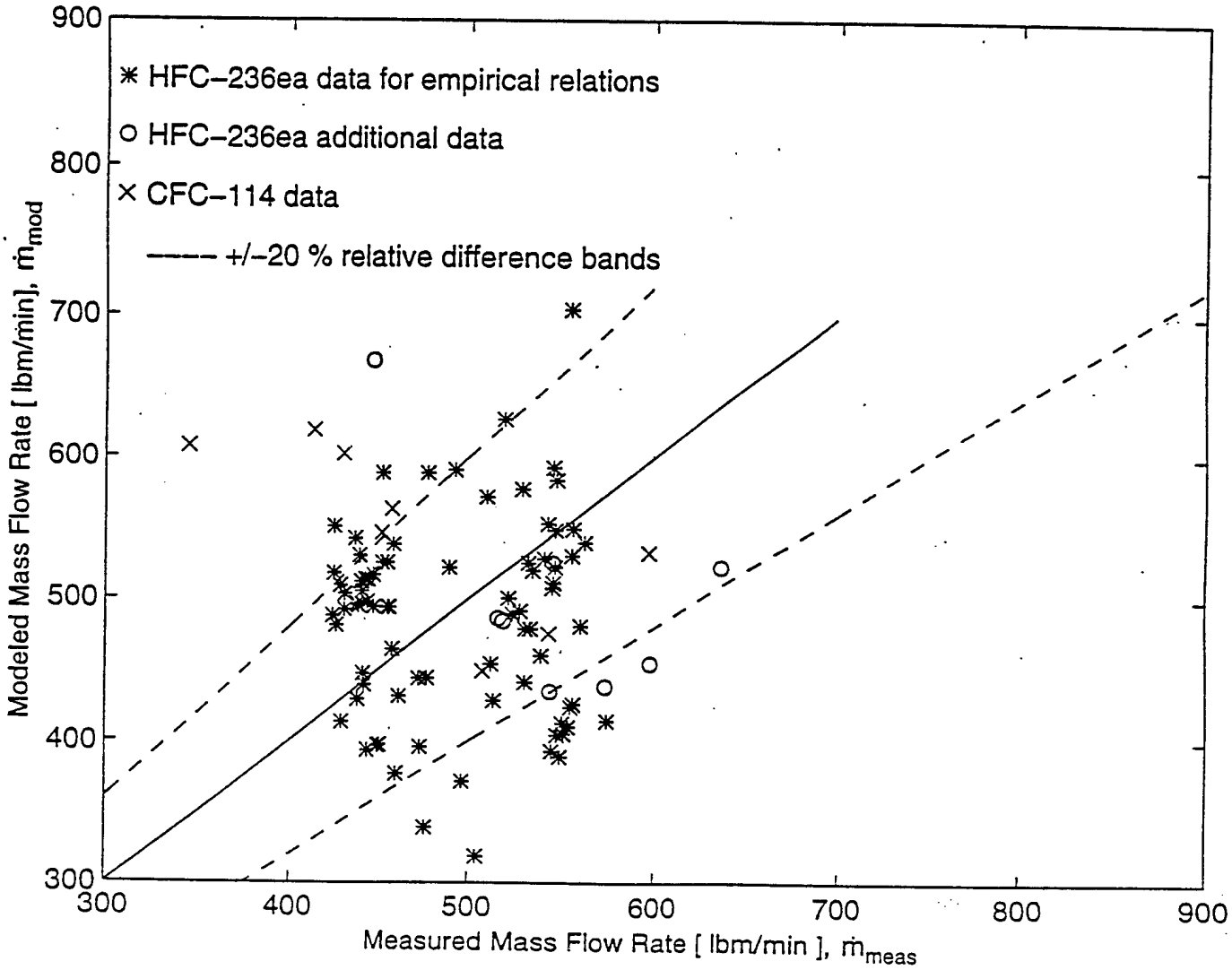

Figure 5.4. Comparison between modeled and measured refrigerant flow rates.

The data points for which the compressor parameters were optimized are marked by stars in Figure 5.4. The relative differences between measured and modeled flow rates are substantial, having the relative differences for several points well beyond ± 20 percent. The ability of the model to predict the flow rate through the compressor appears to be poor. The average absolute relative difference in the flow rate modeling for this data set was 13.96 percent, with the maximum of 36.81 percent.

The additional HFC-236ea data points have the average flow rate absolute relative difference of 22.27 percent and the maximum of 49.71 percent, which can be considered a poor flow rate modeling. Even worse accuracy was obtained for the CFC-114 data points in Figure 5.4, in which the average value was 30.67 percent while the maximum was 76.25 percent.

Since the inlet guide vane settings have not been included in this compressor model, the possible influence of the inlet guide vane angle on the flow rate prediction was investigated. The flow rate relative differences were plotted versus the inlet guide vane angle in Figure 5.5. It appears that the flow rate prediction error is a function of the inlet guide vane position. The observed functional dependence was curve-fitted with the following power function of the inlet guide vane angle, α_1 [degrees open]:

$$\frac{\dot{m}_{meas} - \dot{m}_{mod}}{\dot{m}_{meas}} x100[\%] = 50 - 1.5969e03\ \alpha_1^{-0.97016} \qquad (5\text{-}15)$$

The magnitude of the relative difference in flow rate gets as large as 80 percent of the measured mass flow rate. These excessive differences between measured and modeled flow rates are observed for the data points having low inlet guide vane angles, indicating that the flow rate prediction discrepancy gets larger with an increase in the flow throttling. Also, the relative differences in the mass flow rate modeling are significantly larger, Figure 5.5., for data points which were not used in the optimization procedure.

The curve-fitting of Equation 5-15 was performed on the entire data set shown in Figure 5.5. The flow rate prediction relative difference was calculated as the difference between the measured and the modeled flow rates divided by the measured mass flow rate. The correction equation, Equation 5-15, was incorporated in the model to correct for the modeled refrigerant mass flow rate. The corrected solution for the mass flow rates is compared to measured flow rate in Figure 5.6.

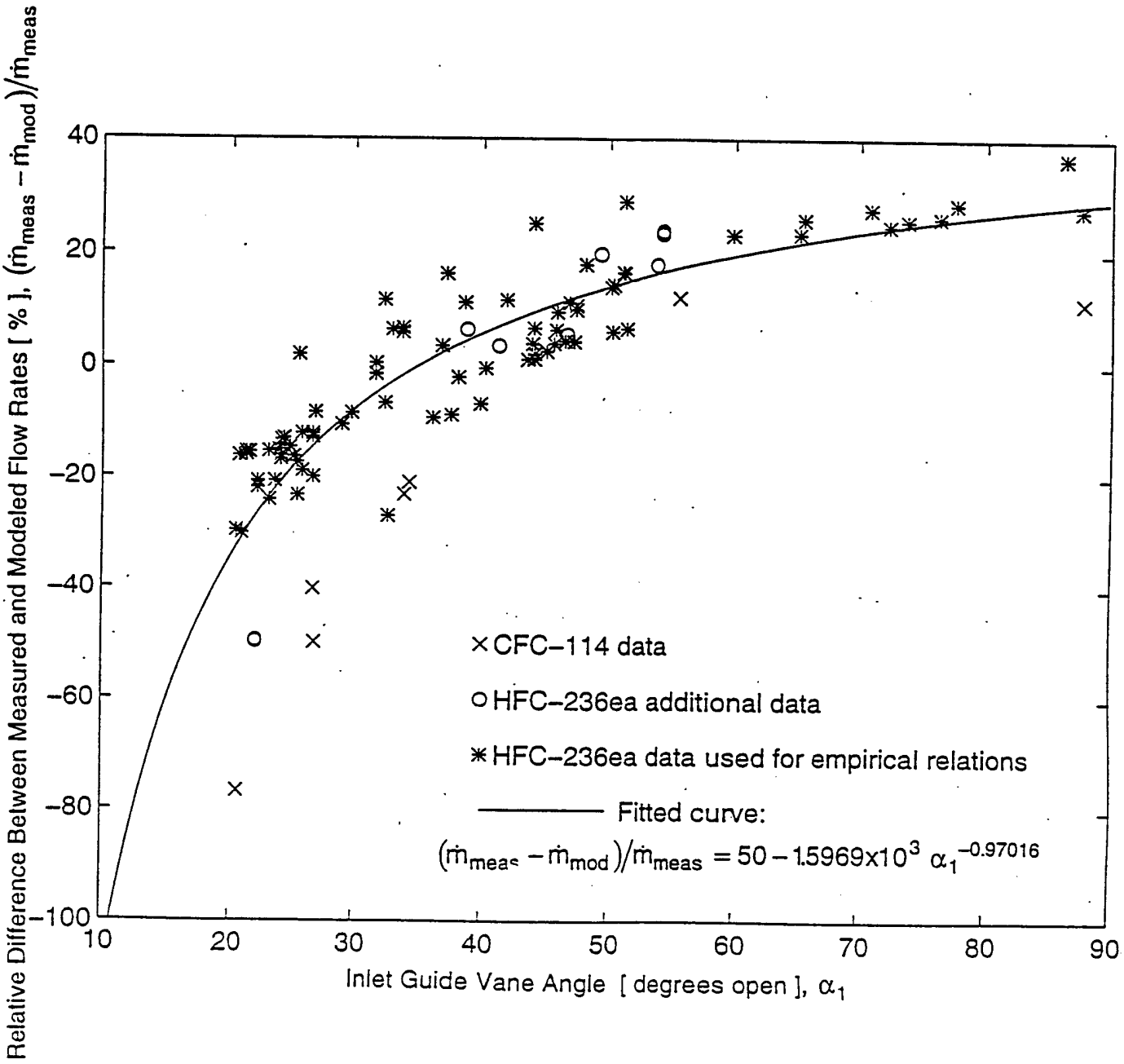

Figure 5.5. Flow rate prediction error as function of guide vane angle.

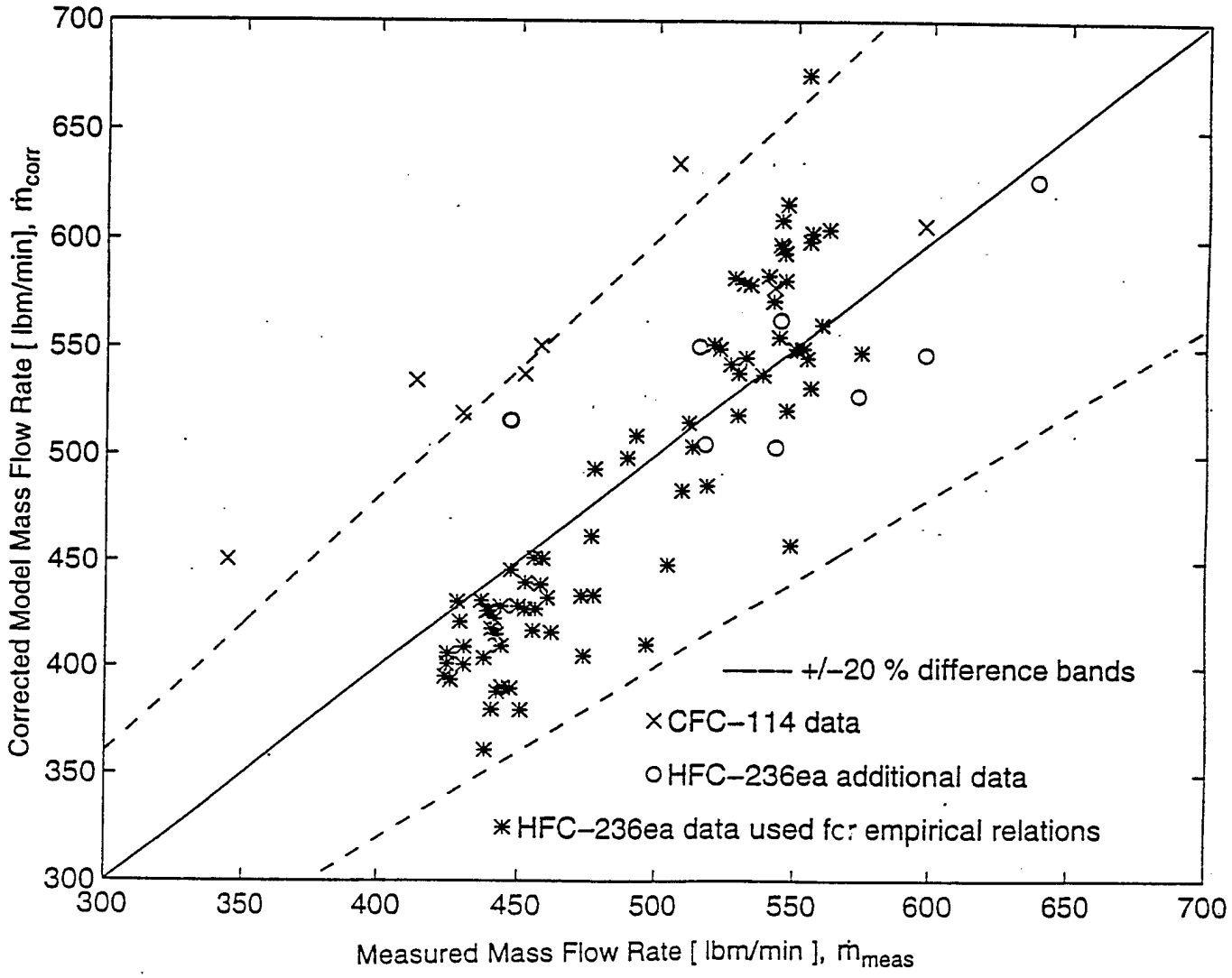

Figure 5.6. Comparison between corrected and measured refrigerant flow rates.

Most of the data points now lie within a ± 20 percent relative difference margin, significantly improving the flow rate prediction accuracy when Figures 5.6 and 5.4 are compared. The HFC-236ea data used to optimize the model have an absolute average relative difference between measured and modeled flow rates of 6.33 percent with a maximum of 21.85 percent. The absolute average relative difference for the additional HFC-236ea data set is 7.66 percent with a maximum of 15.57 percent. It can be concluded that the modified model predicts flow rate satisfactorily. The CFC-114 flow rate prediction has been significantly improved with the flow rate correction formula, but the average relative difference in the flow rate model is still close to 20 percent. This suggests that the model depends on refrigerant type.

The modeled exit state enthalpy for the HFC-236ea refrigerant data points was compared with values obtained from the measured set of data in Figure 5.7. The exit state enthalpy for the HFC-236ea data points was modeled within ± 2 % relative difference, with the larger differences between measured and modeled enthalpies associated with the additional HFC-236ea data points. The data shown in Figure 5.7 also contain HFC-236ea data points operating with the by-pass valve open.

The CFC-114 data exit enthalpy prediction is shown in Figure 5.8. It can be observed that all CFC-114 exit state enthalpies are underestimated up to about five percent. This pattern might be an indication of a systematic error occurring when different refrigerants are applied in the model. The optimized parameters (blockage factor and reference enthalpy) may be a function of the refrigerant type, since there were just too few CFC-114 data points available. The optimization procedure was not utilized for the refrigerant CFC-114 data points.

Exit state temperatures corresponding to the modeled enthalpies are compared to the temperatures measured on the test facility in Figure 5.9. The prediction pattern is similar to the enthalpy results. The relative difference of 2 percent between measured and modeled enthalpy approximately corresponds to a 5 F temperature prediction. The continuous solid line in Figure 5.9 corresponds to the perfect model in which measured and modeled temperature values would coincide.

The absolute average temperature prediction for the optimized data set was 1.22 F, while the maximum difference between measured and modeled exit temperature of the data set was 3.43 F. The additional data set indicated the absolute average temperature prediction difference of 3.49 F, while the CFC-114 data set had an absolute average temperature prediction difference of 13.97 F.

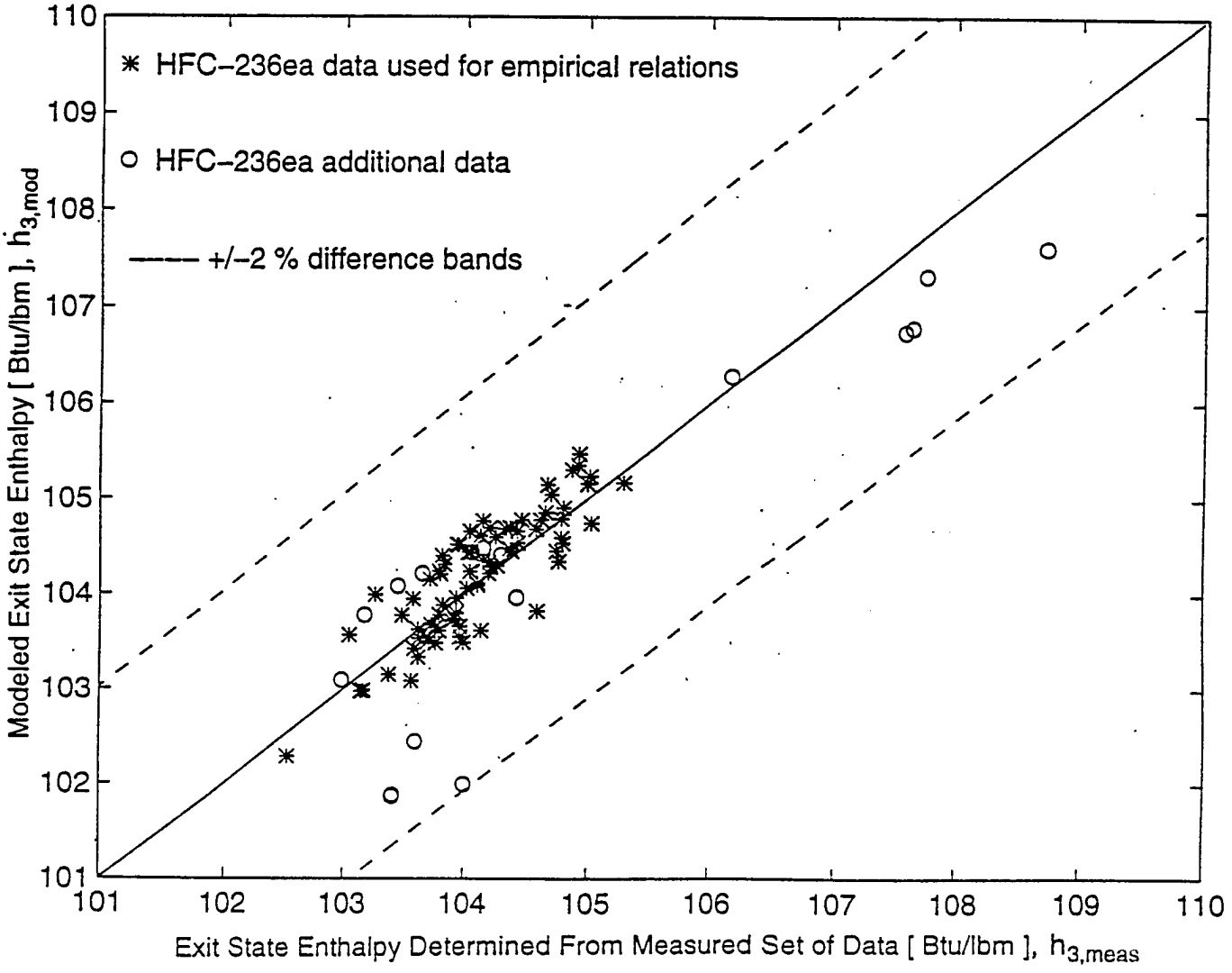

Figure 5.7. Comparison between modeled and measured exit enthalpies for HFC-236ea data points.

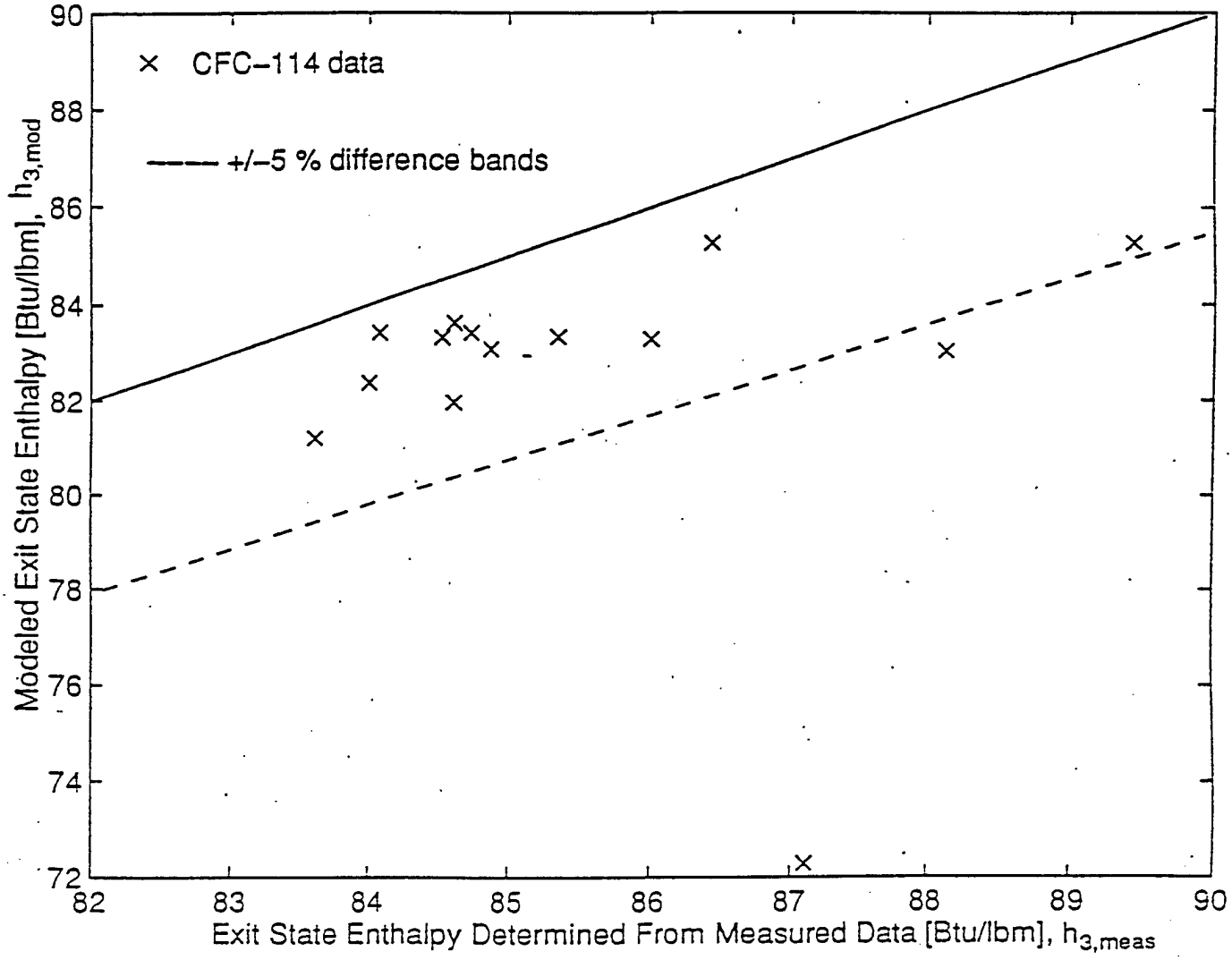

Figure 5.8. Comparison between modeled and measured exit enthalpies for CFC-114 data points.

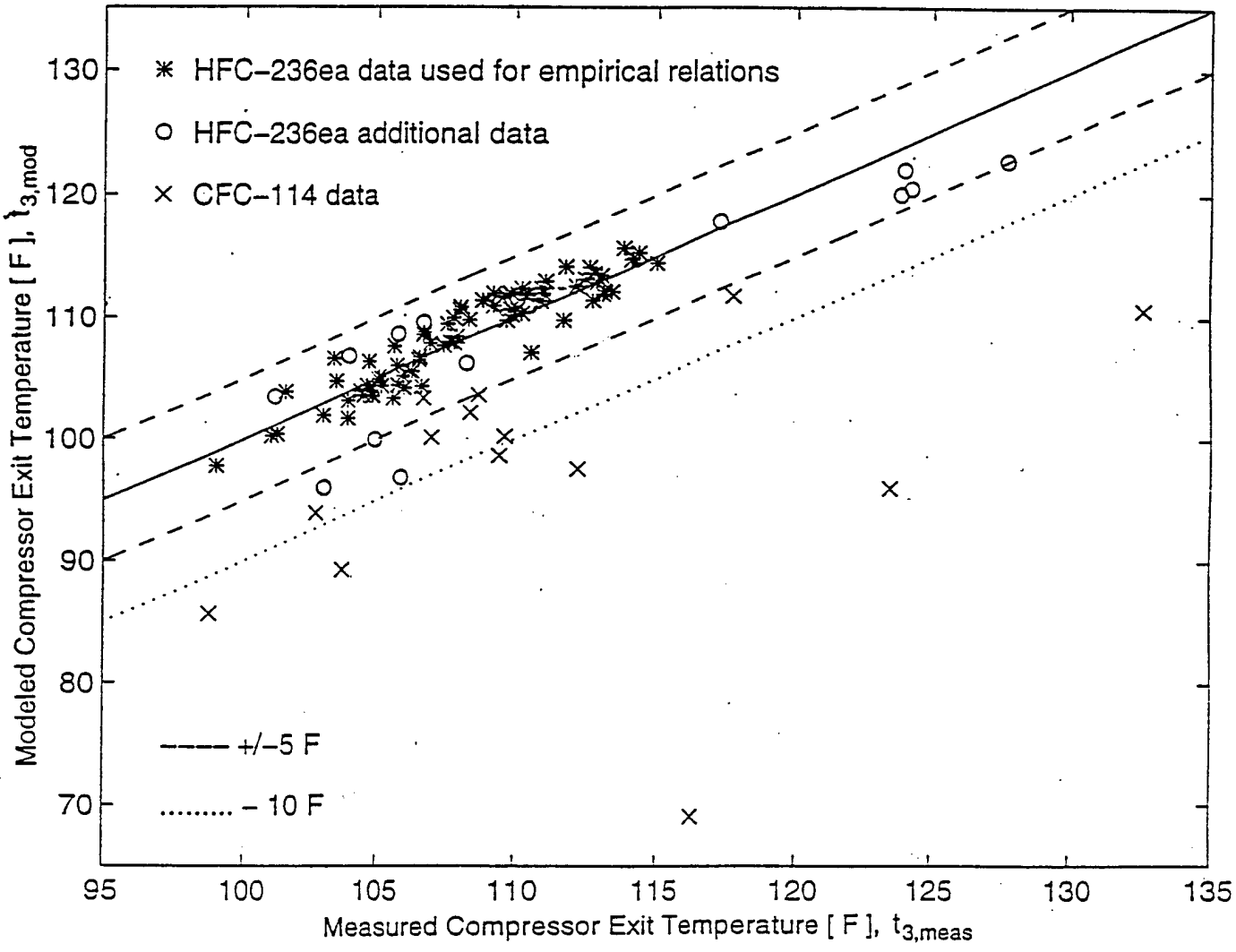

Figure 5.9. Comparison between modeled and measured exit temperatures.

5.3 NEW COMPRESSOR MODEL

A model of similar complexity and based on similar ideas as the existing model described in the previous section was developed seeking better accuracy in compressor performance prediction and better physical significance.

The new model is based on the following ideas and premises:

- the compressor impeller and diffuser are modeled separately,
- the refrigerant state in between these two compressor components is estimated,
- the performance of each compressor component is characterized by its end refrigerant states,
- two empirical relations are developed from the experimental data set available from the chiller test facility,
- the inlet guide vane settings are incorporated in the model,
- the compressor inlet and outlet state velocities are included in the model, and
- the impeller performance is not characterized as isentropic.

5.3.1. NEW MODEL LAYOUT

The inlet guide vane angle and an estimate of the slip factor are incorporated in the model as improvements to the Braun et al. (1987) model. Inlet velocities are also taken into account, because they are the link by which the inlet guide vane angle is incorporated in the model. The inlet velocity effects were neglected in the Braun et al. (1987) model.

The impeller perimeter velocities are proportional to the compressor shaft speed. The fluid in an impeller is accelerated from the inlet to the outlet radius. The peripheral velocity, $U_i = \pi d_i \, RPM$, can be treated as a known value.

Assuming an ideal inlet velocity diagram, as described in Section 3.2., the relevant inlet velocity vectors are defined in Equations 5-16 and 5-17. The inlet guide vane angle, α_1, represents the inlet fluid flow incidence angle, as the ideal inlet velocity diagram was assumed:

$$V_1 = \frac{U_1 \tan\beta_1}{\sin\alpha_1 + \tan\beta_1 \cos\alpha_1} \tag{5-16}$$

The inlet absolute velocity incidence angle is assumed to coincide with the inlet guide vane angle. Therefore, the absolute velocity is a function of the inlet guide vane angle, the inlet impeller blade tip angle, and the impeller rotational speed. The tangential component of the absolute velocity vector is given as:

$$V_{u1} = V_1 \cos\alpha_1 \tag{5-17}$$

When the Euler equation is incorporated into the steady state first law for the impeller assuming that the impeller control volume is adiabatic, the following is obtained:

$$h_2 + V_2^2/2 - \left(h_1 + V_1^2/2\right) = U_2\, V_{u2} - U_1\, V_{u1} \tag{5-18}$$

The refrigerant mass flow rate is incorporated in the model by estimating that the radial velocity component represents an average velocity on which the flow rate can be approximated, taking into account the appropriate impeller departure area. The flow coefficient, ϕ_2, is proportional to the flow rate:

$$\phi_2 = \frac{V_{r2}}{U_2} = \frac{\dot{m}}{A_2\, k_B\, U_2\, \rho_2} \tag{5-19}$$

The blockage factor, k_B, is taken to be 0.9 based on a physical interpretation of one of the empirical relations developed later. This assumption is addressed in Section 5.3.7. of this chapter.

The impeller exit state (the state denoted by 2) is determined with two refrigerant properties: enthalpy and density. The impeller exit state pressure can be evaluated by an equation of state for the particular refrigerant:

$$p_2 = f(h_2, \rho_2) \tag{5-20}$$

The impeller exit state isentropic enthalpy, $h_{2,is}$, is now introduced as the enthalpy at the end of isentropic process between the compressor (impeller) inlet state and the impeller exit state pressure, p_2:

$$h_{2,is} = f(p_2, s_1) \tag{5-21}$$

The impeller exit state isentropic enthalpy is used to define the impeller isentropic efficiency:

$$\eta_{im} = \frac{h_{2,is} - h_1}{h_2 - h_1} \tag{5-22}$$

The slip factor, σ ,which was described in Section 3.1.4, is implemented in the model:

$$\sigma = \frac{V_{u2}}{U_2} \div \frac{\phi_2}{\tan\beta_2} \tag{5-23}$$

The slip factor is assumed to be a constant value, and it was evaluated by the expressions given in Equations 3-9 through 3-11 in Section 3.1.4. The slip factor was estimated by an empirical relation as a function of the impeller outlet blade tip angle and the number of impeller blades.

The following equation is derived from the impeller exit velocity triangle, and it completes the impeller part of the model:

$$V_2^2 = V_{r2}^2 + V_{u2}^2 = U_2^2\,\phi_2^2 + V_{u2}^2 \tag{5-24}$$

The diffuser is modeled only by the energy balance equation, assuming that there are no losses involved in the conversion of the dynamic to the static head.

$$h_3 + V_3^2/2 = h_2 + V_2^2/2 \tag{5-25}$$

The diffuser outlet velocity was not neglected in order to obtain another link of the refrigerant flow rate through the compressor to the model:

$$V_3 = \frac{\dot{m}}{A_3\,\rho_3} \tag{5-26}$$

Finally, the compressor exit density can be determined from the refrigerant equation of state:

$$\rho_3 = f(p_3, h_3) \tag{5-27}$$

A summary of the input and the output values of the new compressor model is presented in Table 5.2. The model system of equations should be first solved for the 12 unknown parameters, and the solution can then be used to generate empirical relations.

Table 5.2. Compressor model input/output summary.

	INPUT	OUTPUT
1.	RPM Compressor shaft speed.	V_1 Inlet absolute velocity.
2.	r_1, r_2 Inlet and outlet impeller radii.	V_{U1} Tangential component of inlet velocity.
3.	α_1 Inlet guide vane angle.	h_2 Impeller exit state enthalpy.
4.	β_1, β_2 Inlet and outlet blade tip angles.	V_2 Impeller exit absolute velocity.
5.	Refrigerant inlet state: (h_1, s_1).	V_{U2} Tangential component of V_2.
6.	A_2, A_3 Impeller and diffuser exit areas.	ϕ_2 Flow coefficient.
7.	K_B Blockage factor.	ρ_2 Impeller exit state density.
8.	σ Impeller slip factor.	p_2 Impeller exit state pressure.
9.	p_3 Compressor exit state pressure.	$h_{2,is}$ Impeller exit state isentropic enthalpy.
10.	$\dot{m}$ Compressor mass flow rate.	η_{im} Impeller isentropic efficiency.
11.	h_3 Compressor exit state enthalpy.	ρ_3 Compressor exit state density.
12.		V_3 Compressor exit velocity.

5.3.2 MODEL SOLUTION

The compressor performance is depicted by Equations 5-16 through 5-27. Having the compressor end state refrigerant properties, mass flow rate, compressor shaft speed, and inlet guide vane angle known, the model system of equations can be solved. The unknowns in the compressor model are listed in Table 5.2 in the output column, while the values required to be entered in the model are listed in Table 5.2 in the input column. The solution of the model system of equations yields the properties at the impeller outlet (state 2), various unknown velocities, and the impeller isentropic efficiency.

The solution was obtained by the consecutive substitution method of solving a system of equations, since it was not possible to solve the system of equations by the simultaneous solution method. The flow diagram of the order of the consecutive substitution is given in Figure 5.10

The system of equations can be solved without any iteration loops, as indicated in Figure 5.10, implying that the system solution is stable.

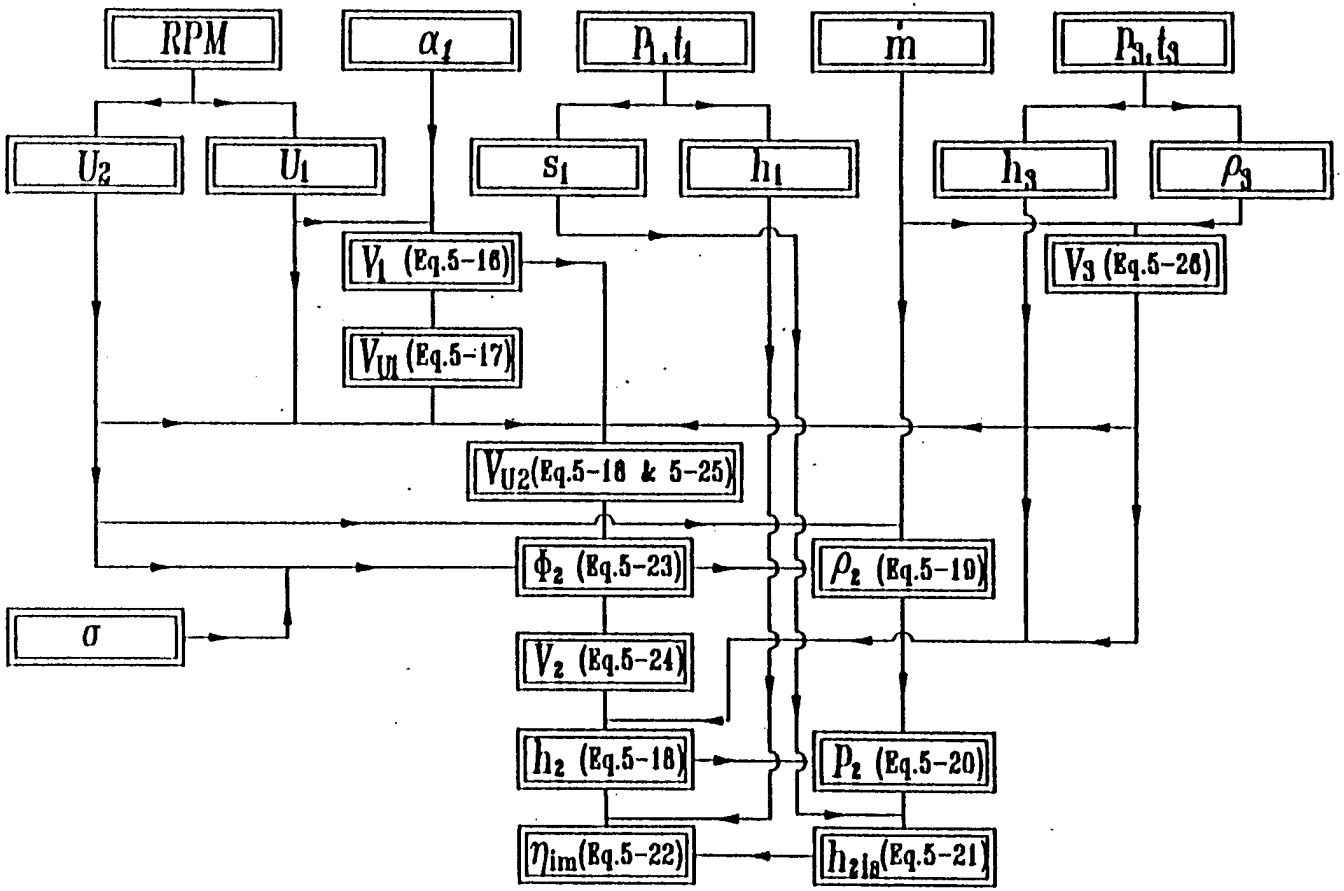

Figure 5.10. The compressor model, Equations 5-16 through 5-27, solution flow diagram.

5.3.3. GENERATION OF EMPIRICAL RELATIONS

As noted in the previous section, every empirical relation added to the model increases the model degrees of freedom by one. The model objective was to predict refrigerant mass flow rate and the refrigerant exit state; therefore, two empirical relations were needed to obtain a solvable system of equations.

The compressor model seems to have a weak dependence on the inlet guide vane angle, since the vane angle position is utilized only in determination of the inlet refrigerant velocity vectors in Equations 5-16 and 5-17. Therefore, an empirical relation was sought to correlate the inlet guide vane angle position to a parameter from the compressor model.

The most sound correlation found is given in Figure 5.11. The impeller isentropic efficiency appears to be a strong function of the inlet guide vane angle. The fact that two data points have efficiency greater than 100 percent may be attributed to errors generated to determination of the compressor mid state as well as the choice of the blockage factor discussed in Section 5.3.7.

The best fit functional relation found is a second degree polynomial given in Equation 5-28. The standard deviation of the mean of 3.34 percent corresponds to the fitted function:

$$\eta_{im}[\%] = ca_0 + ca_1\,\alpha_1 + ca_2\,\alpha_1^2 \qquad [\alpha_1 \text{ in degrees}] \tag{5-28}$$

$$ca_0 = -0.59625 \qquad ca_1 = 1.7049\,[1/\text{degrees}] \qquad ca_2 = -6.6480\times10^{-3}\,[1/\text{degrees}]^2$$

This empirical relation has a sound physical interpretation. As the incoming refrigerant flow is throttled (inlet guide vane angle decreased), the compressor impeller performance deteriorates (the isentropic efficiency drops). On the other hand, as the refrigerant flow is less diverted by the inlet guide vanes, the impeller performance improves, with the isentropic efficiency reaching unity in Figure 5-11.

The inlet guide vane angle is related to the compressor mid state (state 2) through the impeller isentropic efficiency, which was calculated from the experimental data. The empirical relation was then appended to the compressor model, and the new system of equations was solved for the mass flow rate. The resulting errors in the refrigerant mass flow rate prediction were proportional to the errors observed in the fitting of the first empirical equation. This empirical relation can be regarded as being related to the determination of the refrigerant flow rate.

Some other potential relations of the inlet guide vane angle with the compressor parameters were investigated, and the results are discussed next with respect to Figures 5.12 and 5.13.

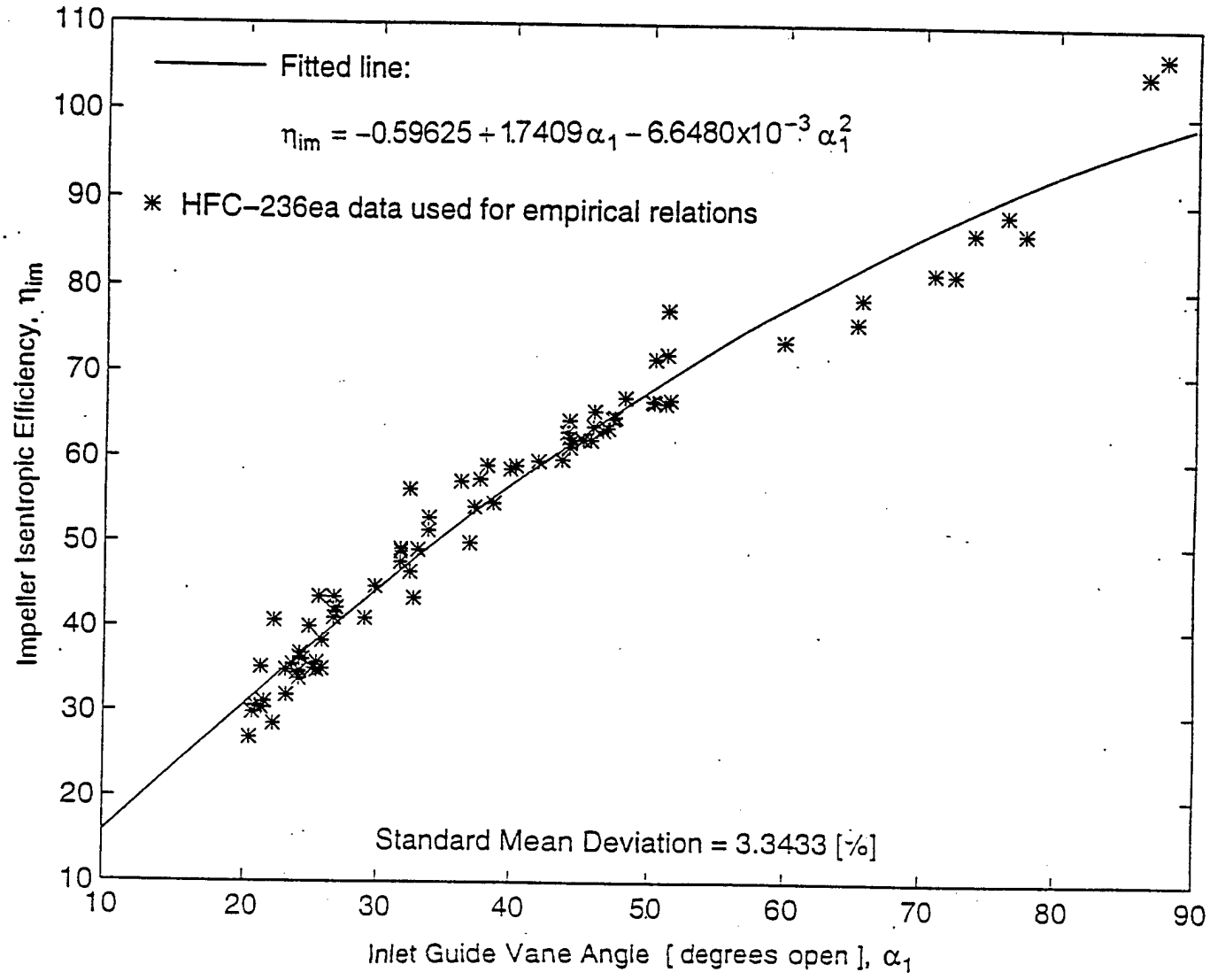

Figure 5.11. Impeller isentropic efficiency as a function of inlet guide vane angle.

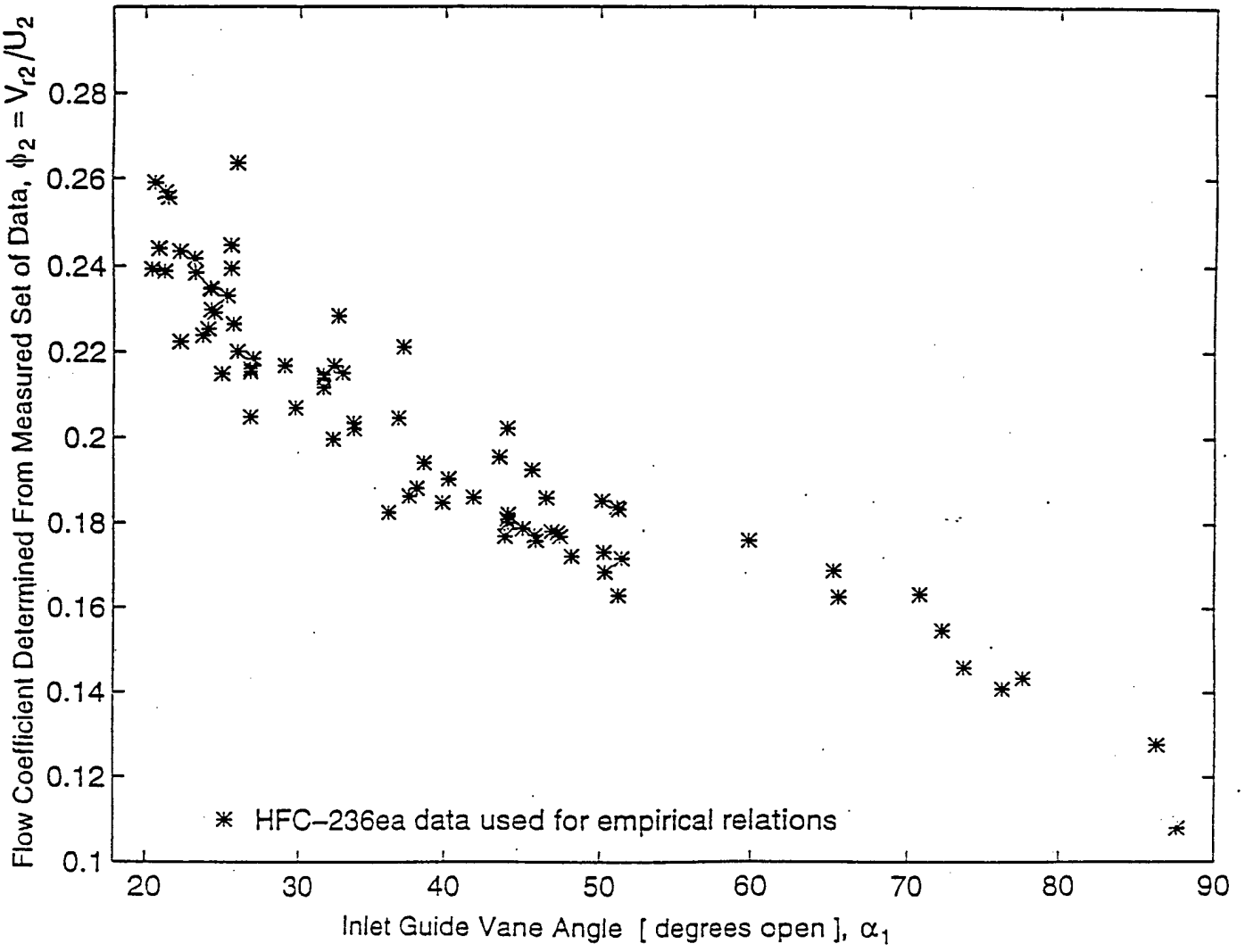

Figure 5.12. Flow coefficient as a function of inlet guide vane angle.

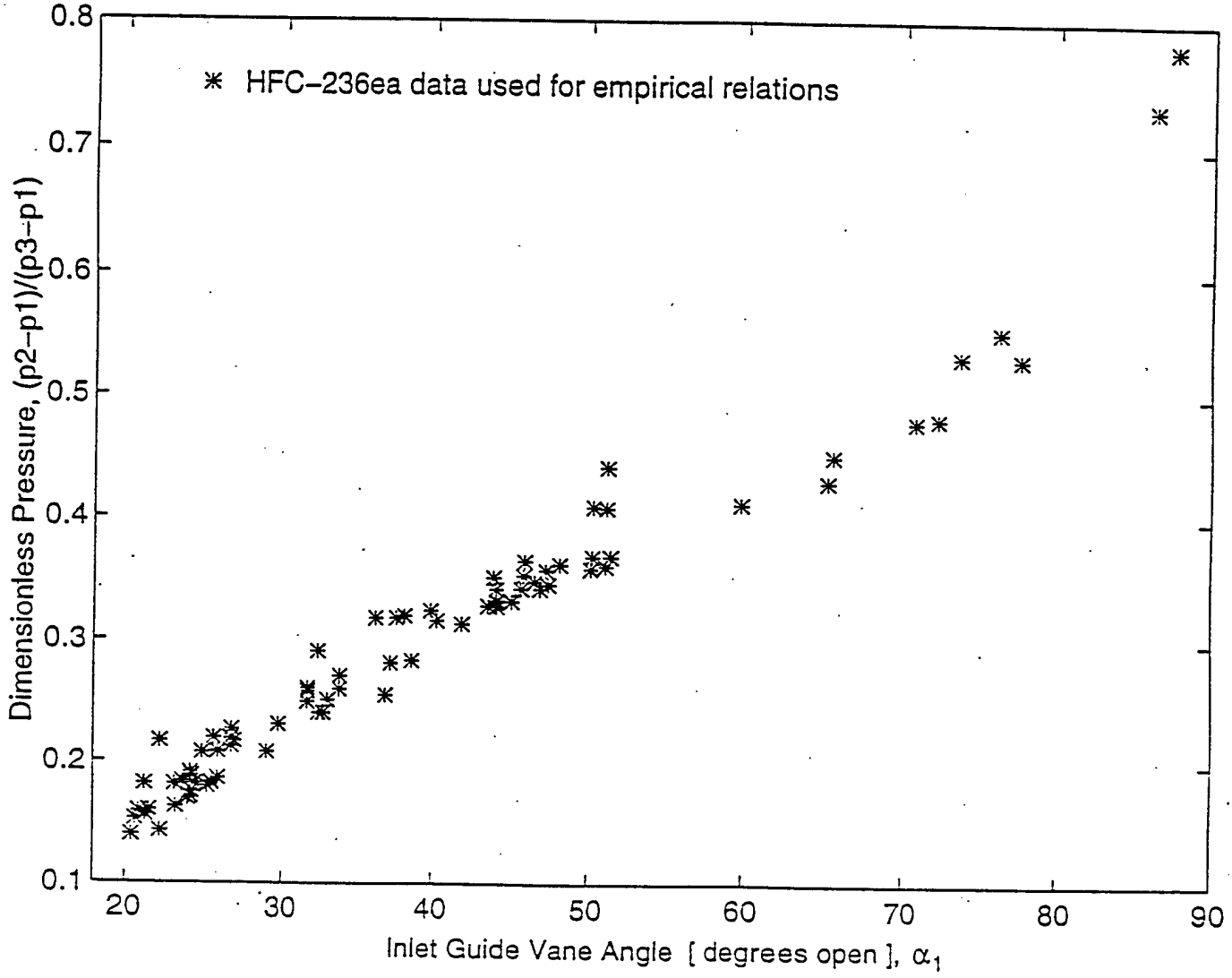

Figure 5.13. Dimensionless pressure as a function of inlet guide vane angle.

The flow coefficient decreases with increasing inlet guide vane angle (less flow throttling) as shown in Figure 5.12. The flow coefficient is directly related to the mass flow rate, but inversely related to the impeller exit state density, Equation 5-19. Thus, throttling of the flow (flow rate decrease) at the compressor inlet also reduces the impeller exit density. The reduction in the impeller exit density can be related to a lower pressure at the impeller exit (reduction in pressure rise across the impeller). Since the flow coefficient appears to be a negatively sloped function of the inlet guide vane angle in Figure 5.12, it can be inferred that the inlet guide vanes have stronger influence on the impeller exit state than on the mass flow rate.

This observation can be justified by Figure 5.13, in which it can be clearly seen that the pressure rise across impeller, $(p_2 - p_1)$, is a function of the flow throttling at the compressor inlet. This is an indication that the inlet guide vane angles affect significantly the impeller performance, as already observed in the first empirical relation in Figure 5.11. The pressure rise across impeller, according to data in Figure 5.13, goes from as low as 15 percent of total pressure rise across the compressor for extremely throttled flow to as high as almost 80 percent for non-throttled flow.

The compressor (diffuser) exit state enthalpy is correlated to the flow coefficient through the dimensionless enthalpy in Figure 5.14. This appeared to be the best functional dependence between compressor parameter pairs in the compressor model solution. The magnitude of the dimensionless enthalpy varied over a very narrow range for different flow coefficients, but the whole set of HFC-236ea data utilized for the empirical relations showed strong dependence on the flow coefficient.

The best fit to the data in Figure 5.14 is a power function given by Equation 5-29:

$$h_{dim} = \frac{h_2 - h_1}{h_3 - h_1} = 0.67 - 0.0092598\,\phi_2^{-0.95383} \qquad (5\text{-}29)$$

This relation was taken to be the second model empirical relation, and it is related to the determination of the compressor exit state refrigerant enthalpy, h_3.

5.3.4 SOLUTION OF THE COMPLETE COMPRESSOR MODEL

The complete model has 16 equations and 16 unknowns, including the two new unknown parameters: the mass flow rate and the exit state enthalpy, and two empirical relations given by Equations 5-28 and 5-29. The consecutive substitution solving method was applied to obtain the solution of the new system of equations. The flow diagram of the solving order is presented in Figure 5.15.

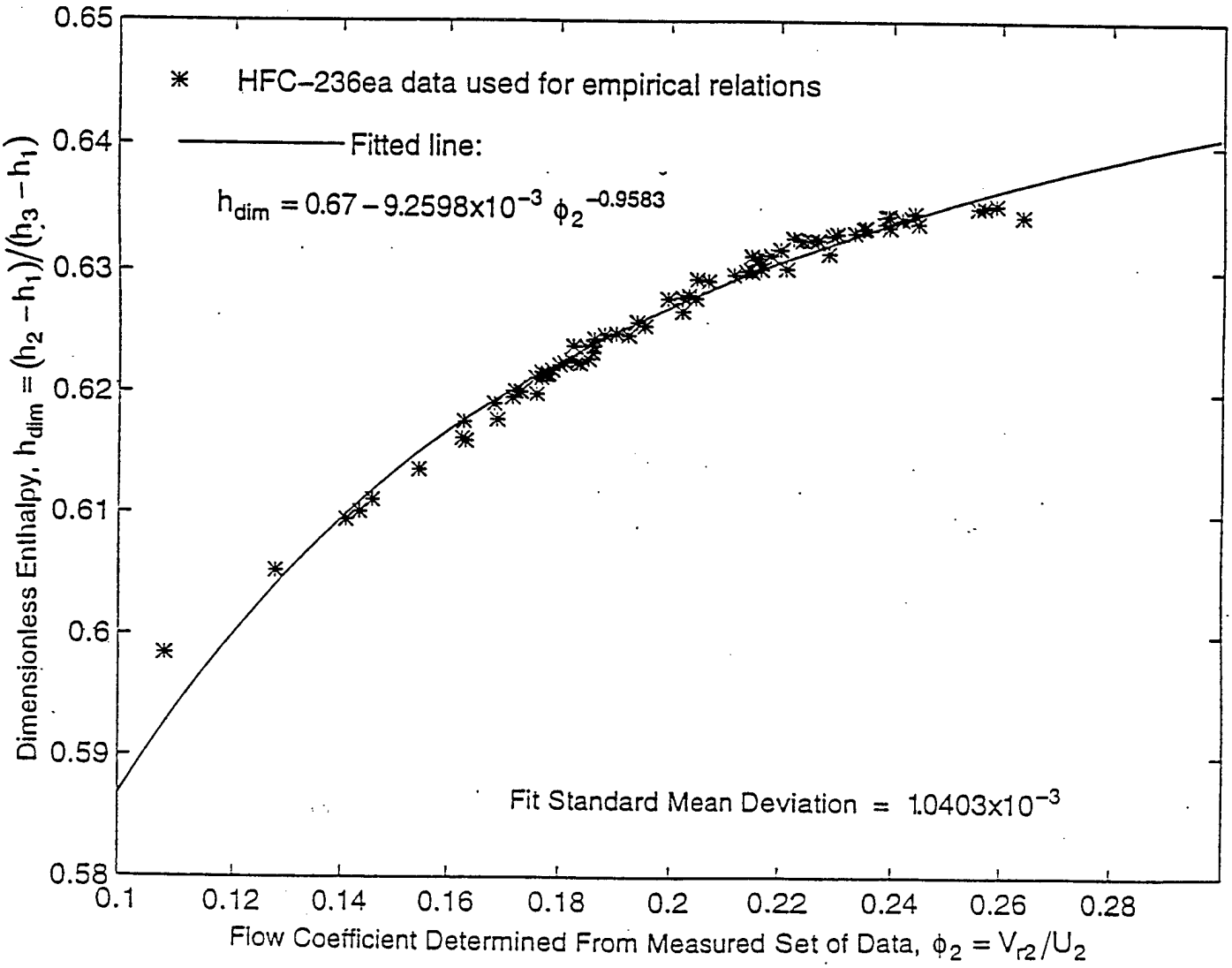

Figure 5.14. Dimensionless enthalpy as a function of flow coefficient.

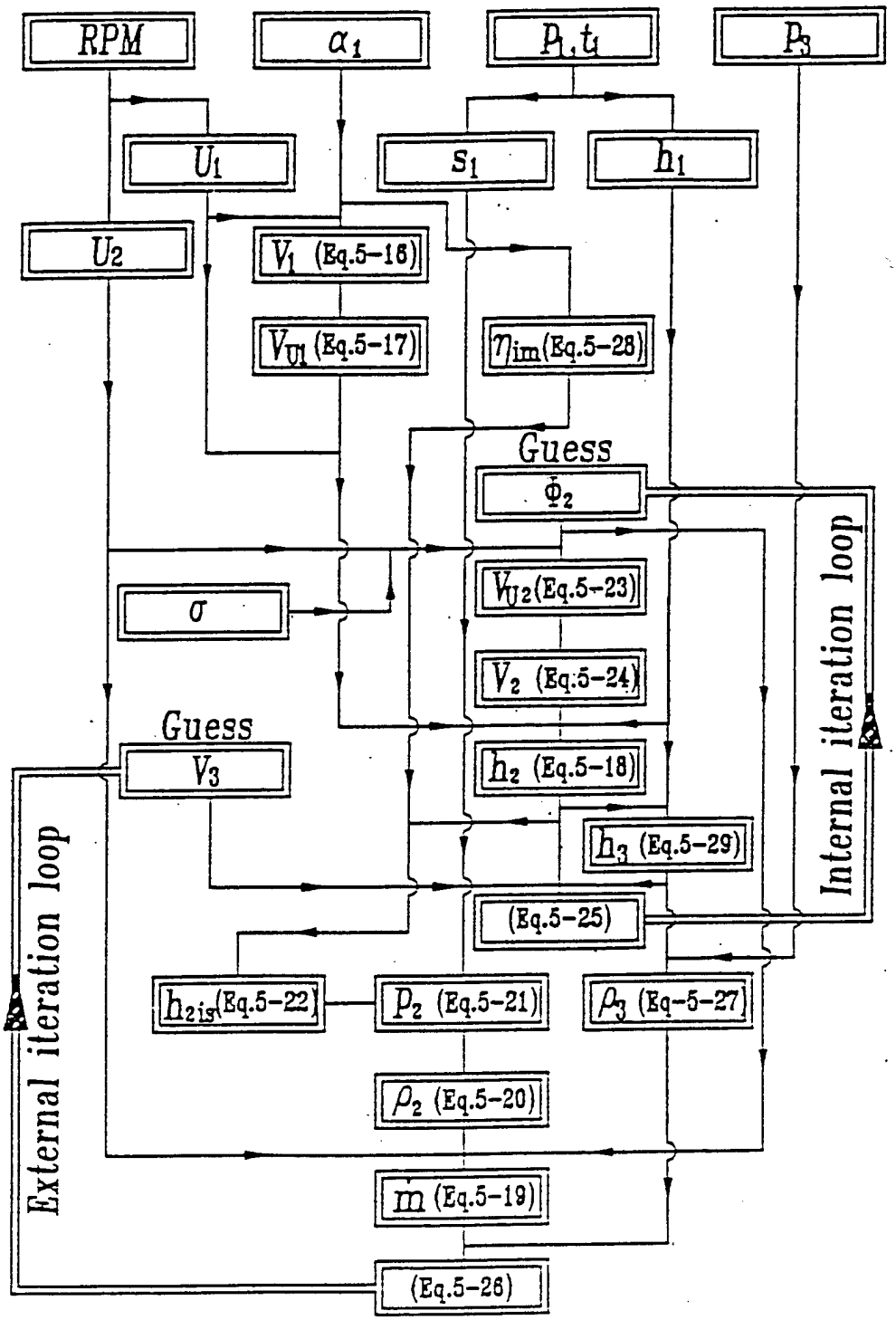

Figure 5.15. Solution flow diagram for compressor model.

As observed in Figure 5.15, two iteration loops were implemented to solve the system of equations. Both loops utilized the secant numerical method to converge to the solution. The velocity leaving the compressor, V_3 (Equation 5-26), which is a parameter not affecting the solution significantly, was chosen in the external loop for fast convergence. It was bounded between zero and approximately one-third of the absolute velocity leaving the impeller, V_2. The flow coefficient, ϕ_2, being the parameter which greatly affects the compressor model (appears most frequently in the model system of equations), was chosen for the internal iteration loop in the solving order of the system of equations (Figure 5.15). The flow coefficient was set between 0.1 and 0.5, and it was iterated by the secant method until a preset accuracy was achieved on the diffuser energy balance equation, Equation 5-25.

5.3.5. SOLUTION ANALYSIS

The solution obtained from the complete compressor model, Equations 5-16 through 5-29, has the flow rate prediction shown in Figure 5.16. The data for which the hot gas by-pass valve at the compressor outlet was used to control refrigerant flow rate were excluded from the plot.

The HFC-236ea data for which empirical relations were utilized have a mass flow rate predicted within a $\pm$ 20 percent relative difference between measured and modeled flow rates. The absolute average of the observed flow rate prediction differences is 4.45 percent with the maximum of 19.51 percent. All additional HFC-236ea data points are within a $\pm$ 20 percent relative difference margin, but they have a higher average absolute relative difference of 12.57 percent.

Five out of eight CFC-114 data points for which the by-pass valve was closed are beyond the 20 percent error margin line. The overall flow rate prediction error average is around 23 percent, with the maximum being around 55 percent. These results for CFC-114 data suggest that the compressor model is not independent of the refrigerant type. This is only considered a tentative conclusion, since there were just a few CFC-114 data points available for this analysis.

In summary, the prediction of the mass flow rate falls in the $\pm$ 20 percent relative difference margin for the HFC-236ea data points. There is an improvement in the mass flow rate prediction for HFC-236ea data over the modified Braun et al. (1987) model analyzed in Section 5.2. However, the CFC-114 data flow rate prediction has not been improved from the modified Braun et al. (1987) model, repeating a similar error pattern when the results in Figures 5.6 and 5.16 are compared. It can be concluded that the CFC-114 flow rate prediction is rather poor. The CFC-114 data flow rate prediction fell into the very limited range of values from 450 to 600 lbm/min, while the values of measured flow rate are in the range from 300 to 600 lbm/min. This observation may indicate that the compressor model is moderately insensitive to the different operating conditions for CFC-114 data points.

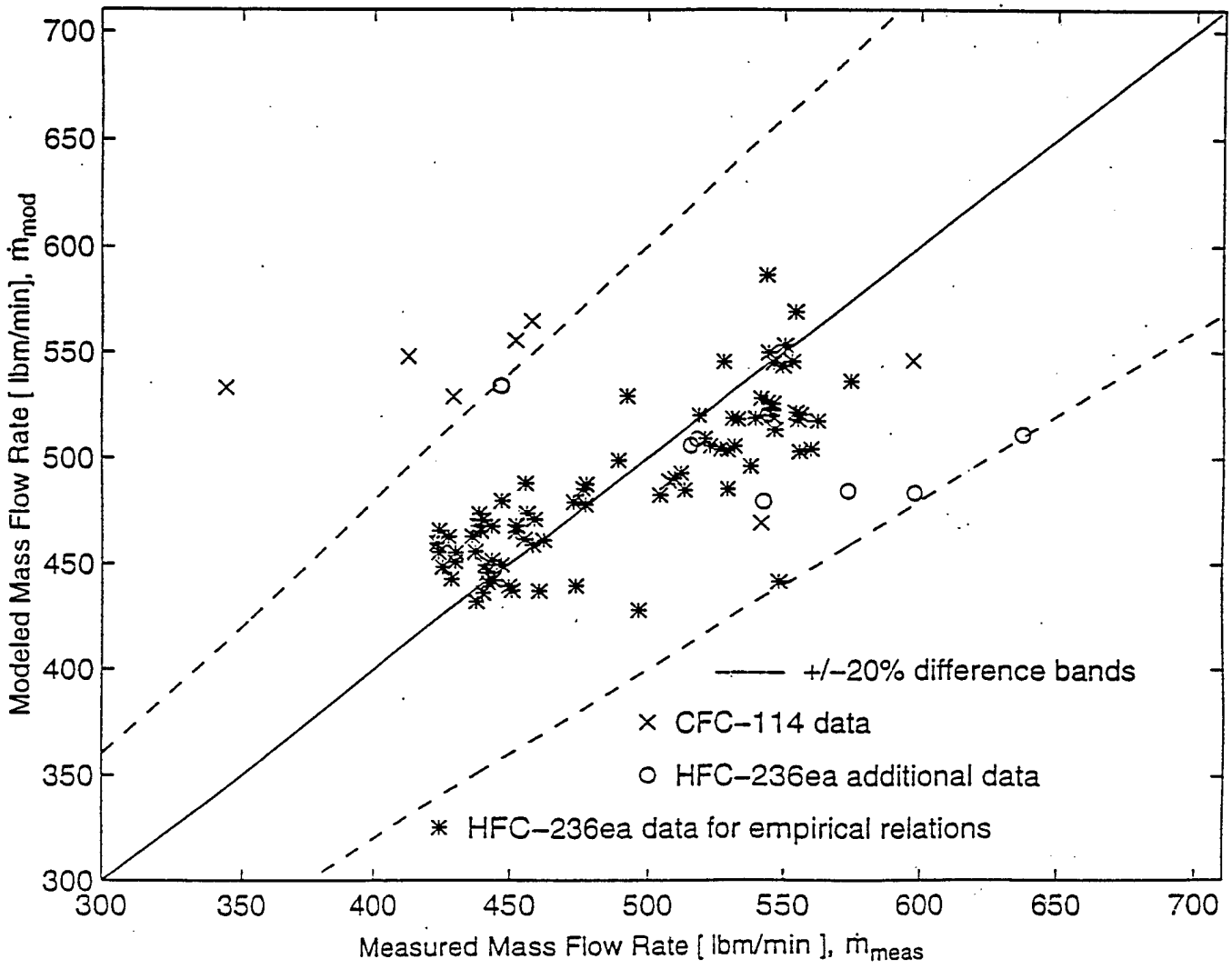

Figure 5.16. Comparison between measured and modeled flow rates.

The relative difference between measured and modeled flow rate is plotted versus the inlet guide vane setting in Figure 5.17 to check whether there is a functional dependence between these two values. The relative difference variance is not constant for the data points used in generating the empirical relation, but it does appear to be distributed symmetrically around the zero difference condition. It may be concluded that the difference occurring in the flow rate prediction is independent of the vane guide setting.

The CFC-114 data points having low inlet guide vane settings (throttled flow) indicated the largest errors. This is another indication of the model developed being inadequate for predicting accurately the CFC-114 data points.

There are six HFC-236ea data points in which the by-pass valve was used to control the chiller capacity. The flow rate through the compressor in that mode of operation is greater than the flow rate through the rest of the chiller. As explained in Chapter 4, the refrigerant flow rate was calculated as the average refrigerant mass flow rate through the chiller heat exchangers, and this flow rate value was referred to as the measured flow rate magnitude. The refrigerant flow rate measured on the installation is divided by the modeled flow rate, since the flow rate with the by-pass valve open must be greater in the compressor than in the rest of the installation. This yields a flow rate fraction. The flow rate fraction of measured to modeled flow rate is plotted versus the percentage of the by-pass valve openness in Figure 5.18.

The compressor operating mode in which the by-pass valve is not fully closed should denote the case of the flow rate ratio equal to one. The function between the HFC-236ea data on Figure 5.18 appears to be strongly linear. This limited number of data is curve-fitted with the following regression line, as indicated on Figure 5.18:

$$\text{By-pass valve}[\%\ \text{open}] = 117.58 - 119.0563\frac{\dot{m}_{meas}}{\dot{m}_{mod}} \qquad (5\text{-}30)$$

At the time when the CFC-114 data were taken, the by-pass valve position was not recorded; therefore, it was not possible to check this model against the CFC-114 data points.

This empirical relation in Equation 5-30 was used to correct the modeled mass flow rates for the mentioned six HFC-236ea additional data points with by-pass valve open. The corrected values of modeled flow rate are compared to the measured values in Figure 5.19.

The by-pass valve data points with corrected mass flow rates show very good agreement with the flow rates measured on the installation. These good prediction results may indicate that there were errors incorporated in the data taking of the additional HFC-236ea experimental data points.

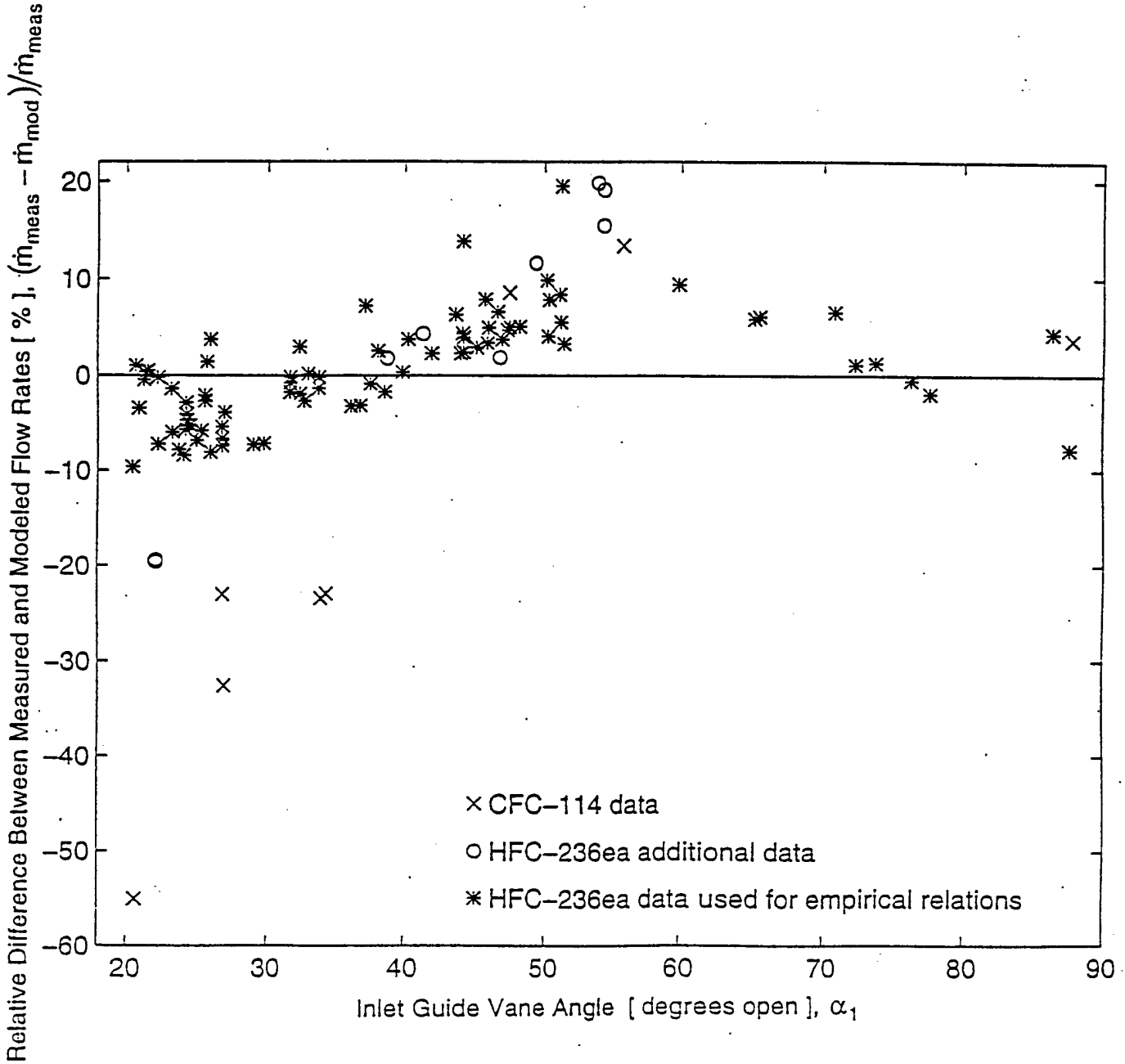

Figure 5.17. Relative difference between measured and modeled flow rates as a function of inlet guide vane setting.

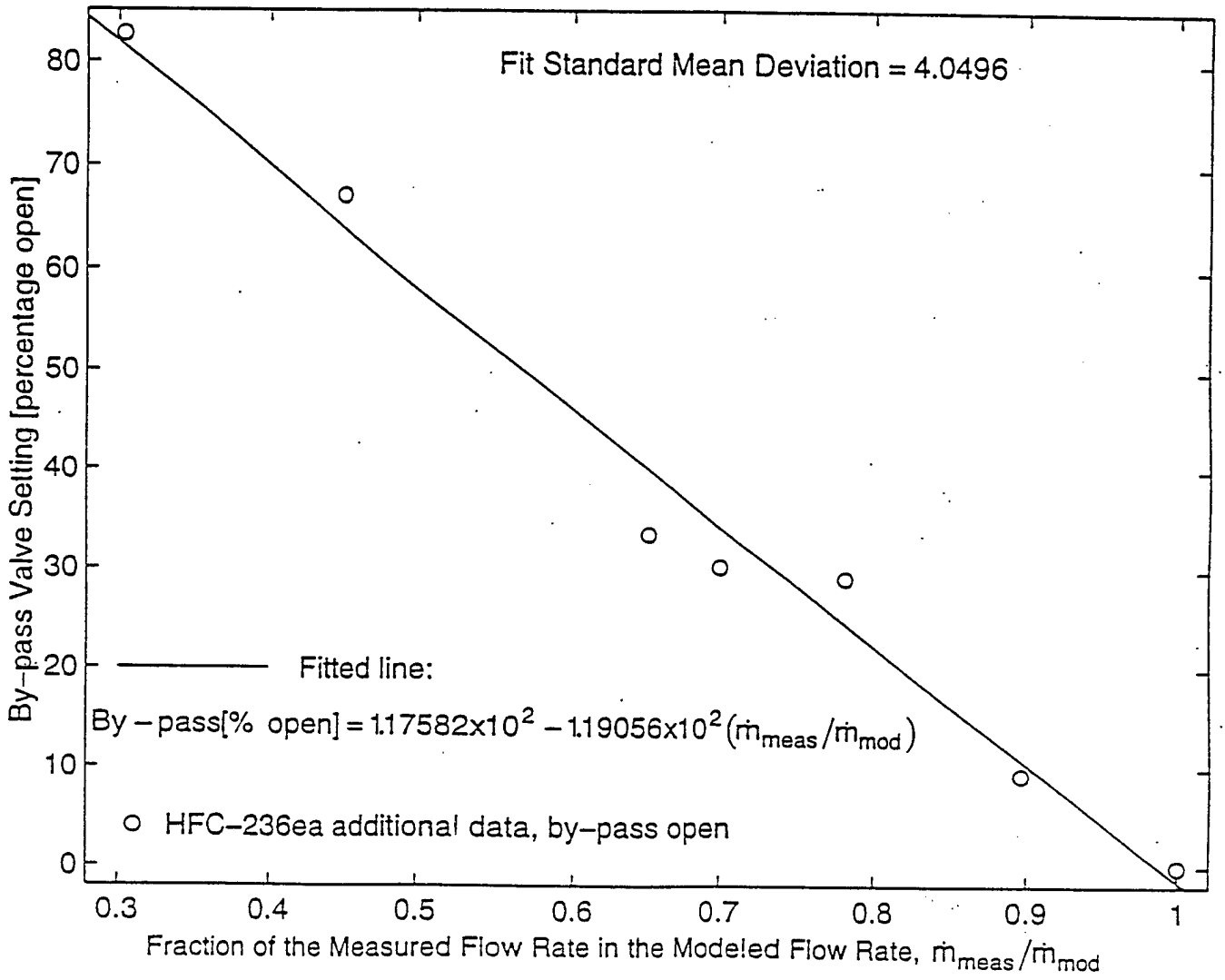

Figure 5.18. By-pass valve position as a function of fraction of measured to modeled flow rate.

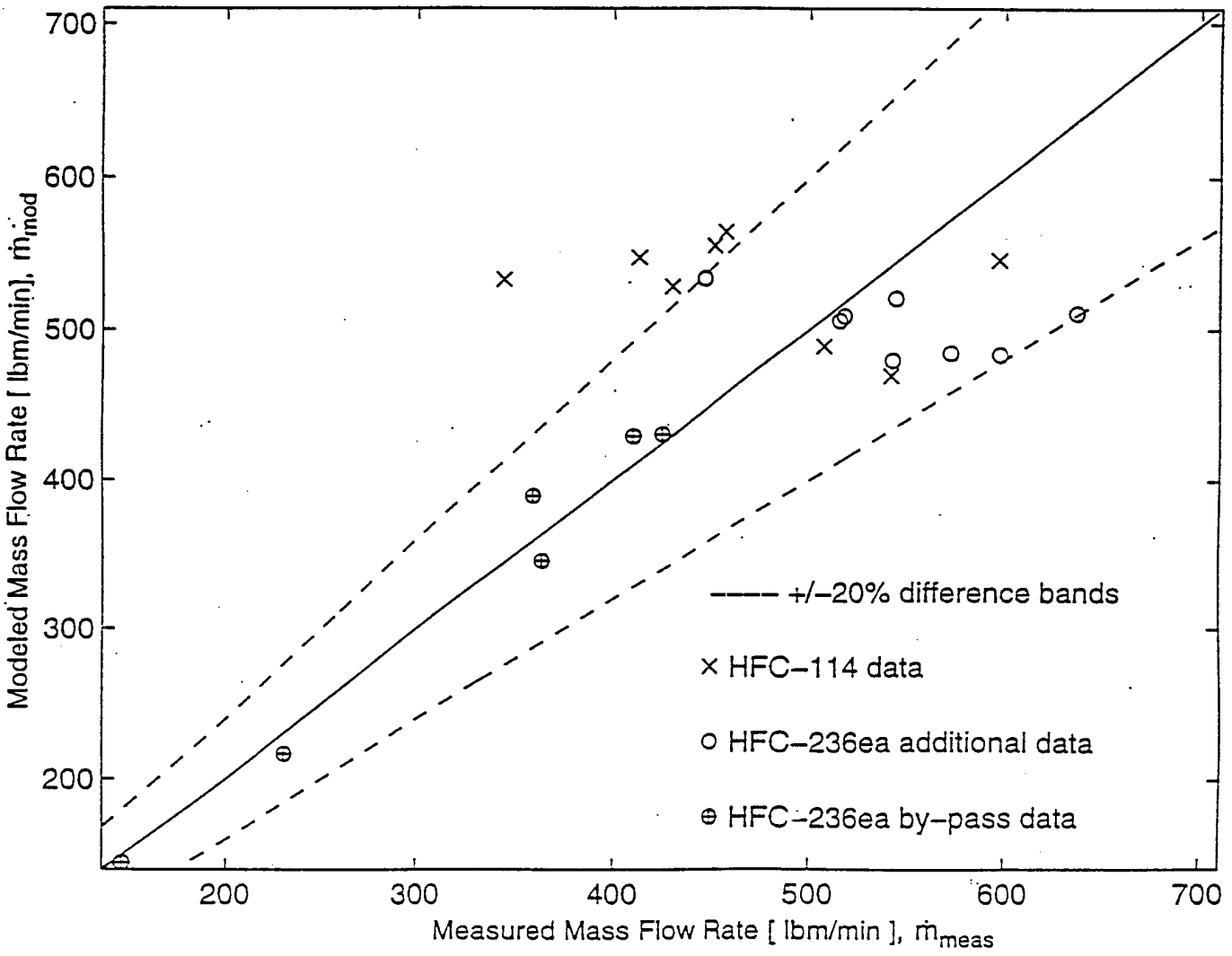

Figure 5.19. Comparison between measured and modeled flow rates for additional HFC-236ea and CFC-114 data.

The refrigerant enthalpy at the compressor exit, h_3, was modeled and used with the known compressor exit state pressure, p_3, to define the compressor exit refrigerant state. Figure 5.20 contains the comparison between modeled enthalpy and that determined from the measured set of HFC-236ea data points. The relative differences between measured and modeled compressor exit enthalpies are well within a ± 2 percent margin. There is a slight improvement in enthalpy modeling in the new compressor model compared with the enthalpy modeling results obtained in the Braun et al. (1987) optimized model analysis in Figure 5-5. It can be concluded that the model predicts the compressor exit state satisfactorily for the HFC-236 data points.

The modeled exit state refrigerant enthalpy for CFC-114 is compared with the measured compressor exit enthalpy in Figure 5.20. The CFC-114 data points are presented on the different plot because the enthalpy values for CFC-114 are lower in magnitude than those values for HFC-236ea at the same pressures and temperatures. Most of the data points are within a ± 2 percent relative difference margin. The model solution underestimates enthalpy for the entire set of CFC-114 data points when compared to the measured exit state enthalpy. It appears that there is a systematic error incorporated in the compressor model when solving for CFC-114 data points. This observation provides further evidence of the model's dependence on the refrigerant type.

The compressor exit refrigerant state temperatures for the HFC-236ea data utilized in generating the empirical relation are compared with the corresponding temperatures measured on the experimental facility in Figure 5.22. The differences between measured and modeled temperatures are well within ± 5 F. The average absolute difference between measured and modeled exit state temperatures is 0.89 F, with the largest absolute difference of 2.21 F.

The additional temperatures are plotted in Figure 5.23, indicating that the exit state temperature can be estimated well within a ± 5 F difference of the measured values. The by-pass valve open data were distinguished from the rest of data in Figure 5.23. The by-pass open HFC-236ea data had temperatures modeled well within ± 5 F of the measured temperatures, apparently a bit better than the points for which the by-pass valve was closed. This observation brings another reason to doubt the additional HFC-236ea data points for which the by-pass valve was closed. On the contrary, the CFC-114 data points showed the opposite trend. The by-pass valve open temperature data are in worse disagreement than the points having the by-pass valve closed. Again it should be emphasized that the model generates a systematic error for CFC-114 data, since the temperatures were underestimated for the entire CFC-114 data set.

The additional HFC-236ea data points had an average difference between measured and modeled temperatures of approximately 2 F, while the maximum was around 6 F. This is a quantitative evidence that the model well predicts the compressor exit state.

The CFC-114 data points indicated the average difference in the temperature model data in proximity of 5 F and the maximum difference of around 15 F.

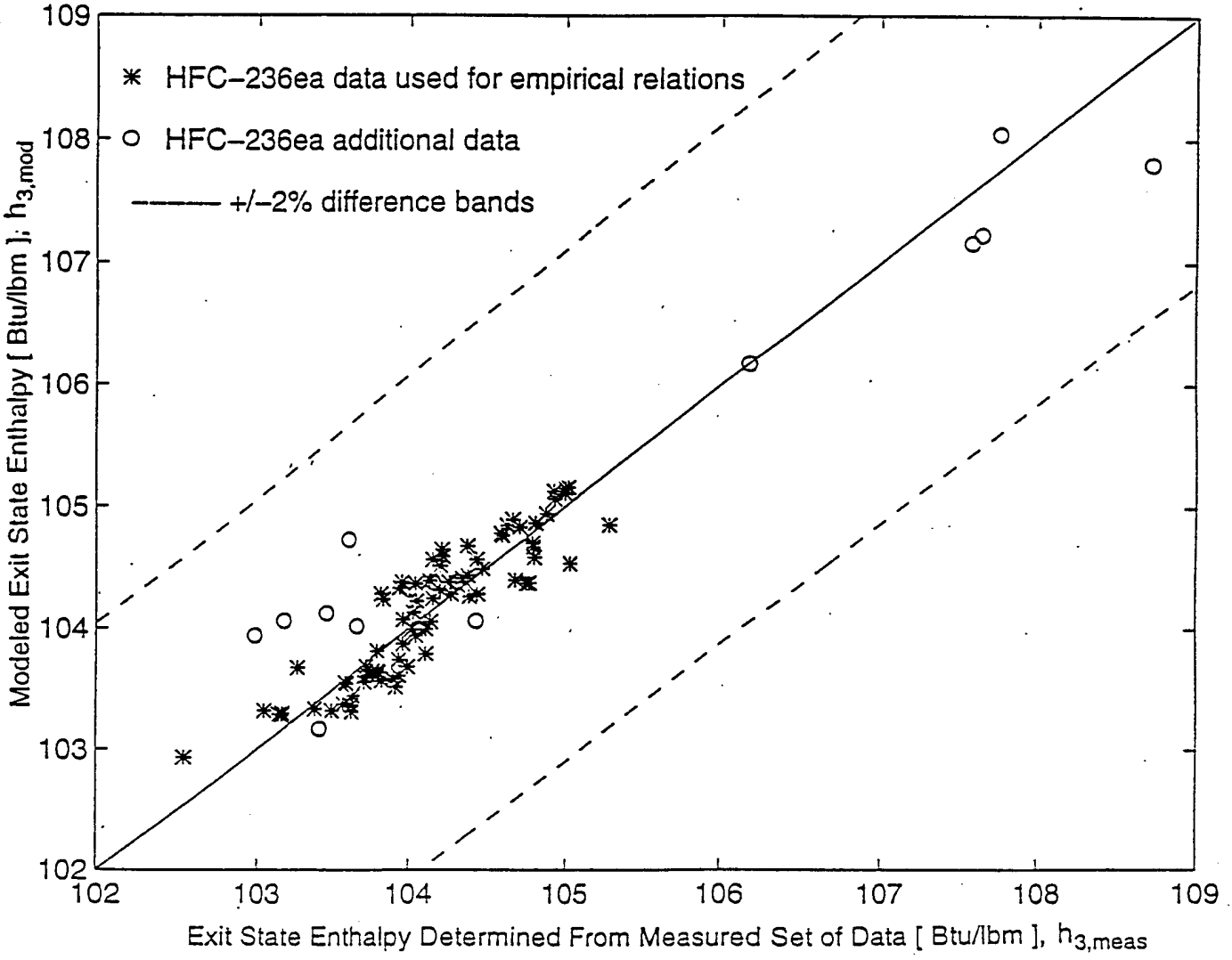

Figure 5.20. Comparison between modeled and measured exit enthalpies for HFC-236ea data.

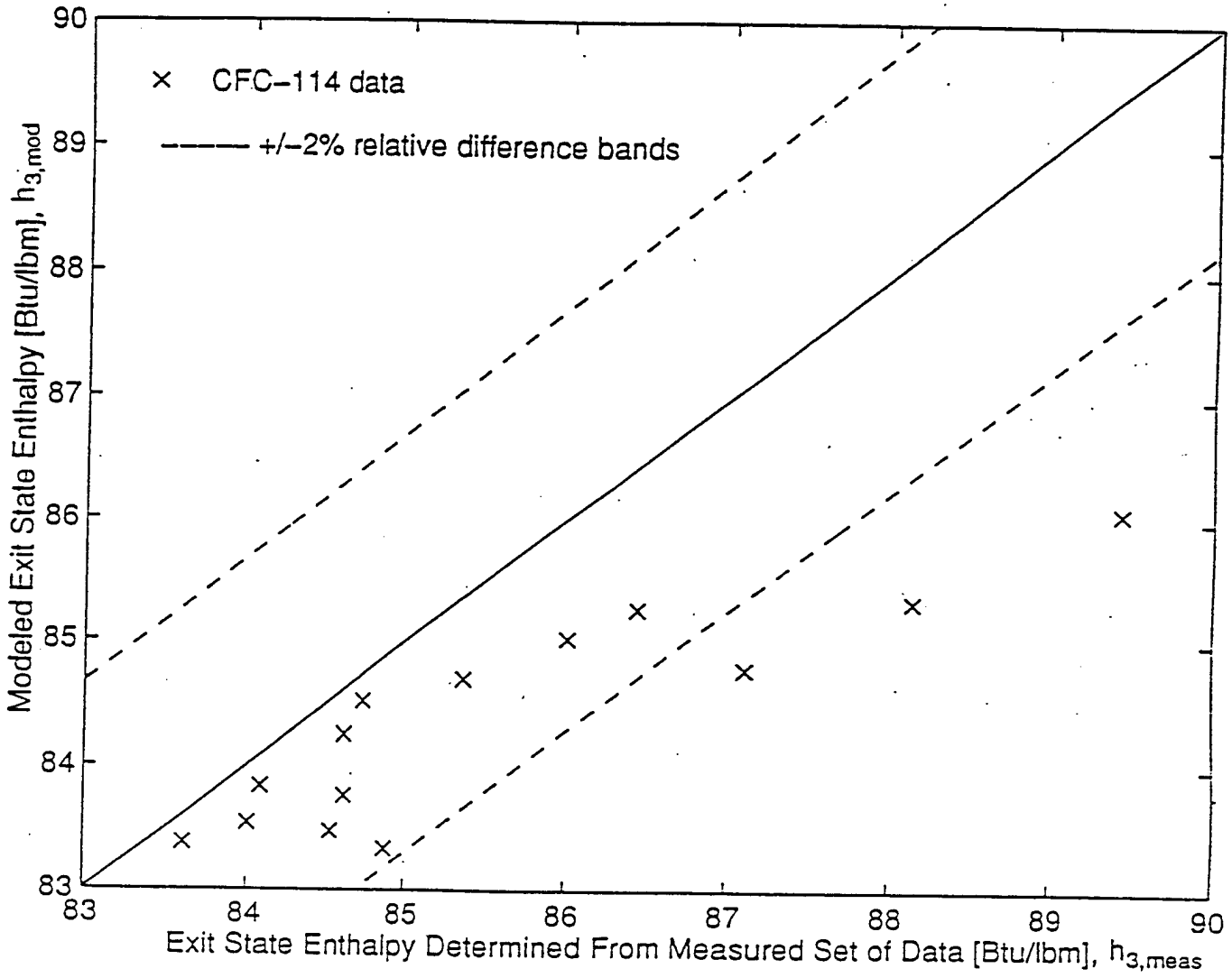

Figure 5.21. Comparison between modeled and measured compressor exit enthalpies for CFC-114 data.

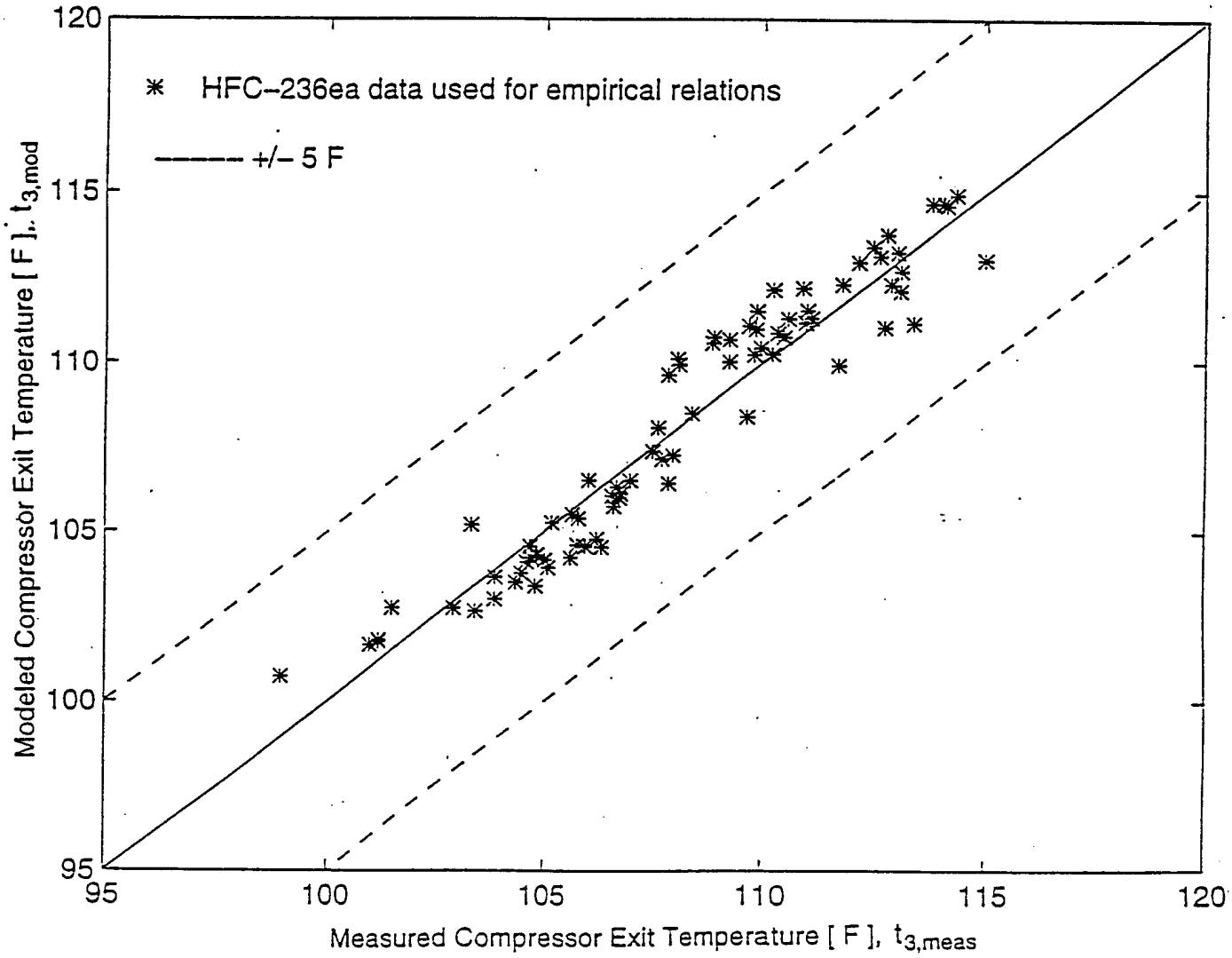

Figure 5.22. Comparison between modeled and measured exit temperatures for HFC-236ea data utilized to generate empirical relations.

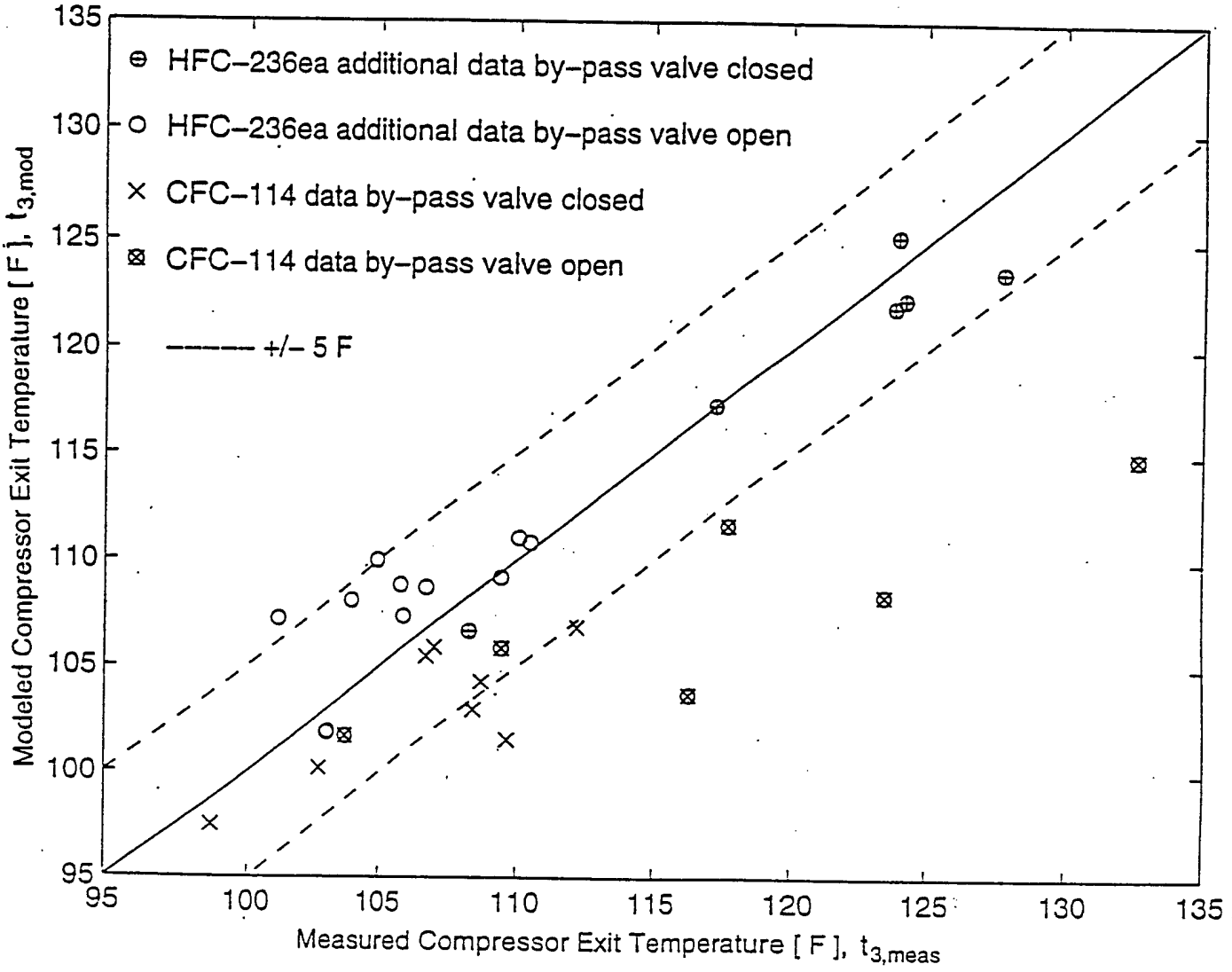

Figure 5.23. Comparison between modeled and measured exit temperatures for additional HFC-236ea data, and CFC-114 data.

The compressor shaft power was modeled within ± 10 percent relative difference between measured and modeled values for the majority of points as shown in Figure 5.24. The shaft power was well approximated as a linear function, Equation 4-1 in Section 4.4, of the product of the flow rate and enthalpy difference across the compressor. The differences occurring in the compressor shaft power modeling correspond to the differences generated in models of the mass flow rate and the exit state enthalpy. However, due to the effects of the error propagation, the observed differences in the compressor shaft power prediction are smaller than the differences in the flow rate prediction.

5.3.6. MODIFICATION OF THE SECOND EMPIRICAL RELATION

The entire experimental data set was used to plot flow coefficient versus dimensionless enthalpy in Figure 5.25 because it was suspected that the additional data points are outside the data range used for the empirical relation's generation. The functional dependence appears to be a parabolic function, which is contrary to the second empirical relation. The function used as the second empirical relation is plotted as a dashed line, while the new curve-fitted line is drawn as a continuous line on Figure 5.25. It was speculated that the new empirical relation should improve at least the exit refrigerant state prediction results. Applying the new empirical relation and using the same solver (the scheme given in Figure 5.15), the obtained solution yielded even worse results in the exit refrigerant state prediction. This illogical behavior of the compressor model solution is shown in Figure 5.26, having increased error in the refrigerant exit state temperature compared with the prediction obtained with the original empirical relation (Equation 5-29) in Figure 5-23. These observations support the assumption that there were some errors incorporated in taking some of the data.

5.3.7. BLOCKAGE FACTOR DETERMINATION

It was already assumed that the blockage factor, k_B, for the new model was 0.9. It was detected that the value of the blockage factor greatly influences the first compressor empirical relation which is presented in Figure 5.27. Reduction in the blockage factor shifts the functional dependence between isentropic efficiency and guide vane angle downward. The data show the same pattern for all different blockage factors.

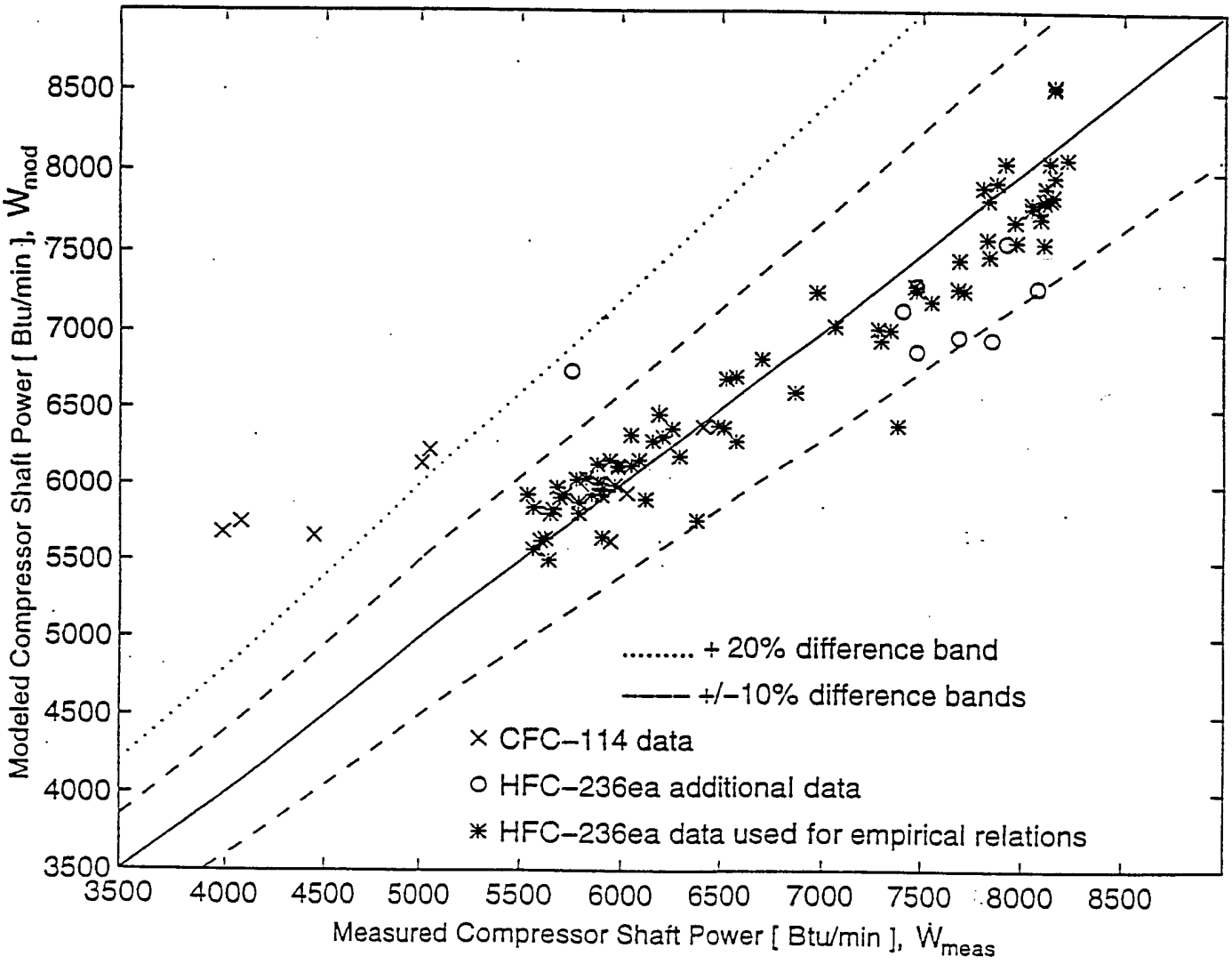

Figure 5.24. Comparison between measured and modeled compressor shaft power.

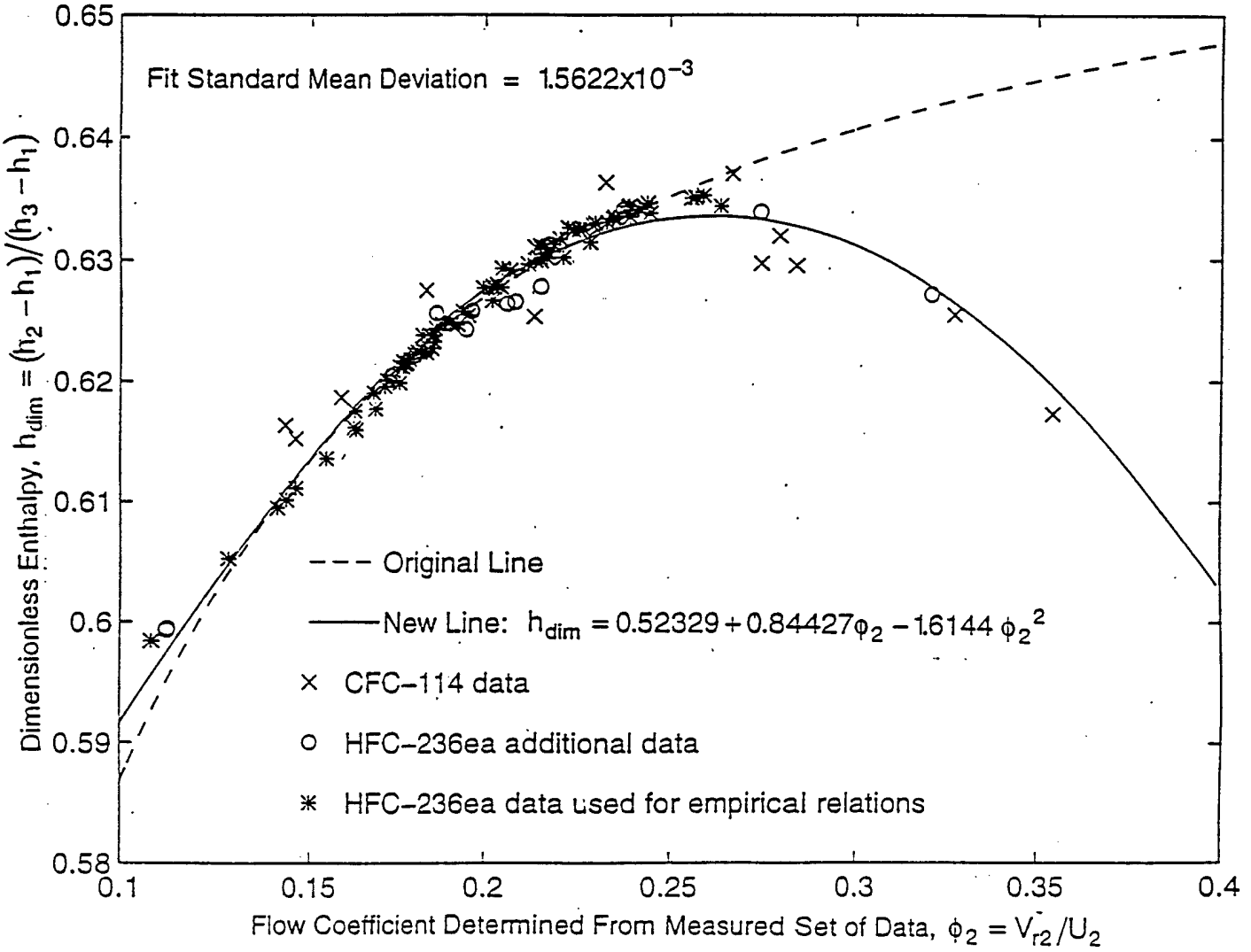

Figure 5.25. Dimensionless enthalpy as a function of flow coefficient for entire data set.

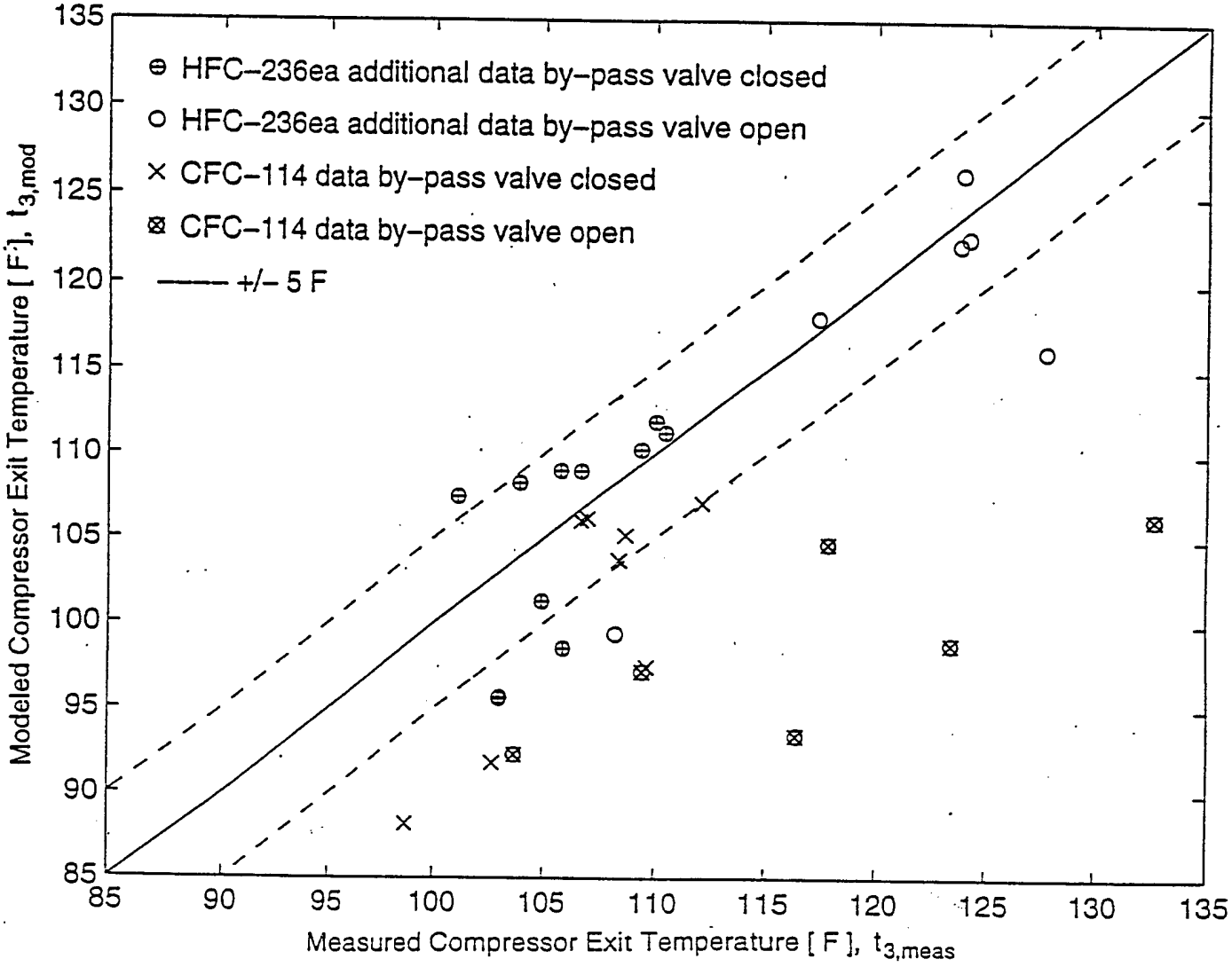

Figure 5.26. Comparison between modeled and measured compressor exit temperatures for additional HFC-236ea data and CFC-114 data in the modified model.

The blockage factor of 1 represents the case in which the effects of blade exit thickness and non-uniform impeller exit velocity profile are negligible. If a curve were fitted through the data for a blockage factor of 1 in Figure 5.27, it would be parallel to the curve-fitted line corresponding to a blockage factor of 0.9, since there is an apparent repeatability in the data pattern. The isentropic efficiency for the curve-fitted function for the blockage factor of 1 would be greater than 100 percent for the inlet guide vanes set close to the fully open position. This would represent an unreal case, since the isentropic efficiency must not be greater than 1; therefore, there is a strong indication of the necessity to account for the blockage factor in the compressor model.

The reduction of the blockage factor shifts the first empirical relation (solid curve) downward in Figure 5.27. The efficiency of the impeller operating without the influence of the inlet guide vanes was assumed to be close to, but less than, the ideal efficiency. This is a reasonable assumption since a number of authors reported impeller efficiency to be over 90 percent. The fitted line on Figure 5.27, which is the first empirical relation in the model, Equation 5-28, has the maximum isentropic efficiency of 96 percent. Therefore, the blockage factor of the 0.9 curve-fitted data was taken to be the upper acceptable limit for the first empirical relation.

A further reduction in the blockage factor shifts the isentropic efficiency to the region of negative values on Figure 5-27, which is unacceptable. Therefore, the blockage factor of 0.65 was then taken to be the lower acceptable limit.

The valid range for the blockage factor was determined to be from 0.65 to 0.9. A constrained optimization was performed on the compressor model, having the blockage factor as the only variable constrained (between values 0.65 and 0.9). The optimization objective function was the relative difference between measured and modeled mass flow rates. The optimum was found to be at a blockage factor of 0.9, but it should be mentioned that there was no substantial accuracy improvement in the flow rate prediction over the range of the valid blockage factor values.

The blockage factor of 0.9 was chosen to minimize the flow rate relative differences and to keep the first empirical relation within realistic magnitudes. The blockage factor for the Braun et al. (1987) model was optimized to a value of 0.237 in Section 5.2.3. The blockage factor of 0.9 is by far a more reasonable value than the unrealistically small value determined in the existing model, giving the new model an edge in being more physically meaningful.

5.4. REFINED NEW COMPRESSOR MODEL

A more detailed centrifugal compressor model was built on the model outlined in Section 5.3.1 of this chapter. In addition to the new model, the refined model contains the following improvements:

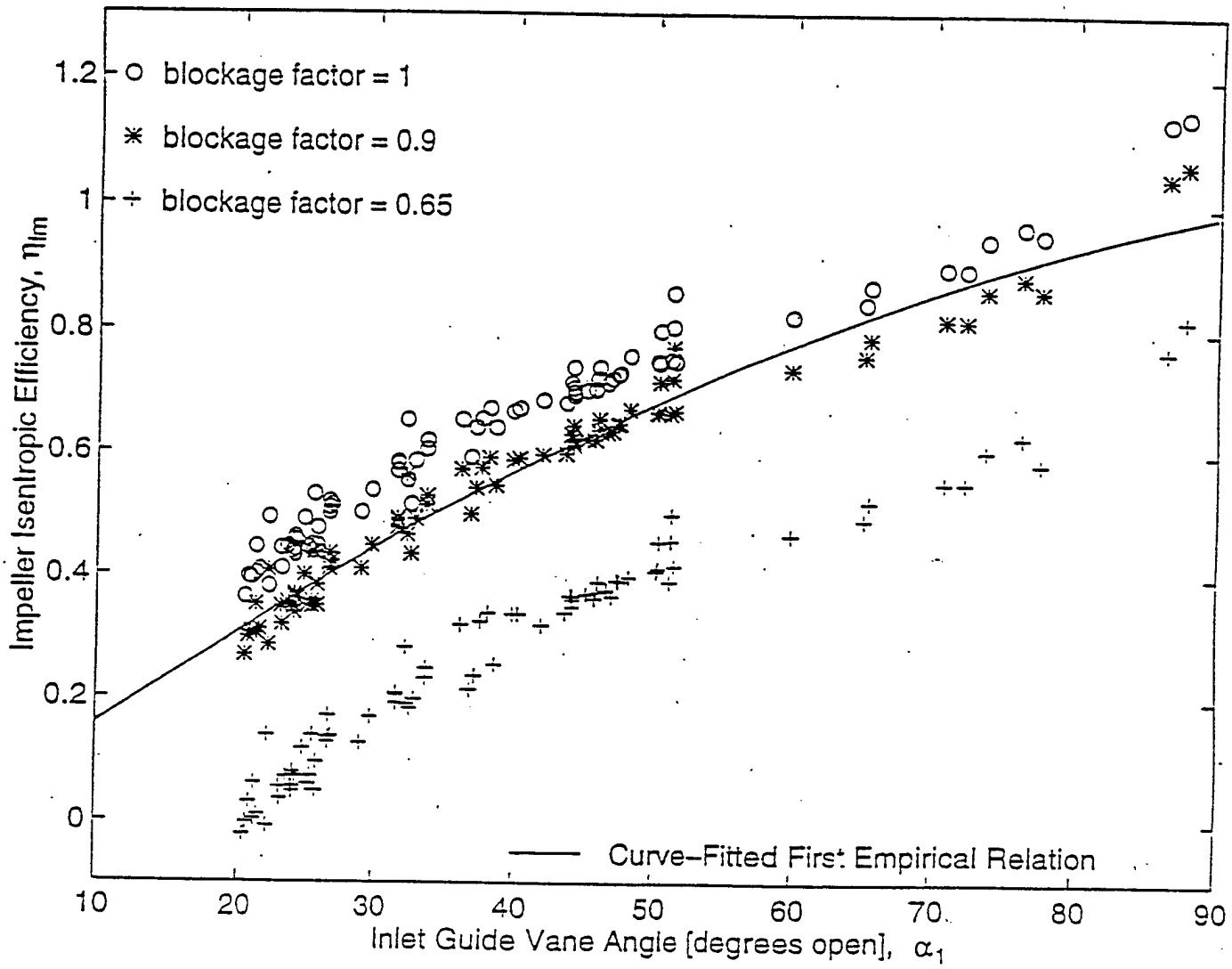

Figure 5.27. Effect of blockage factor on the first empirical relation built into the new model.

- a variable slip factor, and
- a more detailed diffuser model.

The refined model, which is given in Appendix A, is based on a two-dimensional theory developed by Dean and Senoo (1960) in which the jet and wake regions of the fluid flow are distinguished and the ratio of the flow regions, ε, is used to characterize the solution. A detailed description of this theory is given in Section 3.3.1 of Chapter 3.

The slip factor is corrected for the assumption of the jet and the wake flow regions with the correction given by Equation 3-13 in Section 3.1.4. The vaneless diffuser model developed by Johnston and Dean (1966) was utilized in this refined model. The diffuser model, described in Section 3.4.1, has friction and mixing pressure losses accounted for by the jet-wake two-dimensional theoretical approach.

The model parameters were solved by the consecutive substitution method, having all the parameters measured on the installation known. Again, two empirical relations were required in order to predict the mass flow rate and the exit state enthalpy. The empirical equations developed are of the same form as those given in Figures 5.11 and 5.14. The friction pressure loss in the diffuser accounted for approximately 3 percent of the ideal pressure rise across the diffuser for all HFC-236ea data used to construct the empirical relations. The pressure loss due to mixing of the jet and the wake regions was determined to be between 7 and 10 percent for the operating conditions investigated. These combined pressure losses correspond to the total diffuser efficiency of approximately of 90 percent, which is regarded as a reasonable value.

Having the empirical relations incorporated in the refined model, the solution was sought for the flow rate and the exit state enthalpy. A reasonable solution of the system of equations was impossible to find. Simultaneous solution of the refined model system of equations never yielded any results, or ,in the other words, the system was unsolvable. The system of equations was very sensitive. Also, it was detected that the parameters in the model have vastly different magnitudes, which usually leads to a stiff system of equations that are difficult to solve. Hence, the simultaneous solving of the system of equations was abandoned.

In addition, the consecutive substitution method of solving the system of equations did not yield reasonable solutions either. The solving order affected significantly the amount of error generated in the modeling of the parameters. Consequently, it can be stated that the error propagation was found to be a function of the solving order. For these reasons, the refined model investigation was abandoned.

Many different solving orders were attempted, and even different empirical relations were applied to the model, all with futile results. The best solution obtained from the refined model had a worse accuracy than the simpler model. However, it is reasonable to assume that the model should be a better prediction tool of the compressor performance if the solution can be found. A more powerful solver may yield a reasonable solution to the refined model; hence, the model was outlined in Appendix A. The complexity of the model appears to bring up

the problems related to the solving of large systems of equations for a questionable gain in prediction accuracy. In this case, no solution was found; hence, the model appears to be useless.

5.5 CONCLUSIONS

The Navy chiller compressor can be quite successfully depicted analytically with either of two simple compressor models. The models predict flow rate, exit state enthalpy, and the compressor shaft power within ± 20 percent of the measured values. Both models showed the following characteristics:

- several operating data points are required to develop the model parameters,
- both models were developed using the same set of HFC-236ea data points,
- either model required two empirical relations to obtain a solvable set of equations,
- both models were functions of the refrigerant type, since the CFC-114 data points run through the models had systematic errors occurring in the prediction of the compressor parameters,
- the refrigerant mass flow rate was the most sensitive parameter in the model's analysis; hence, it is the model parameter with the largest difference from the measured values, and
- both models indicated excellent prediction of the compressor exit state.

The first model (existing model) which is described in Section 5.2 was adopted from the Braun et al.(1987) chiller model. The existing model had to be optimized to obtain reasonable mass flow rate values and was adjusted to account for the inlet guide vanes's effect.

The second model (new model) presented in Section 5.3 was built on the basis of the generation of the empirical relations from the experimental data base. Two physically meaningful empirical relations were built into a theoretical model.

The new model has more physical validity than the existing model for the following reasons:

- The blockage factor in the new model was derived to be 0.9, while the existing model blockage factor was optimized to the value of 0.24. In the ideal case the blockage factor is unity and any reduction in the blockage factor accounts for the blade thickness influence on the impeller discharge area. The blockage factor value of 0.9 is by far more reasonable then the value of 0.24, since it reduces the impeller discharge area by 10 percent. In the existing model, the blockage factor must have accounted for some other compressor performance effects, diminishing the model's physical relevance.
- The existing model required the polytropic exponent and the reference polytropic efficiency to be estimated as input.

- The existing model inlet guide vane setting was introduced in the model as the flow rate correction factor, while in the new model the inlet guide vane angle was a fundamental factor upon which the model was developed.

Quantitatively, the two compressor models are compared in the Table 5.3 for several performance parameters.

Table 5.3. Quantitative comparison between two compressor models.

Comparison between measured and modeled compressor parameters	HFC-236ea data used to build empirical relations		HFC-236ea additional data points.		CFC-114 data points	
	Average *	Max †	Average	Max	Average	Max
The Existing Model						
Flow rate w/o IGV cor. [%] ‡	13.96	36.81	22.27	49.71	30.67	76.25
Flow rate IGV corrected[%] ‡	6.33	21.85	7.66	15.57	19.22	31.01
Exit state temperature [F] §	1.22	3.43	3.49	9.07	13.97	47.31
Shaft power [%] ‡	15.67	21.04	20.27	39.40	33.04	52.99
The New Model						
Flow rate prediction [%] ‡	4.45	19.51	12.57	19.84	22.84	55.08
Exit state temperature [F] §	0.89	2.21	2.13	6.11	6.21	17.81
Shaft power [%] ‡	3.13	13.38	9.26	17.22	20.54	42.61

* The mean value for a set of absolute differences between measured and modeled particular compressor parameters for the data set in question.

† The maximum absolute difference between measured and modeled particular compressor parameter for the data set in question.

‡ The comparison results are presented in terms of the absolute relative difference between measured and modeled particular compressor parameter, X, given as percentage: $\text{Difference}[\%] = \left|(X_{meas} - X_{mod})/X_{meas}\right| 100$

§ The comparison between measured and modeled compressor exit state temperatures is given in terms of absolute difference between measured and modeled temperatures in degrees Fahrenheit for the particular data set;

$$\text{Difference}[F] = \left|t_{3,meas}[F] - t_{3,mod}[F]\right|$$

From the comparison results presented in Table 5.3, it can be inferred that the new model estimates the compressor performance parameters better than the existing model. In addition to the increased physical validity of the new model, this improvement in the parameter estimation definitely classifies the new model as the better of the two.

The new model is dependent on the refrigerant type. The model represented here is developed for HFC-236ea data; hence, a different set of empirical relations should be developed for a different refrigerant operating in the same compressor. There were not enough CFC-114 data points available in this study to develop a CFC-114 model.

The new HFC-236ea model can estimate the flow rate within ± 20 percent relative difference between the measured and modeled flow rates, the exit state temperature within ± 3 F, and the compressor shaft power within ± 14 percent relative difference.

The better HFC-236ea compressor model (the new model) will be the basis for the design analysis in the next chapter.

CHAPTER 6

DESIGN STUDY

6.1. INTRODUCTION

The compressor model described in Chapter 5 includes several geometric parameters. These parameters can be defined as the compressor model design inputs. The compressor input parameters which represent different compressor operating points should be distinguished from the design inputs. The compressor operating parameters, as already described in Chapter 5, consist of: the compressor inlet state, the shaft speed, the inlet guide vane setting, and the compressor outlet pressure.

The compressor design inputs which were taken to be design variables in this analysis were: the number of impeller blades, the blade nominal tip angles, the impeller inlet and outlet diameters, and the impeller exit axial width. The compressor operating input was kept constant, while the effects of the compressor design parameter variation were investigated on the compressor output. Such an analysis may suggest alteration in the compressor design to enhance the compressor performance. Each design parameter was varied individually, keeping the other compressor design parameters and the compressor operating input constant.

Five compressor output performance parameters were considered to be significant. The compressor or impeller performance is characterized by the work coefficient and the impeller exit pressure. The flow rate represents another vital compressor performance parameter. The exit state enthalpy was investigated to check the overall performance of the compressor and to indicate its influence on the changes in the compressor shaft power, which was the fifth performance parameter investigated.

Three characteristic HFC-236ea data points were taken into consideration for the purpose of this design analysis. The representative points presented in Table 6.1 were chosen based on the following conditions:

- data for the inlet guide vane (IGV) setting are well spread over the entire range of IGV settings, and
- data indicated low prediction errors in the compressor model analysis.

Table 6.1. Representative data nomenclature.

	Inlet Guide Vane (IGV) Position [degrees open]	Pressure Ratio	Data Labels in the Plots of Chapter 6
1	20.63	3.51	*
2	45.91	4.19	o
3	76.27	4.35	+

The inlet guide vane (IGV) setting was considered to be an important compressor operating parameter, characterizing the particular data point. Having the representative data spread over the entire range of IGV settings, the effects of IGV setting on design analysis were observable.

In the following four sections of this chapter, following nomenclature has been adopted:

- Compressor actual design parameters are labeled as the nominal design parameters, i.e. X_{nom}.
- The variation of the design parameters were plotted on the abscissa in all figures in Chapter 6 in terms of the relative design parameter. A particular design parameter, X, is expressed in terms of the nominal design parameter, X_{nom} ; therefore, the relative design parameter is defined as X/X_{nom} . The relative design parameter is one when the design parameter is equal to the nominal design parameter.
- Since the compressor manufacturer treats compressor design parameters as confidential, the actual design parameter values are not disclosed, but are presented here in terms of the relative design parameters.
- The analyzed compressor performance parameter behavior as function of the variation in the design parameters is plotted on the ordinate. Figures in this chapter contain marked compressor nominal case points for each representative data point. The nominal case points are shown as intersections of dotted lines. The abscissa has the relative design parameter of one while the ordinate values are given as the magnitudes of the compressor parameters as they are measured on the compressor.
- The inlet guide vane (IGV) angle is inversely related to the amount of the flow throttling; therefore, the larger the IGV angle, the less flow throttling occurs.

6.2. NUMBER OF IMPELLER BLADES

The number of impeller blades was introduced in the model through the expression for the slip factor. Slip factor is discussed in Section 3.1.4 of Chapter 3 and analytically defined by Equations 3-9 through 3-11. The slip factor value from Equation 3-9 is related to the number of blades. As the number of blades approaches infinity, the slip factor approaches unity. A large number of blades could be regarded as the ideal flow with no

slippage present if only the slip factor equation (Equation 3-9) is considered. Realistically, the number of blades has to be limited to allow refrigerant flow though the compressor and also to prevent large friction losses.

The estimate of slip factor was incorporated in the compressor model in Section 5.3.1 by Equation 5-23 in which the slip factor simply represents the sum of the work coefficient and the flow coefficient for a constant impeller exit tip angle.

The work coefficient, μ_2, plotted in Figure 6.1 as a function of relative number of blades, Z/Z_{nom}, indicates that an increase in the number of blades corresponds to an increase in the work coefficient. The compressor performance is directly related to the compressor work coefficient. As the number of blades increases, there is a better physical contact between the impeller and the fluid, yielding better impeller performance.

As observed on Figure 6.1, the throttling of the refrigerant flow with the inlet guide vanes results in a decrease in the work coefficient. The points labeled with stars correspond to the data with the most flow throttling, while the points labeled with pluses had the least flow throttling. The differences between these characteristic points is greatest in the vicinity of the compressor nominal case.

Since the compressor model solution behaved as expected regarding the compressor work coefficient, one might anticipate that the flow coefficient would indicate the same trend. On the contrary, increasing the slip factor (number of impeller blades) causes a decrease in the flow coefficient. The flow coefficient is directly related to the flow rate and inversely related to the refrigerant density at the impeller exit state (see Equation 5-19). Variations of the flow coefficient will be analyzed in terms of these two parameters.

Refrigerant mass flow rate, $\dot{m}$, which is directly related to the compressor flow coefficient (Equation 5-19), is plotted as a function of the number of blades in Figure 6.2. A decrease in flow rate is observed as the number of blades increases. It is realistic to assume that an increase in the number of impeller blades would choke the flow, hence reducing it. The change in flow rate magnitude is very significant for small variations in the number of impeller blades from the nominal case. The plot indicates that the removal of a few blades would increase the flow rate through the impeller considerably.

As expected, the plot also indicates that increasing the guide vane angle setting (i.e., increasing the opening for flow) results in larger refrigerant flow rates.

The compressor mid-state pressure, p_2, has a positive gradient with the number of impeller blades. The position of the nominal case in Figure 6.3. indicates that an increase in the number of impeller blades will not produce a significant pressure increase across the impeller, because the nominal case is located close to the asymptotic value of the maximum impeller exit pressure for the given operating input. This indicates that the number of impeller blades was designed to be near the optimum.

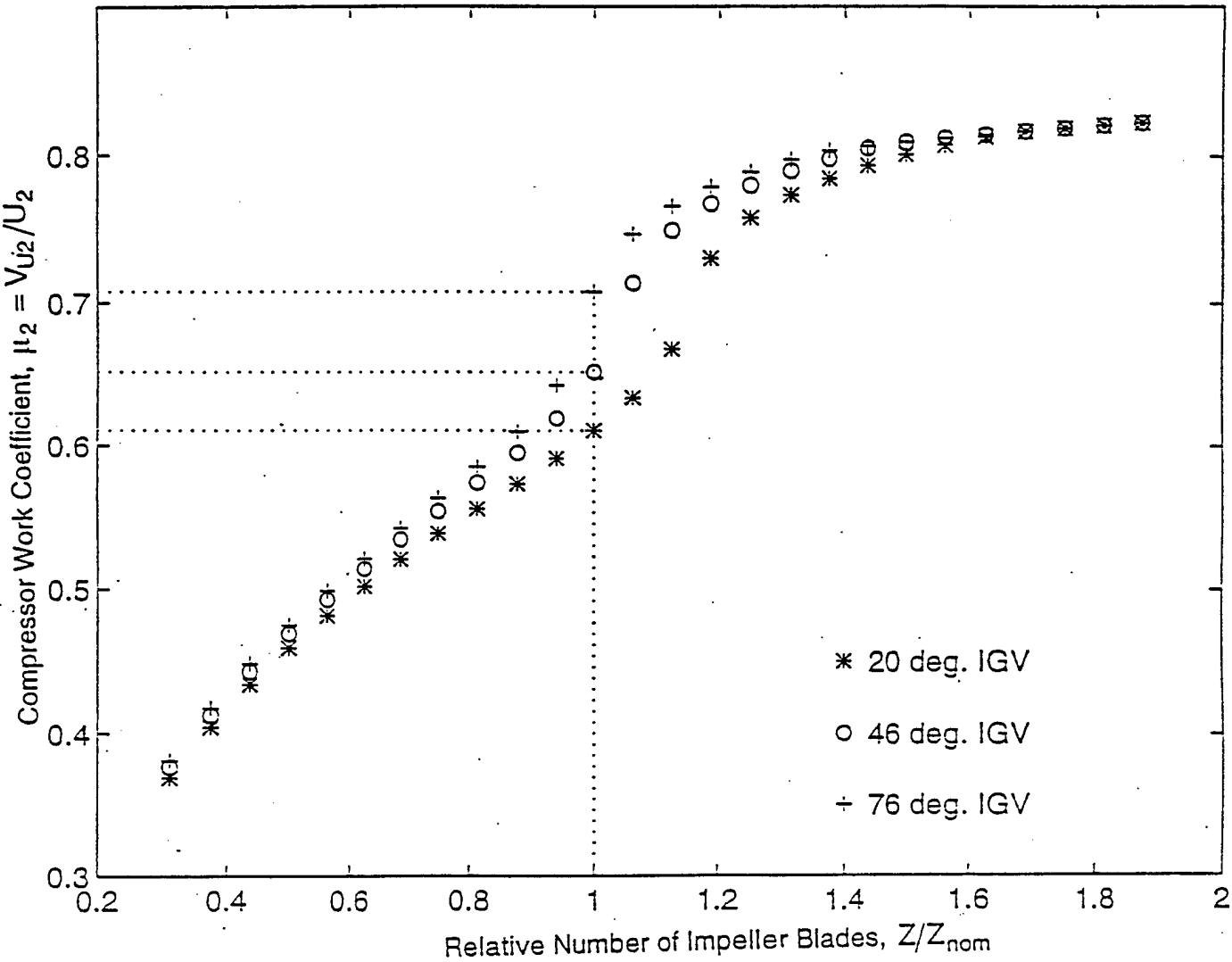

Figure 6.1. Impeller work coefficient as a function of the number of blades.

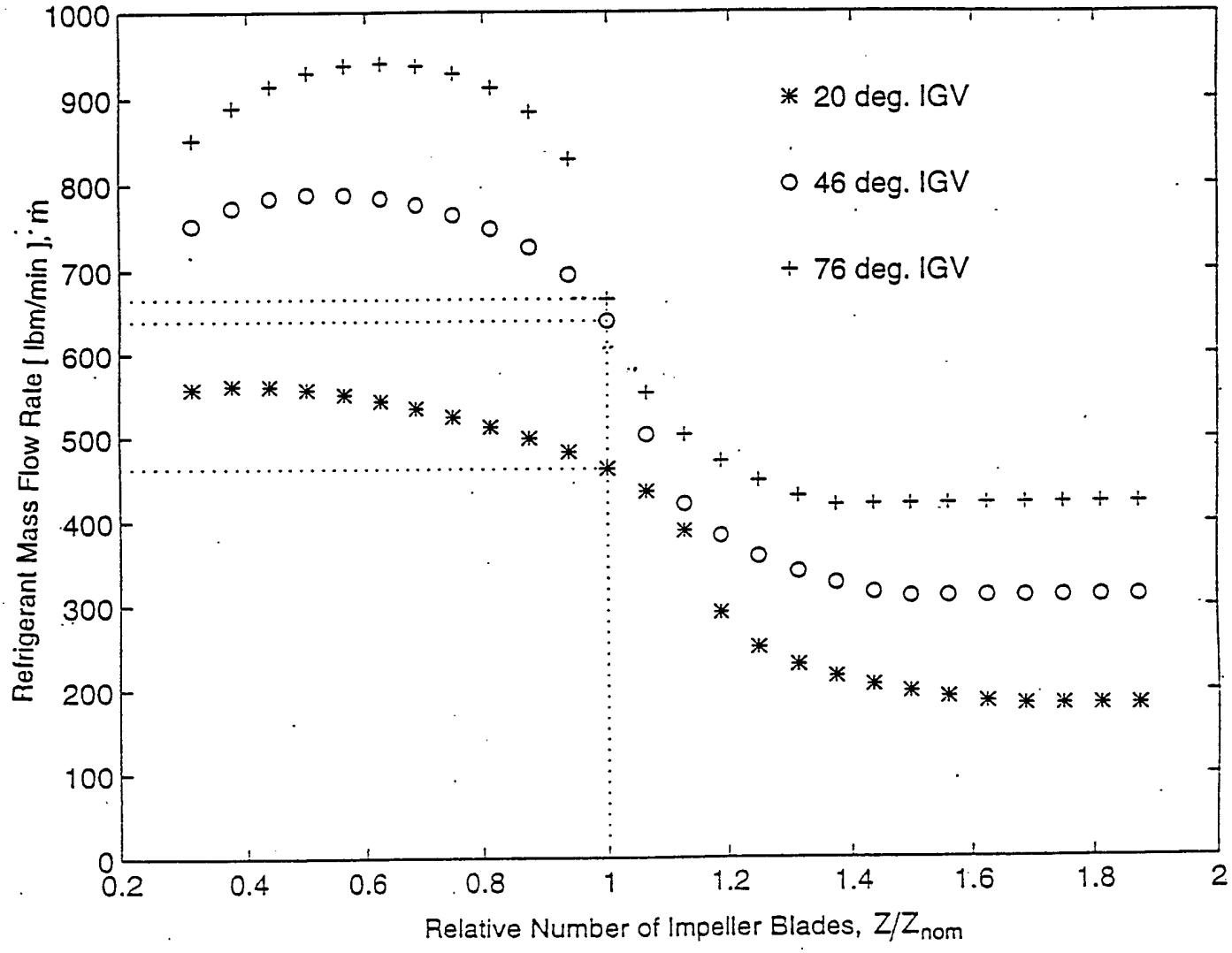

Figure 6.2. Refrigerant mass flow rate as a function of the number of blades .

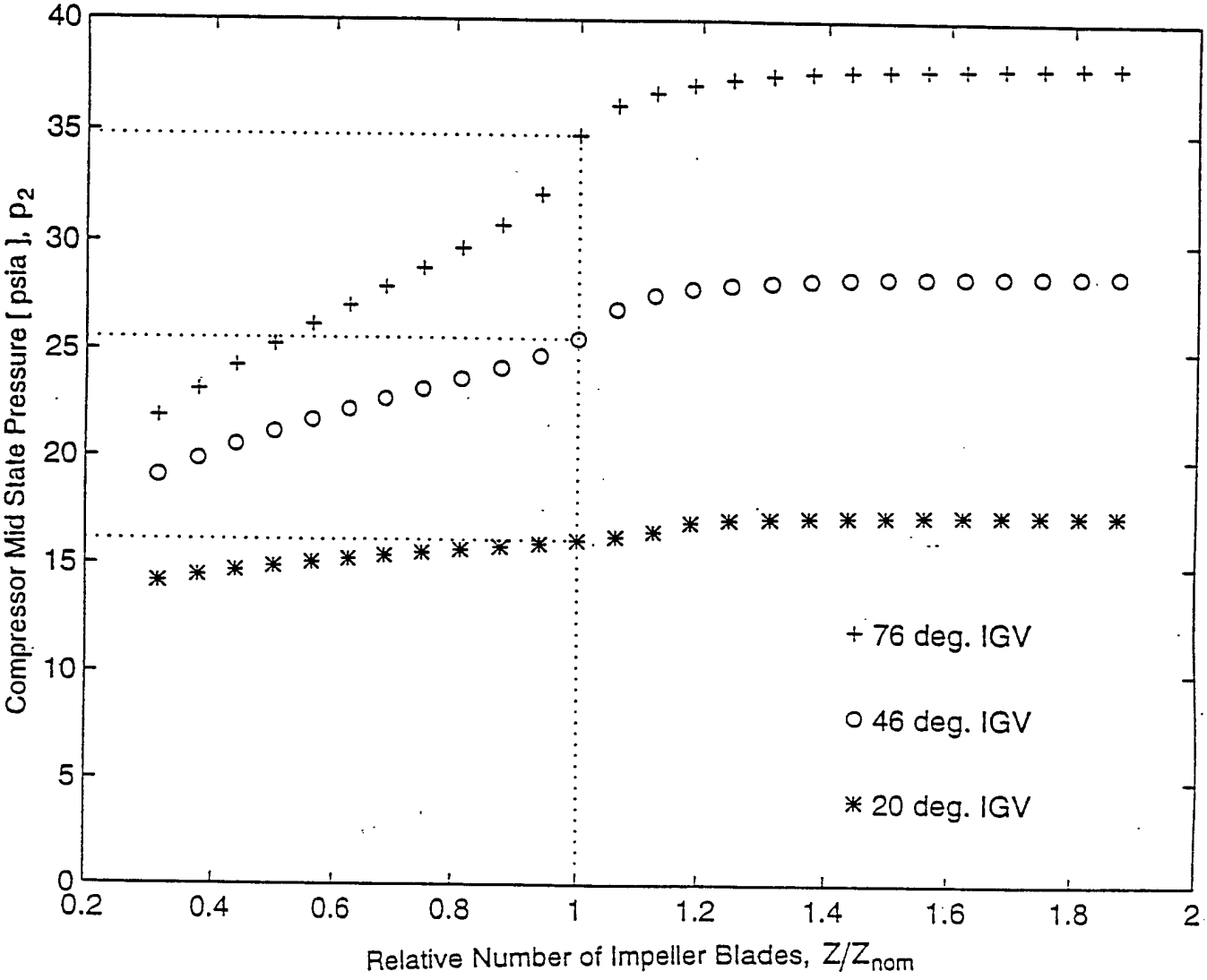

Figure 6.3. Impeller exit state pressure as a function of the number of blades.

The amount of inlet flow throttling influences the amount of pressure change. The mid-state pressure variation diminishes with an increase in the flow throttling as the number of blades is reduced.

Pressure is proportional to density for a compressible fluid if temperature is roughly constant. In addition to the reduction in the flow rate, there is an increase in the mid-state density as the number of blades increases. Both trends observed in the parameters on Figures 6.2 and 6.3 contribute to reduction of the flow coefficient, which can be seen from analysis of Equation 5-19.

The flow coefficient is reduced with an increase in the number of blades. The reduction in the flow coefficient is related to the reduction in the compressor mass flow rate and increase in the pressure across the impeller. These observations are in agreement with an ideal compressor performance chart in which the largest pressure rise is obtained for the smallest flow rate. Since the functional dependence of pressure rise and flow rate is negatively sloped, pressure rise becomes zero for a certain limiting flow rate.

The influence of the variation in the number of blades, or the slip factor value, on the exit state enthalpy is presented in Figure 6.4. There is a slight positively sloped relation between the compressor exit enthalpy and the number of blades. However, the figure indicates that the enthalpy change is not very large for the range of the number of impeller blades investigated. The total change in the exit enthalpy is less than five percent from the nominal case values marked as the intersection of the dotted lines in Figure 6.4. It appears that by increasing the number of blades the exit state enthalpy asymptotically approaches some maximum value. The functional dependence pattern in Figure 6.4 is very similar to the pattern observed in the behavior of the work coefficient with a change in the impeller blade number, Figure 6.1. This suggests that the work coefficient and the exit enthalpy have related behavior.

Compressor shaft power is plotted as a function of the number of impeller blades in Figure 6.5. As already explained in Chapter 4 (Equation 4.1), the shaft power is directly proportional to the total energy transferred to the refrigerant, which is the flow rate multiplied by the enthalpy difference across the compressor. Therefore, the compressor shaft power is directly affected by the variation of the flow rate and the compressor exit enthalpy for a constant inlet enthalpy. As observed in Figure 6.5, shaft power is more affected by a change in the flow rate than a change in the exit enthalpy, since the functional pattern resembles the pattern from Figure 6.2.

In summary, the number of blades is directly related to the slip factor. An increase in slip factor improves impeller performance, which is demonstrated by the variation in compressor work coefficient in Figure 6.1 and the pressure at the impeller exit in Figure 6.2. At the same time, the compressor flow coefficient drops considerably due to the increase in the compressor mid-state density and a significant reduction in the flow rate (Figure 6.3). The compressor exit enthalpy for constant exit pressure is directly related to the slip factor, as shown in Figure 6.4. The compressor shaft power is more affected by changes in flow rate than by variations in the compressor exit enthalpy.

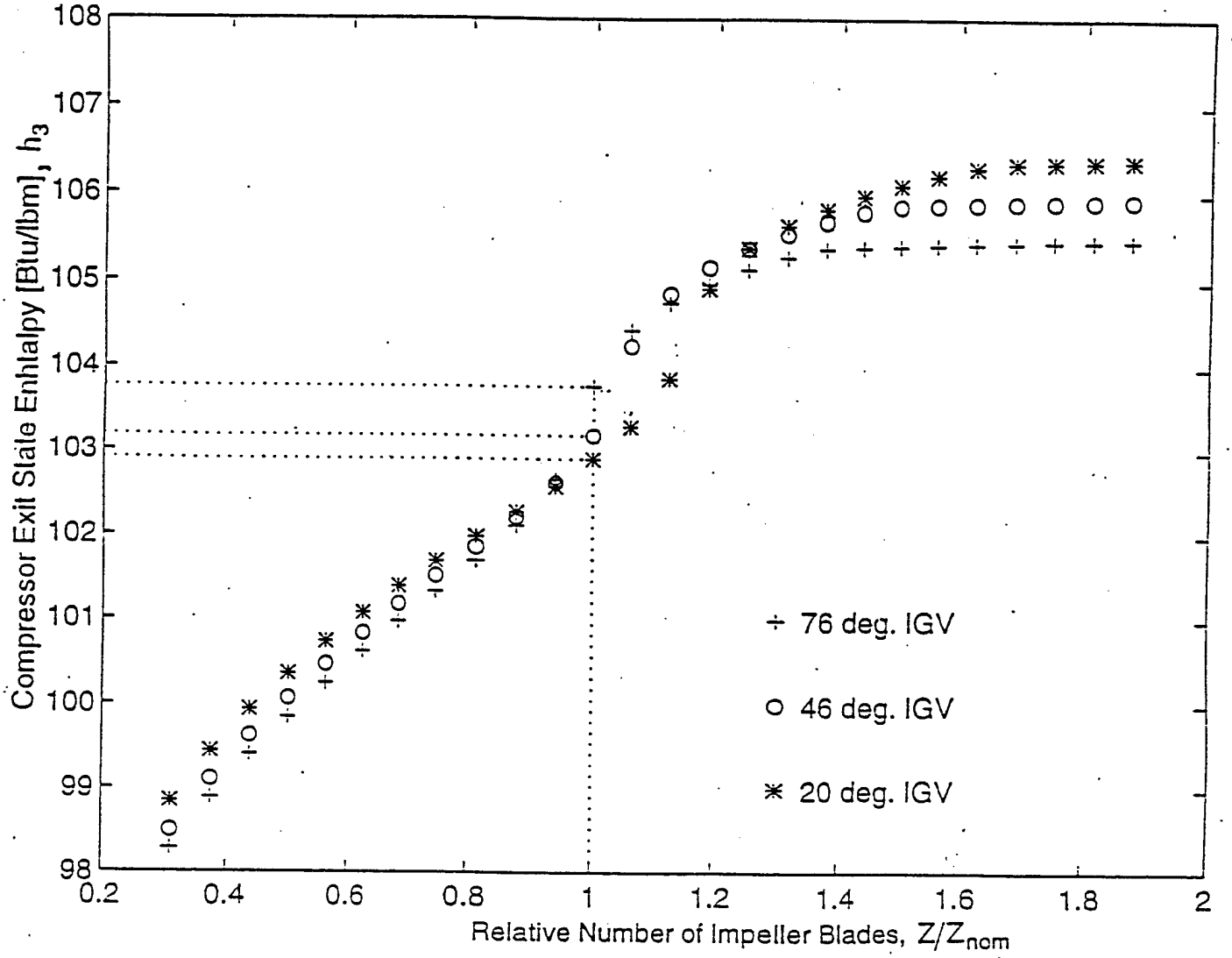

Figure 6.4. Compressor exit state enthalpy as a function of the number of blades.

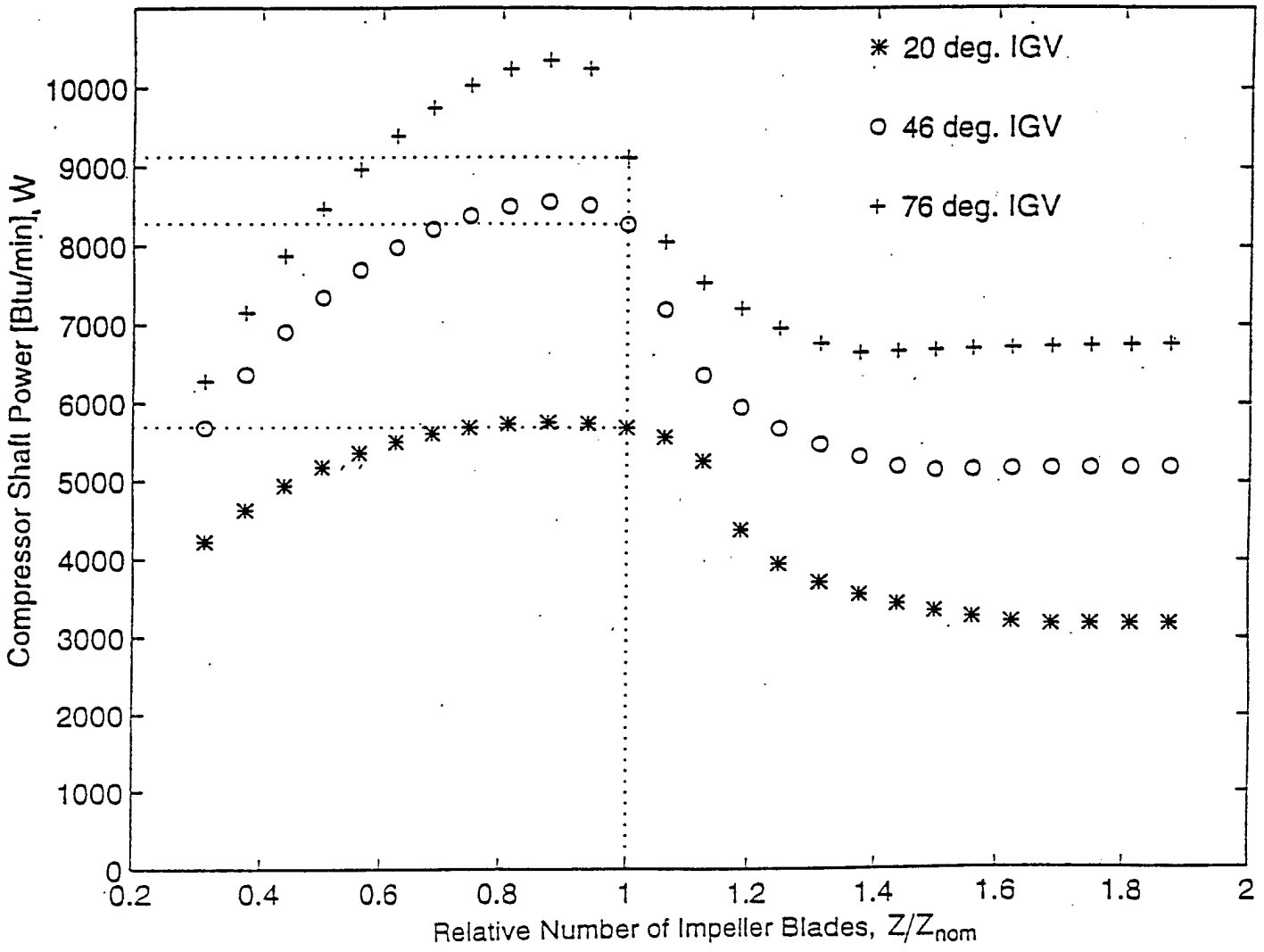

Figure 6.5. Compressor shaft power as a function of the number of blades.

The design analysis based on the compressor suggests that a slight improvement in compressor performance might be achieved if the number of blades were increased by 10 percent. According to the model, this impeller alteration would bring approximately a 10-percent increase in the work coefficient, a 1 to 2 psi pressure rise at the impeller exit, a 15-percent flow rate reduction, and a similar relative drop in the compressor shaft power.

The impeller performance appears to deteriorate drastically with a reduction in the number of blades from the nominal value in Figure 6.1. Conversely, on increasing the number of impeller blades, a much less dramatic effect is observed. An impeller with a smaller number of blades would have a larger flow rate, with the maximum flow rate occurring for approximately the 0.7 relative number of blades. Nevertheless, a higher flow rate is not necessarily desirable, especially with significant deterioration in the compressor performance.

6.3. BLADE TIP ANGLES

6.3.1 INLET BLADE TIP ANGLE

Inlet blade tip angle, β_1, which was introduced into the compressor model by Equation 5-16 in Section 5.3.1, affects the magnitude of the refrigerant inlet velocity. Variation of this parameter did not produce any significant effects on any of the investigated compressor performance parameters. Since the inlet blade tip angle affects only the magnitude of the fluid inlet velocity, which is relatively small compared with the impeller exit velocity, it was reasonable to expect that the impeller inlet tip angle would have a negligible influence on the overall compressor performance.

Design consideration should be given to the inlet guide vane tip angle since it influences the magnitude of the compressor choked flow (Section 3.1.4). Blade tip angle also plays an important role in the interaction between the impeller and incoming refrigerant flow. However, this effect on the overall compressor performance is not detectable by the current compressor model.

6.3.2 OUTLET BLADE TIP ANGLE

The impeller outlet blade tip angle, β_2, is a very important design parameter in the compressor model developed, since it affects the estimated value of the slip factor, Equations 3-9 through 3-11 given in Section 3.1.4, and it is present in the slip factor definition in Equation 5-23.

The blade tip angle is presented in terms of the relative blade tip angle in Figures 6-6 through 6-10 which is the ratio of the blade tip angle to the actual blade tip angle (nominal case), $\beta_2/\beta_{2,nom}$.

The slip factor is inversely related to the blade tip angle; thus, as the blade tip angle is increased, the slip factor decreases for a constant number of impeller blades. As already concluded in Section 6.2, impeller performance improves with an increase in the slip factor. Pursuing this logic, the results presented in Figure 6.6, in which the work coefficient is plotted as function of the outlet blade tip angle, appear to be spurious since the work coefficient is positively sloped with the increase in the blade tip angle. However, as noted above the blade tip angle also plays a role in the definition of the slip factor, Equation 5-23, being inversely related to the slip factor. Apparently, the influence of the blade tip angle on the slip factor as expressed in Equation 5-23 prevails and the net effect is that blade tip angle is positively sloped relative to impeller performance as shown in Figure 6.6.

It should be noted that a reduction in the exit blade tip angle causes the impeller performance to deteriorate significantly, while increasing the blade tip angle leads to a much less significant improvement in compressor performance. Apparently compressors with larger blade tip angles have better performance, eventually approaching the radial blade impeller that is known from a theoretical analysis of the energy transfer in the impeller to be superior (Shepherd, 1956). Compressor impellers are designed as backswept (with the angles less than 90 degrees) due to design limitations such as huge velocities at the impeller exit and stability of compressor operation. With these considerations, an optimum impeller blade tip angle is usually sought.

Similar to the analysis in Section 6.2, the blade tip angle was chosen by the manufacturer to be close to an optimum value. The nominal case is located close to the beginning of a large gradient in the functional dependence of the compressor work coefficient on the blade tip angle. Any further reduction in the blade tip angle from the nominal case would cause a drastic drop in the impeller performance as suggested in Figure 6.6. Also in Figure 6.6, the effect of the inlet guide vane setting appears to be greatest in the vicinity of the nominal case though it is quite insignificant.

The pressure rise across the impeller indicates a similar trend with variation of the blade tip angle as does the compressor work coefficient. The curves presented in Figure 6.7 show a significant pressure drop as the blade tip angle is reduced, and a relatively small raise in the compressor mid-state pressures as the blade tip angle increases. Also, the influence of the inlet guide vane (IGV) setting has a substantial influence on the impeller exit pressure, as already noted with reference to Figure 6.3.

The flow coefficient is inversely related to the blade tip angle, as already noted in the design analysis for the number of impeller blades in Section 6.2. As shown in Figure 6.8., the mass flow rate decreases and then levels out as the exit blade tip angle increases above the nominal value.

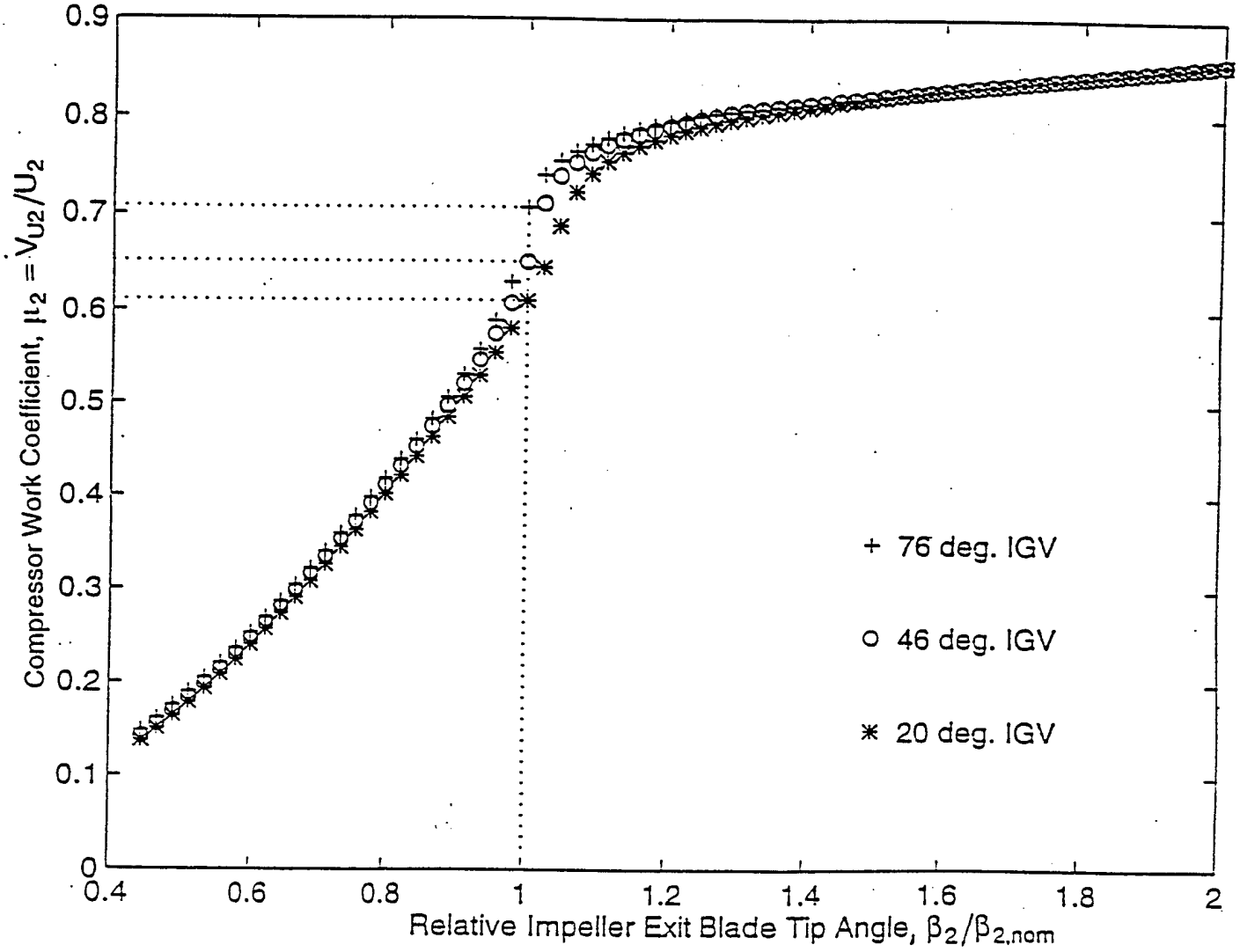

Figure 6.6. Impeller work coefficient as a function of impeller exit blade tip angle.

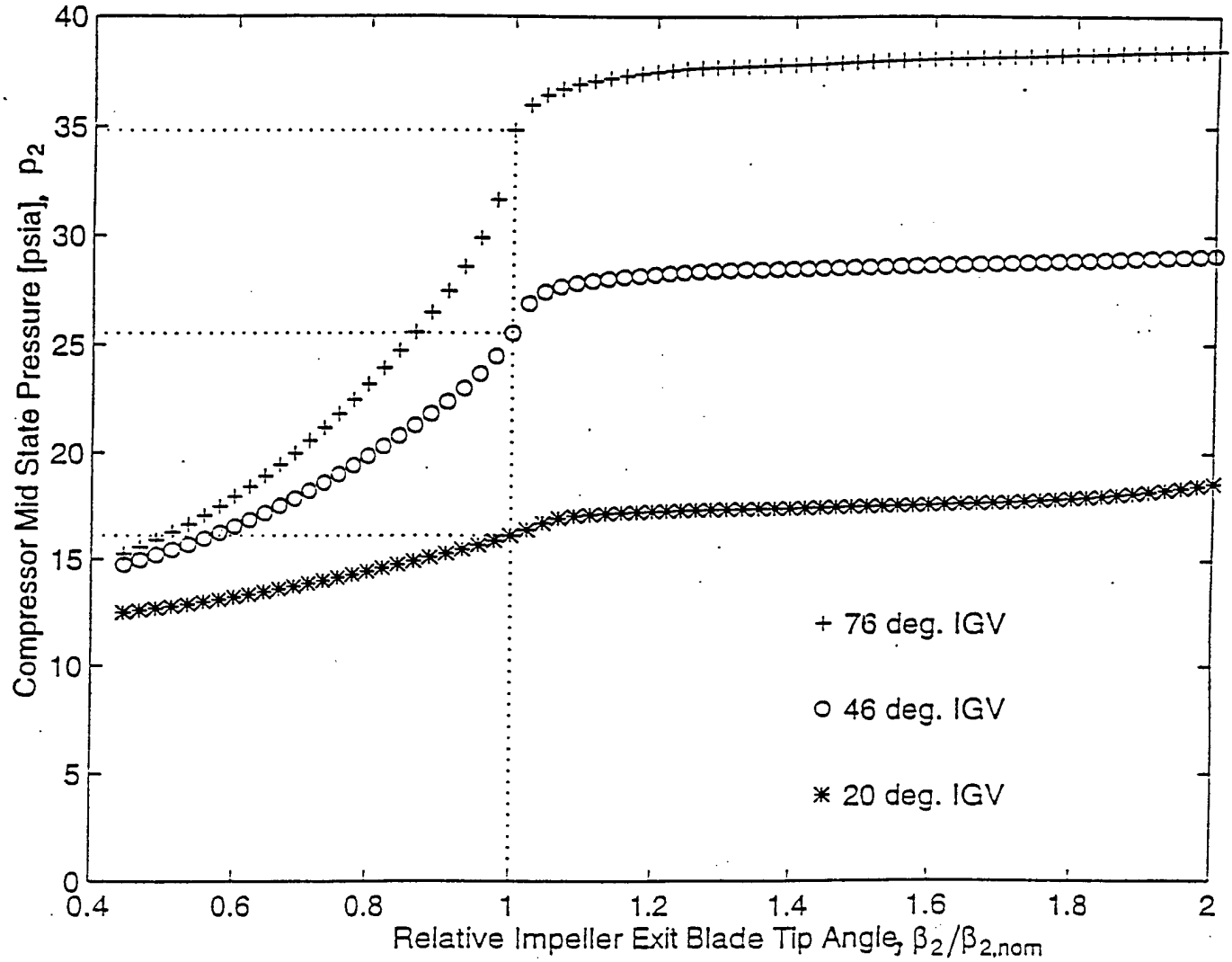

Figure 6.7. Impeller exit state pressure as a function of impeller exit blade tip angle.

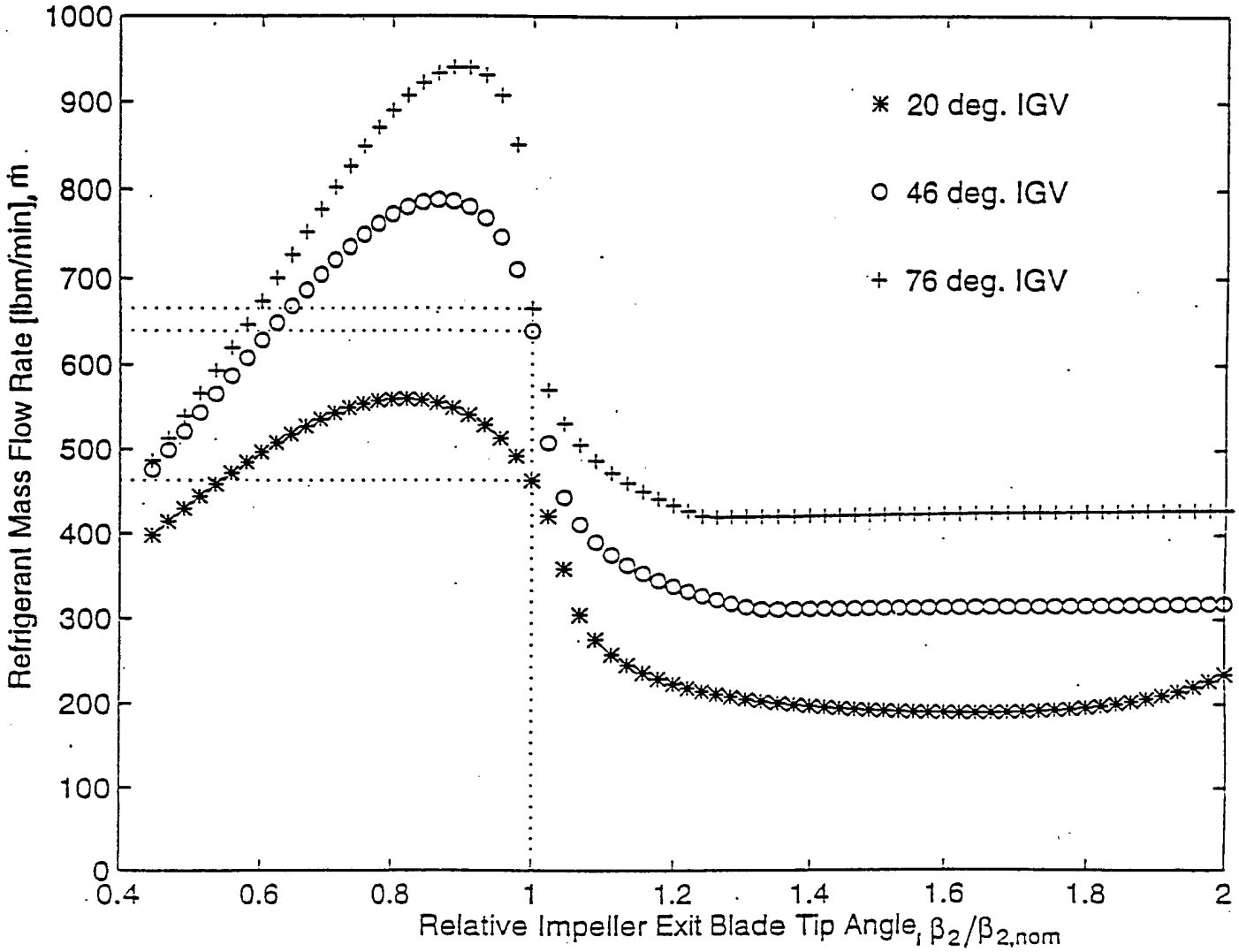

Figure 6.8. Refrigerant mass flow rate as a function of impeller exit blade tip angle.

The behavior of the mass flow rate as the blade tip angle is reduced is intriguing. It appears that there is a maximum flow rate corresponding approximately to the relative exit blade tip angle of 0.9. This observation implies that a small reduction (not larger than 10 percent in this case) of the blade tip angle would greatly increase the flow rate. However, a problem may arise related to compressor stability, since increased flow rate may shift the compressor operating point toward the region of choked flow.

A similar functional behavior is observed for all three inlet guide vane angles in Figure 6.8. Thus, the inlet guide vane angle does not affect the flow rate trend, just its magnitude.

The compressor exit enthalpy increases continually with increasing impeller exit blade tip angle, as shown in Figure 6.9. The pattern in Figure 6.9 is almost the same as the pattern observed in Figure 6.4, in which exit enthalpy was plotted versus the impeller blade number. When the blade tip angle decreases from its nominal value, the exit enthalpy decreases rapidly and appears to be independent of the inlet guide vane angle. For increasing blade tip angle, the curves flatten out but still indicate an increasing trend. Also, the curves diverge somewhat for different inlet guide vane angles and the enthalpy increases are inversely related to the size of the inlet guide vane setting.

The flow rate variation shown in Figure 6.8 is a predominant factor in the changes observed in the compressor shaft power in Figure 6.10. A similar behavior was observed in the design analysis of the impeller blade number in Section 6.2. Figure 6.10 shows that a reduction in the compressor shaft power may be achieved as the blade tip angle is increased slightly.

Similar trends in the investigated parameters are observed with variation of the blade tip angle as with the impeller blade number. According to the present analysis, the nominal blade tip angle appears to be well chosen. The results suggest that a slight increase in the blade tip angle might enhance impeller performance, but with a potentially significant drop in the flow rate.

6.4 IMPELLER DIAMETERS

The effects of the impeller diameters are introduced in the model through the impeller linear velocities (see Section 5.1.3); hence, they influence magnitudes of the velocity vectors substantially. From the literature review presented in Chapter 3, it is recommended that the inlet diameter (hub diameter) be as small as possible, and the outlet diameter be as large as possible. The inlet diameter is limited by the shaft size, while the outlet diameter is limited by the large refrigerant velocities developed at the impeller exit tip that can cause deterioration in the impeller performance due to occurrence of a shock wave.

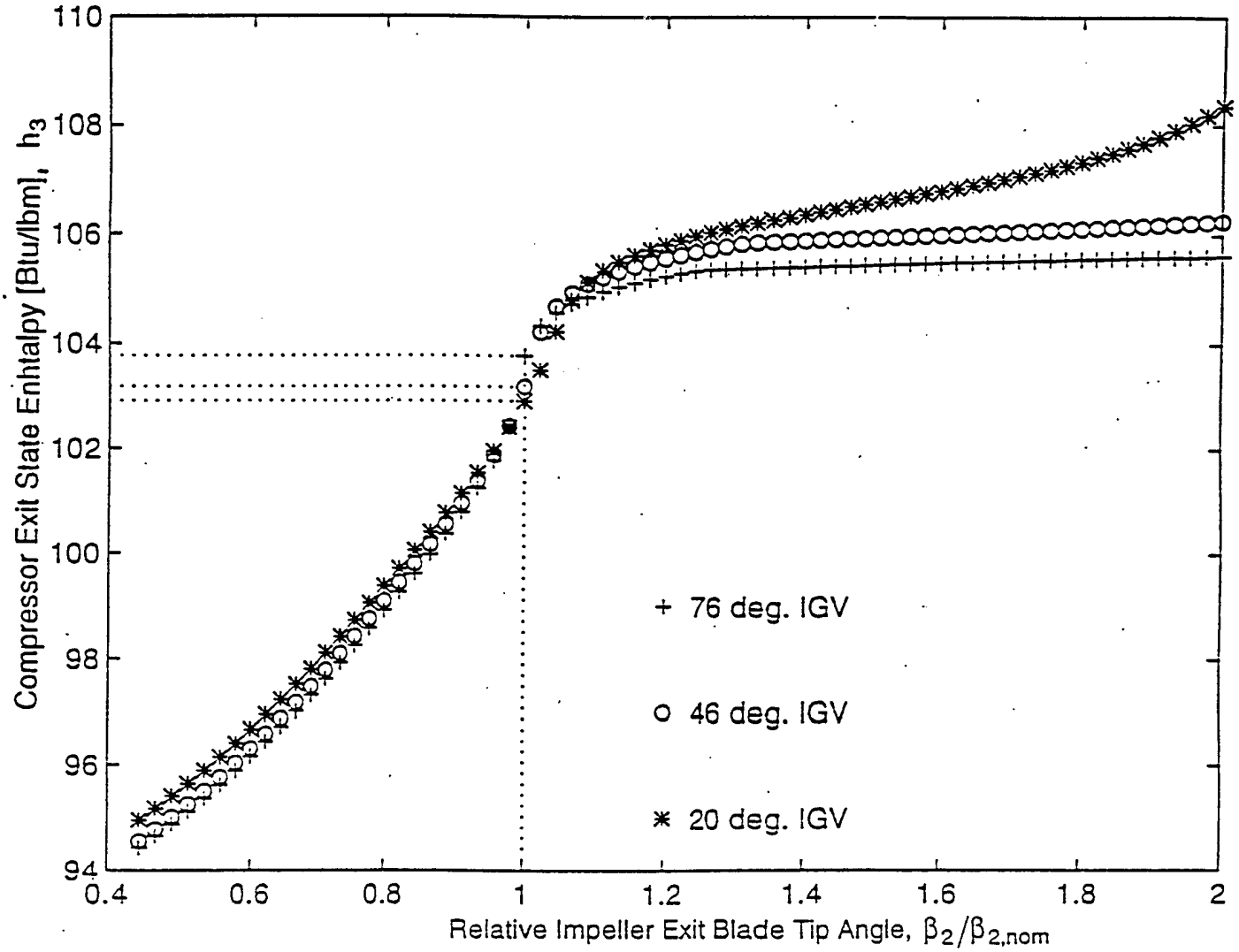

Figure 6.9. Compressor exit state enthalpy as a function of impeller exit blade tip angle.

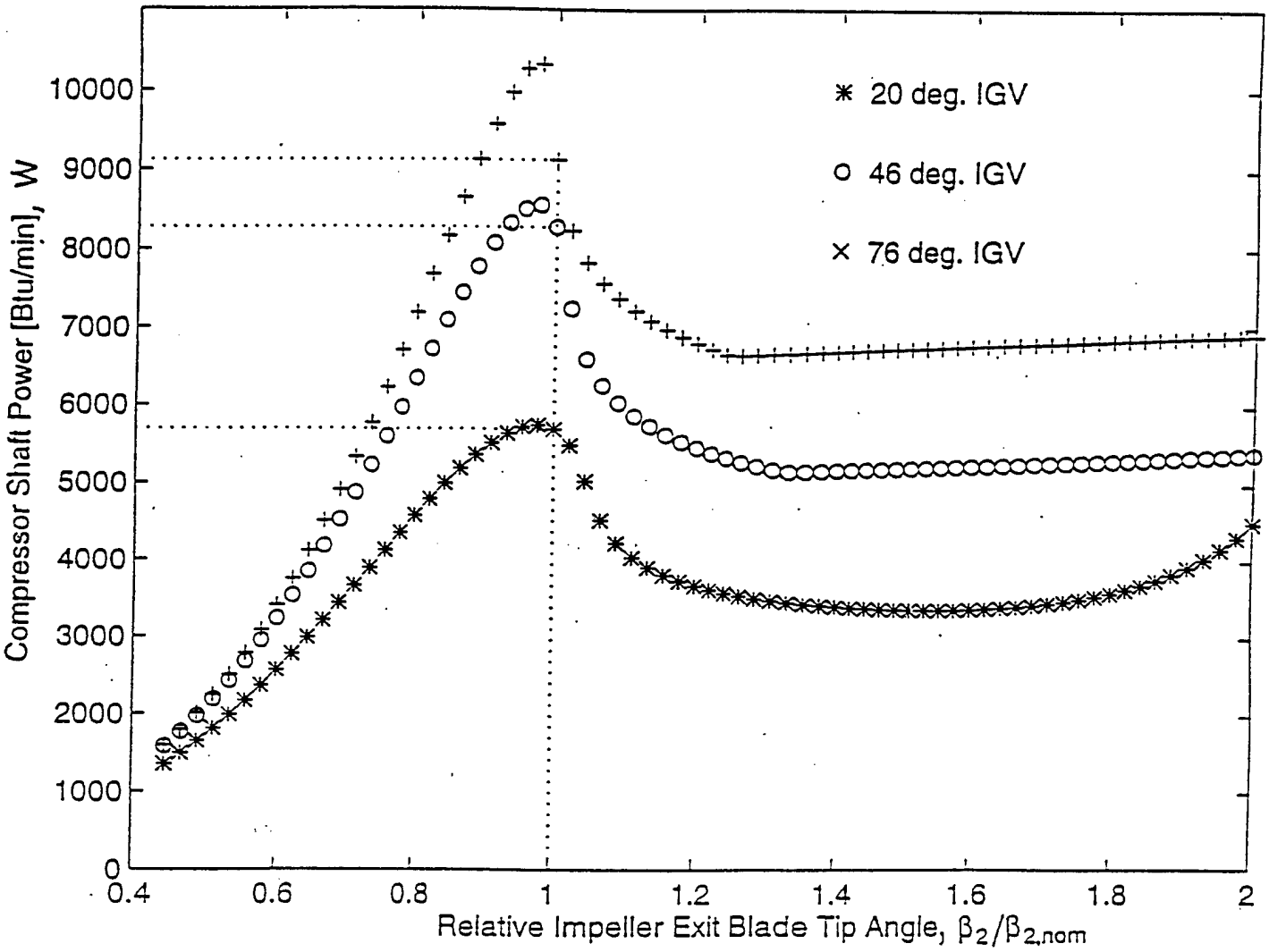

Figure 6.10. Compressor shaft power as a function of impeller exit blade tip angle.

6.4.1 IMPELLER INLET DIAMETER

The impeller inlet diameter, d_1, affects the inlet impeller tip velocity that is calculated at the impeller hub diameter. The impeller inlet linear velocity is directly proportional to the impeller inlet diameter and contributes to the magnitudes of the inlet velocity vectors given in Equations 5-16 and 5-17 in Section 5.3.

The Euler equation (Equation 3-2) indicates that an increase in the inlet velocity would reduce the amount of energy transfer to the refrigerant across the impeller. However, an increase in the inlet impeller diameter improves compressor performance, as suggested in Figure 6.11, where the work coefficient, μ_2, is plotted against the relative inlet impeller diameter, $d_1/d_{1,nom}$. This observation implies that even though the total amount of energy transferred decreases, the impeller performance is enhanced slightly except for the data corresponding to the IGV setting of 20 degrees.

Changes in the work coefficient are relatively small, asymptotically approaching minimum and maximum values on either end in Figure 6.11. The influence of the inlet guide vane angle setting is remarkable, because there is even a very small negative gradient observed for data with the lowest inlet guide vane setting. The influence of the inlet diameter on the impeller performance diminishes as the flow throttling is intensified.

Very insignificant, 10 percent or less, variations are observed in the compressor mid-state pressure in Figure 6-12, implying that the inlet impeller diameter size does not have any significant effect on the compressor mid-state pressure.

The refrigerant flow rate shows the expected trend in Figure 6-13, because the compressor performance improves as the flow rate decreases. This normal trend was observed in all design analysis so far in this chapter, proving that the model indicates a good physical behavior.

A physical interpretation of reduction of the flow rate with an increase in the impeller inlet diameter is that the effective flow cross sectional area diminishes allowing less refrigerant to pass through the impeller. Flow throttling affects changes in the mass flow rate as shown in Figure 6-13, having the largest gradient for the data point with the least throttling (76 degrees IGV) while having no gradient for the data with the most flow throttling.

The compressor exit enthalpy has a small positive gradient with the inlet impeller diameter, but the changes are negligibly small. Therefore, the plot of the exit state enthalpy versus the impeller inlet diameter was excluded. Also the compressor shaft power as a function of the impeller inlet diameter was not presented here, as it shows the same trend as the flow rate variation in Figure 6.13.

The overall influence of the inlet diameter is not substantial on the compressor performance. The compressor performance can be slightly improved by an enlargement in the inlet diameter but at a substantial drop in the flow rate. The flow rate is the compressor parameter that is most affected by the variation of the design parameters, indicating that the flow rate prediction represents the most sensitive part of the compressor model.

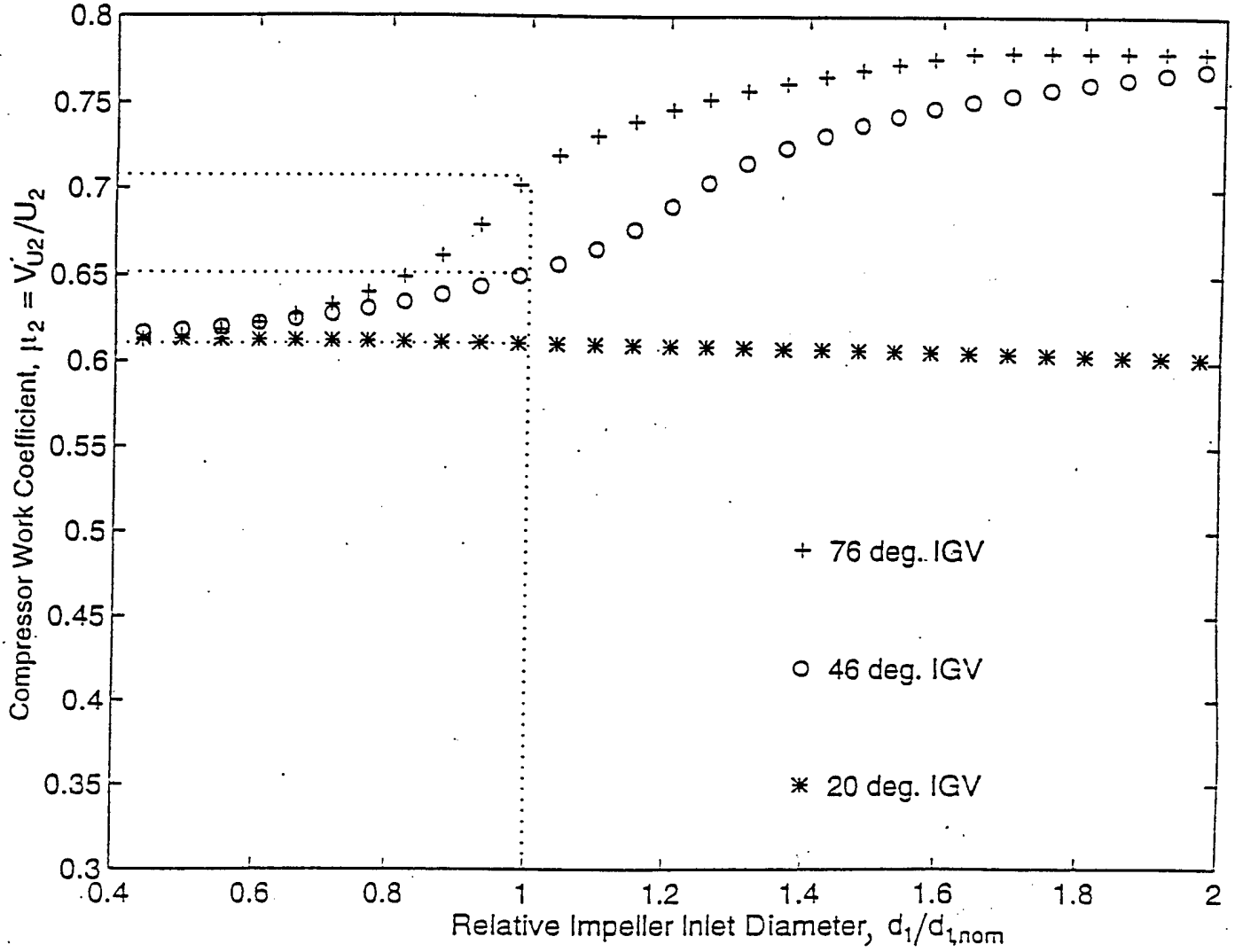

Figure 6.11. Impeller work coefficient as a function of impeller inlet diameter.

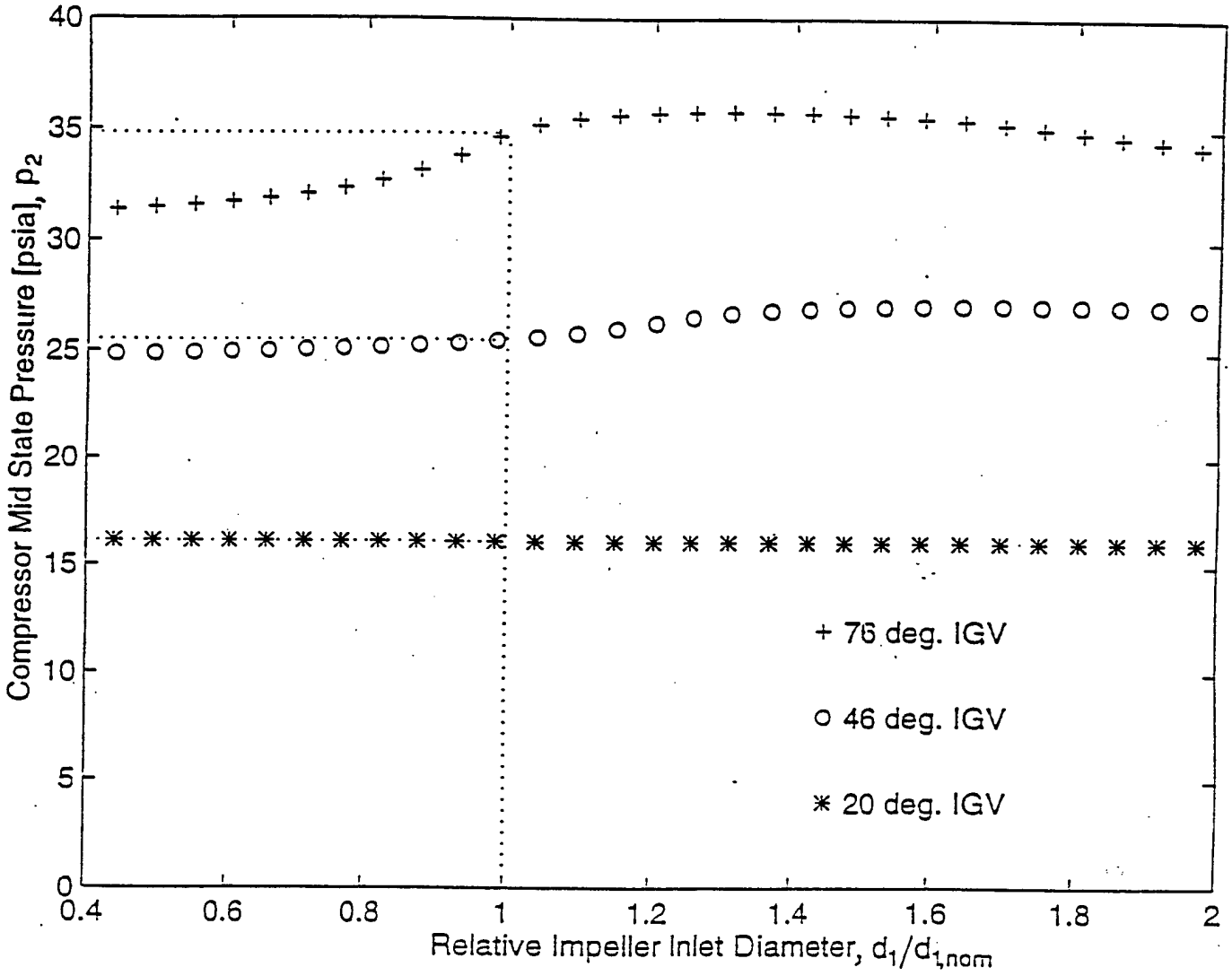

Figure 6.12. Impeller exit state pressure as a function of impeller inlet diameter

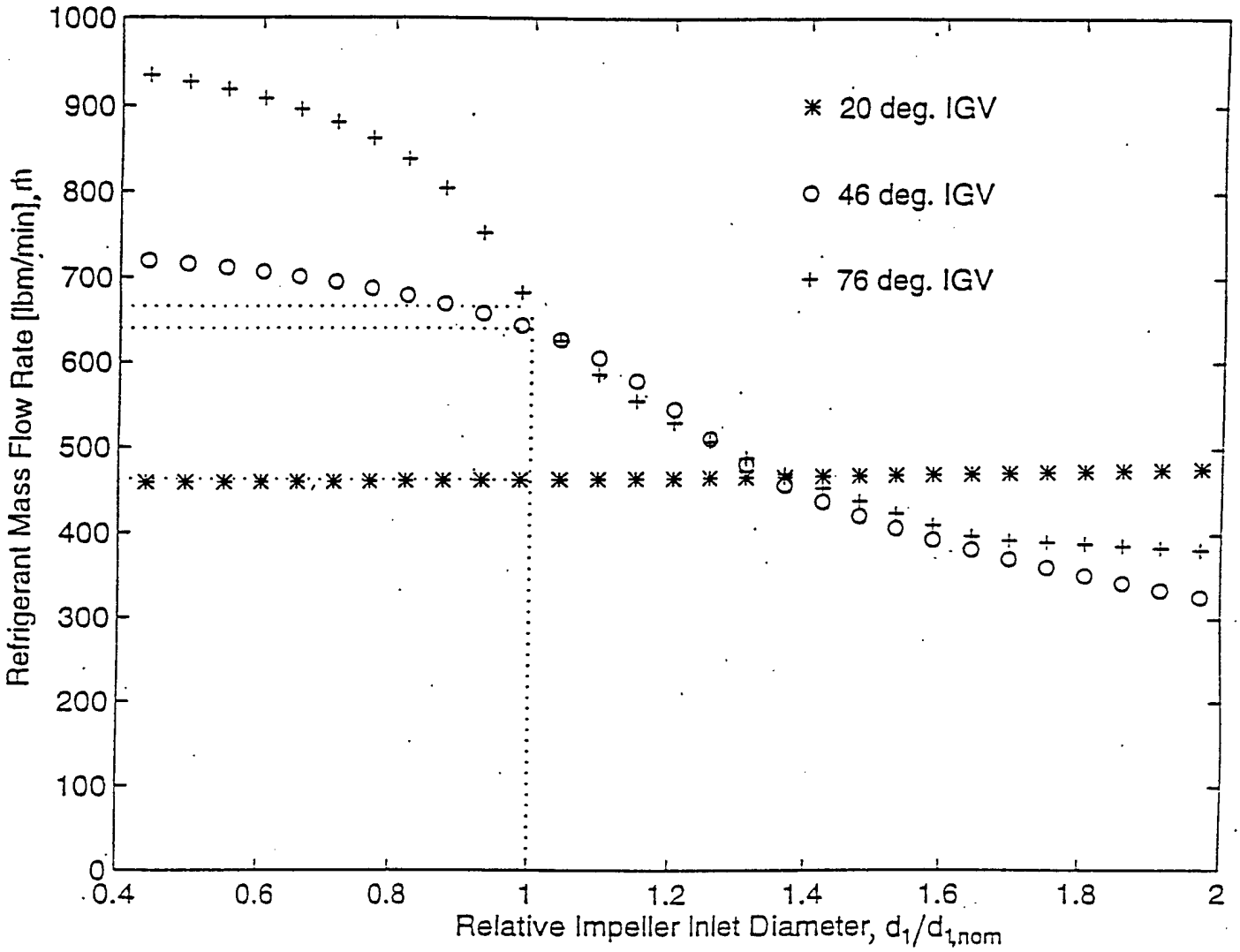

Figure 6.13. Refrigerant mass flow rate as a function of impeller inlet diameter .

6.4.2 IMPELLER EXIT DIAMETER

The impeller exit tip velocity, U_2, is directly related to the impeller exit diameter, d_2. As the relative impeller exit diameter, $d_2/d_{2,nom}$, increases, the exit velocity increases rapidly. An increase in the impeller exit linear velocity should increase the amount of the Euler head transferred to the fluid across the impeller. Also, the exit diameter is directly related to the impeller discharge area; therefore, it is directly related to refrigerant flow rate.

The impeller performance deteriorates as the exit diameter is increased in Figure 6.14, since the compressor work coefficient decreases as the impeller exit diameter increases. This supports the conclusion made in the previous section that the head produced in the impeller is inversely related to the work coefficient, and hence to the impeller performance. It should be noted that a greater flow throttling reduces the impact of the exit diameter.

Contrary to the trends observed in the design analysis so far, variations in impeller exit pressure in Figure 6.15 are opposite to changes in the work coefficient observed in Figure 6.14. The impeller exit pressure increases with an increase in the relative exit diameter. Observing Equation 5-23, it can be inferred that a reduction of the work coefficient introduces an increase in the flow coefficient, ϕ_2, for a constant slip factor (σ). Since the mid-state pressure, p_2, is inversely related to the flow coefficient, the flow rate must be very strongly related to the exit diameter to provide a reduction of the flow coefficient.

This correlation between the relative impeller size and the flow rate presented in Figure 6.16 appears to be exponential. The gradients in Figure 6.16 in which flow rate is shown as a function of the impeller exit diameter are the greatest observed in this design analysis. From the curves of Figure 6.16, it can be concluded that the flow rate is extremely sensitive to the size of the impeller. An increase in the impeller exit diameter allows more fluid flow through the impeller, so this observation has a physical meaning. Such steep gradients as encountered in Figure 6.16 are also due to the increase in the impeller discharge area which results from the increase in the fluid density at the compressor mid-state.

Looking at the huge slope observed for the flow rate variation with the relative impeller exit diameter in Figure 6.16, it is easy to understand the design limitations imposed on the impeller size. A 10-percent increase in the exit diameter produces almost a 100-percent flow rate increase. One must be very cautious in choosing the impeller outer diameter because of its predominant influence on the flow rate through the compressor.

The compressor exit state enthalpy shows a familiar positively sloped trend with no substantial changes in its magnitude across the investigated range of exit diameters, while the compressor shaft power increases directly with an increase in the flow rate.

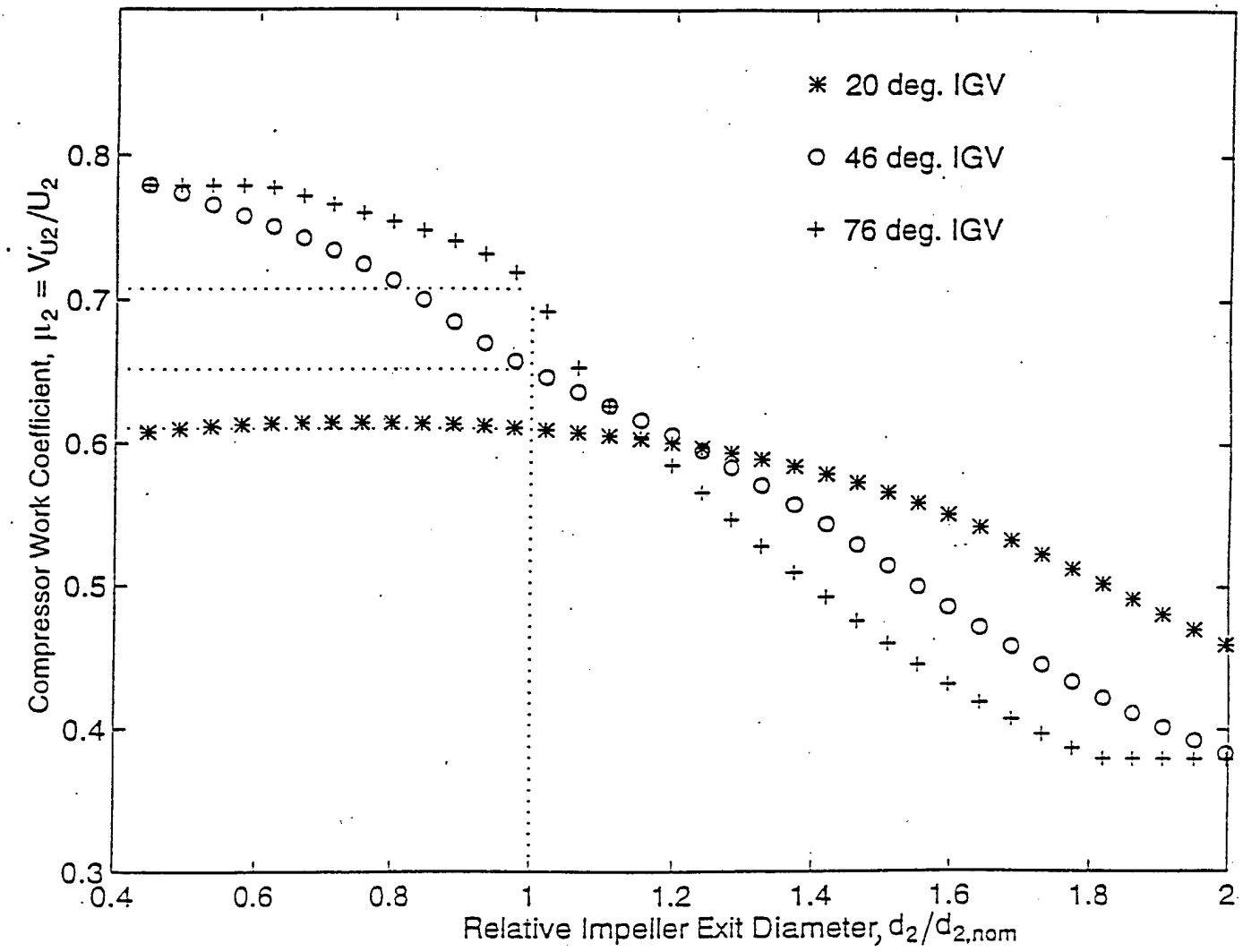

Figure 6.14. Impeller work coefficient as a function of impeller exit diameter.

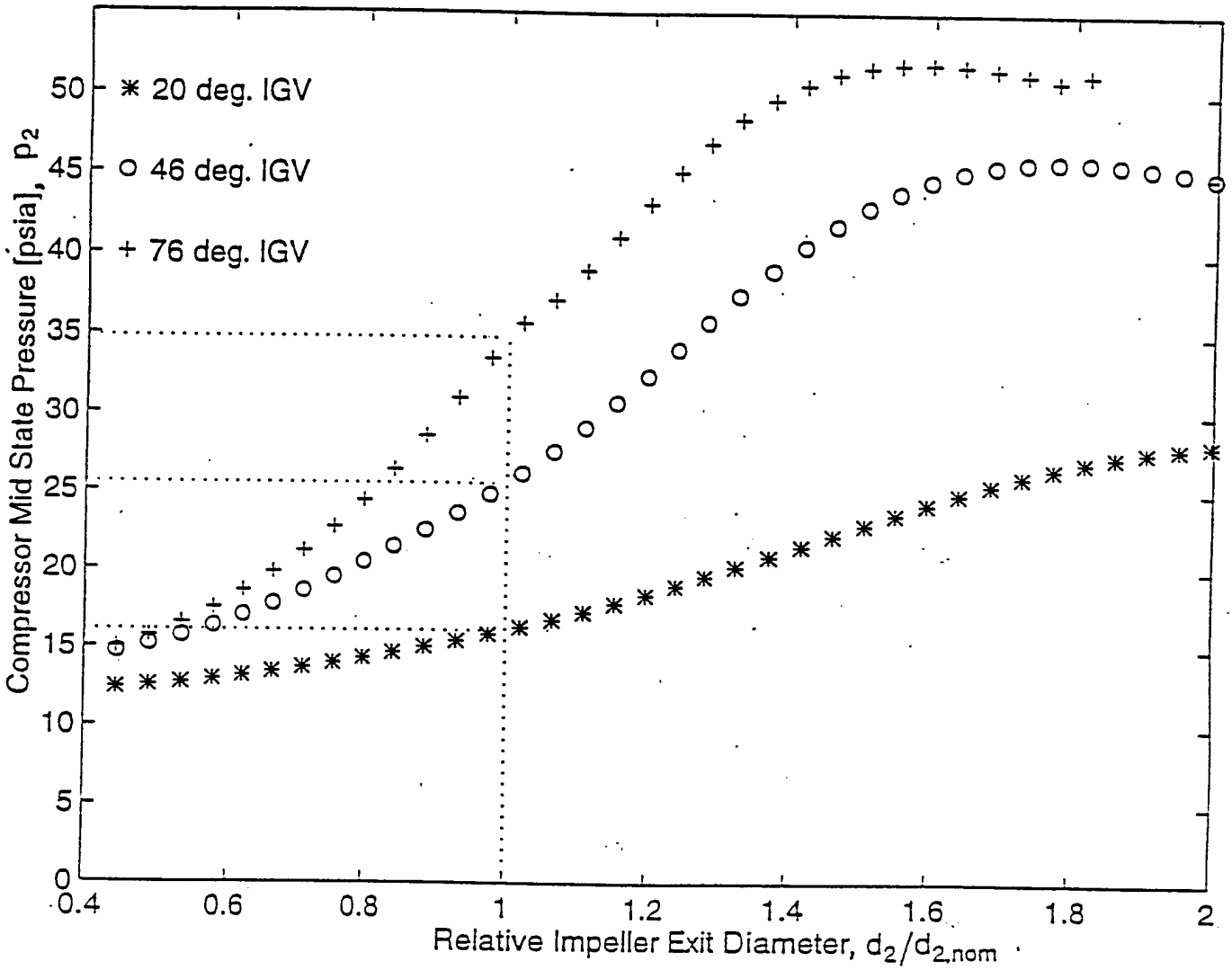

Figure 6.15. Impeller exit state pressure as a function of impeller exit diameter

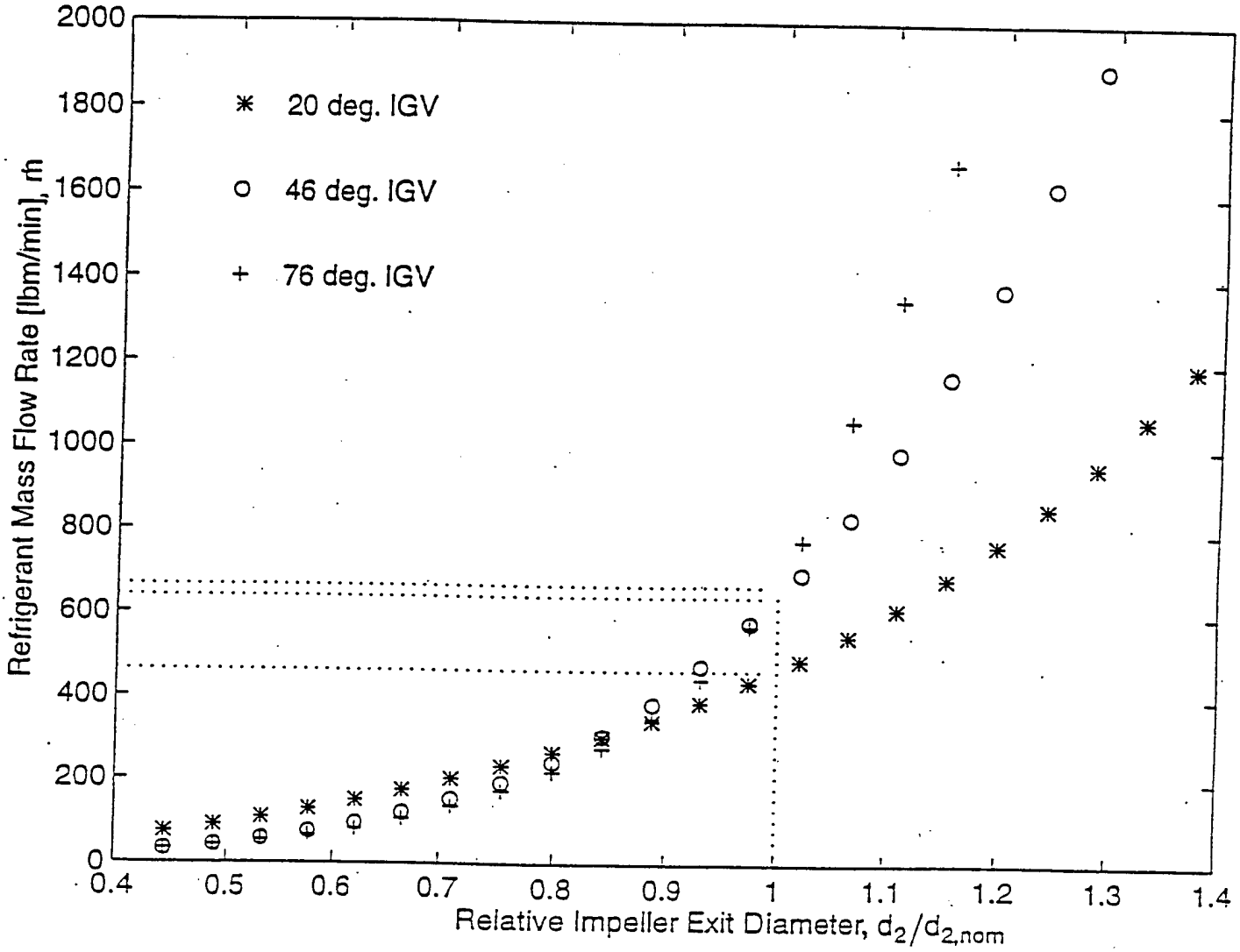

Figure 6.16. Refrigerant mass flow rate as a function of impeller exit diameter

The flow rate through the compressor is very strongly related to the impeller exit diameter, having the strongest dependence observed in this design analysis. The compressor work coefficient appears to be a negatively sloped function of the impeller size, while the impeller exit state pressure indicates an opposite trend.

6.5. IMPELLER EXIT AXIAL WIDTH

The impeller axial width, b_2 (see Figure 3.1), affects the size of the impeller discharge area. Therefore, the flow rate is directly related to the impeller exit axial width through Equation 3.6. This trend can be observed in Figure 6.17 in which the refrigerant flow rate, $\dot{m}$, is plotted as a function of the relative impeller axial width, $b_2/b_{2,nom}$. The substantial gradient observed in Figure 6.17 can be explained by Equation 3-6 in Section 3.1.3.

As already concluded in the design analysis, the flow rate is inversely related to the compressor performance; therefore, the compressor performance should be a negatively sloped function of the axial impeller width, b_2. The compressor work coefficient as the primary indicator of impeller performance shows the anticipated trend in Figure 6.18. It should be noted that changes in the work coefficient are within 10 percent, which is not substantial over the range of impeller exit axial widths investigated.

The second indicator of the compressor performance, the impeller exit state pressure, does not change significantly over the range of axial impeller widths studied. The actual gradient in Figure 6.19 is slightly negative, indicating that in addition to a reduction of the work coefficient there is a small reduction in the impeller exit pressure as the impeller axial dimension increases. Since changes in the exit impeller pressure are insignificant, the effect of the impeller axial width on the refrigerant state at the impeller exit is negligible.

Since the variations of the exit state enthalpy are negligible, within one percent, over the range of the investigated values of the impeller axial width,the exit enthalpy changes are not plotted. The compressor shaft power behaved in the same manner as the flow rate shown in Figure 6.17, since the exit state enthalpy did not vary. Thus the impeller axial width only affects the flow rate value significantly by altering the impeller discharge area.

6.6. CONCLUSIONS

The compressor model appears to be physically reasonable since the following characteristics are observed for changes in the investigated design parameters:

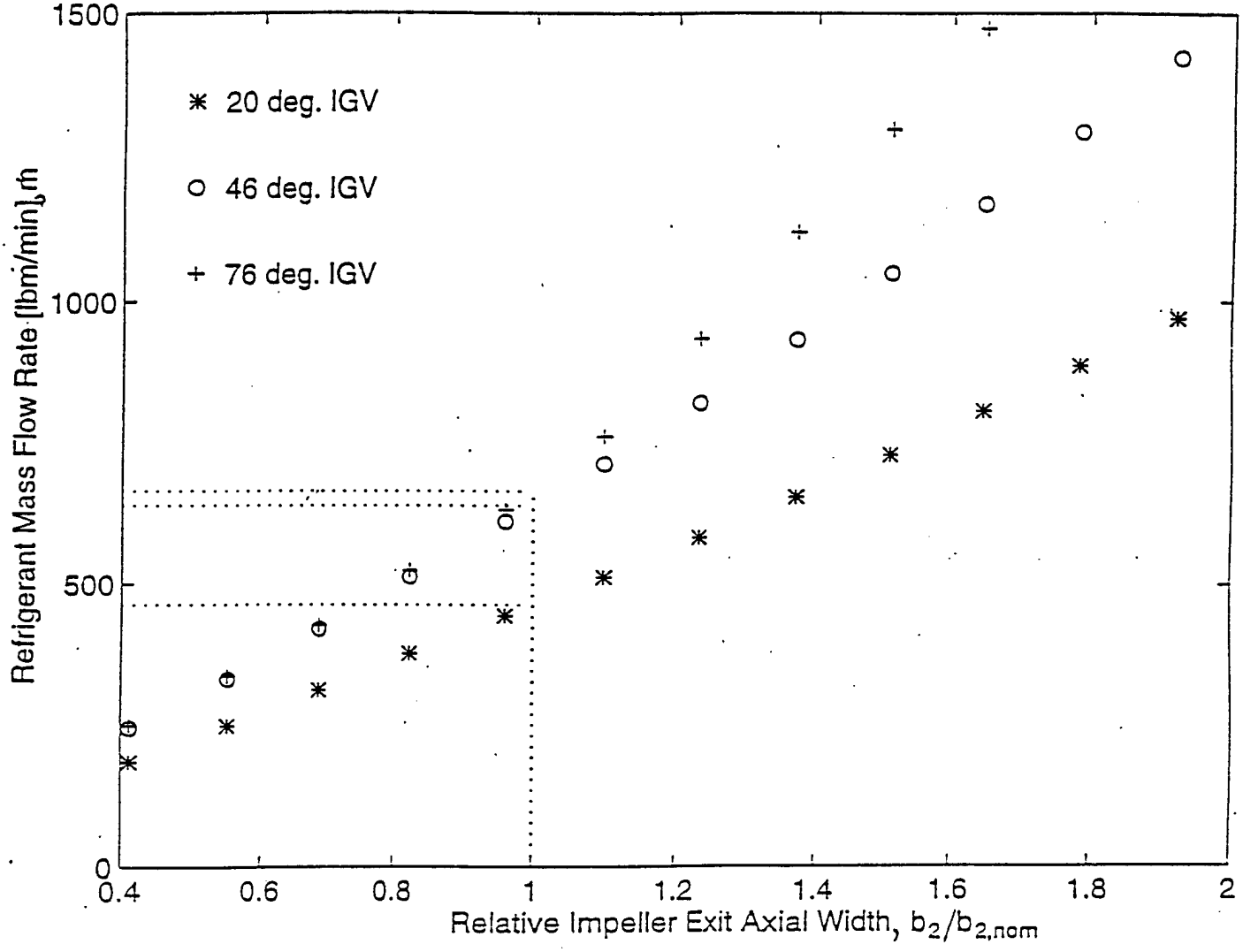

Figure 6.17. Refrigerant mass flow rate as a function of impeller exit axial width.

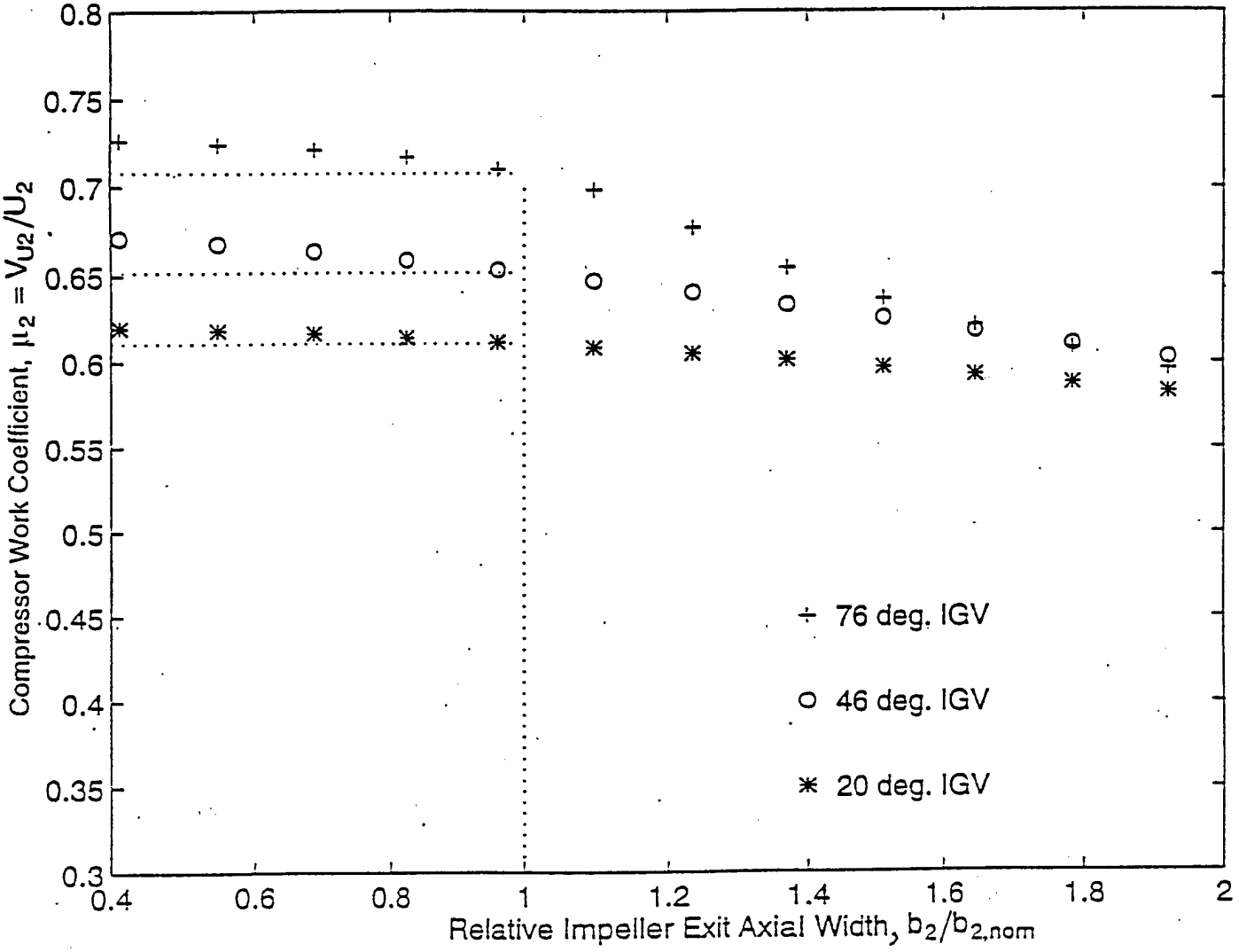

Figure 6.18. Impeller work coefficient as a function of impeller exit axial width.

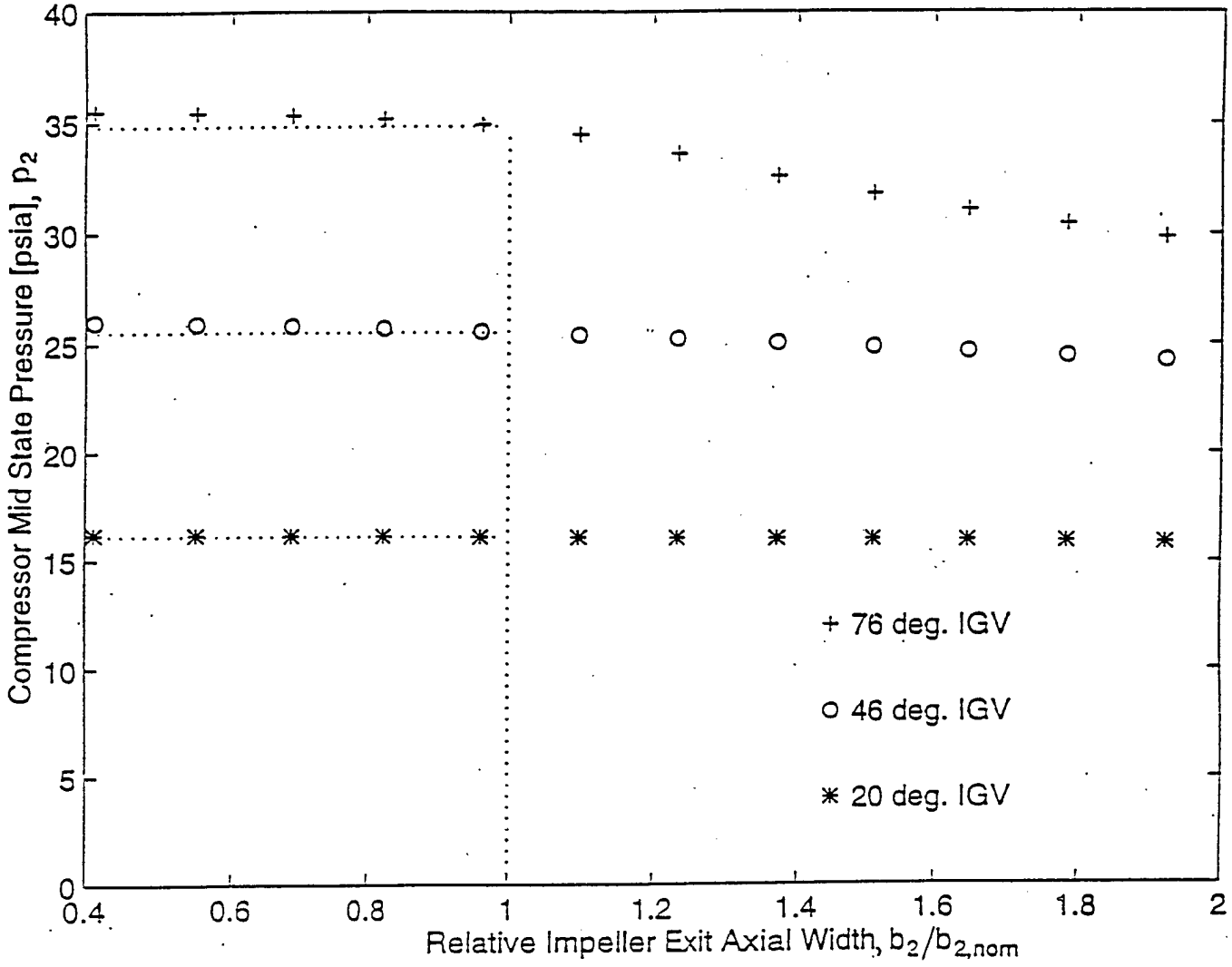

Figure 6.19. Impeller exit state pressure as a function of impeller exit axial width.

- The refrigerant flow rate and the pressure rise across the impeller indicate opposite trends with the variation of the design parameter which was expected from the theoretical analysis. Referring to the standard performance map described in Section 3.4, positively sloped performance curves, would indicate the surging region of compressor operation, while the negatively sloped performance curves correspond to the useful range of compressor operation.
- The nominal design parameters which are the actual compressor design parameters appear to be appropriately chosen.
- Observed variations in the design parameters yielded results which had logical physical explanations on applying the compressor theoretical analysis presented in Chapter 3.
- The net amount of the Euler head is inversely related to the impeller performance. In other words, the larger the amount of energy transferred across the impeller, the lower is the efficiency of this energy transfer.

The effect of the design parameters on the compressor model results are summarized in the following bulleted section:

- The number of impeller blades is directly related to the slip factor. As reported in Chapter 3, impeller performance as a function of the slip factor has a positive gradient, while the flow rate as a function of the slip factor is negatively sloped. These trends were observed in the design analysis, and it appears that the number of blades was chosen appropriately. Increasing the number of blades by about 10 percent might improve compressor performance, but would result in a pressure drop of approximately 15 percent.
- The blade tip angle is inversely related to the slip factor, but still directly related to the compressor performance. The trends observed in the blade tip angle design analysis were very similar to the trends encountered in the number of impeller blades design analysis. The blade tip angle appears to be well chosen. Enlarging tip angle by about 5 percent might improve the work coefficient by roughly 10 percent and reduce the flow rate by about 20 percent, with an increase of 1 to 2 psi in the impeller exit pressure.
- Increasing the inlet impeller diameter improves compressor performance and reduces the mass flow rate. The flow rate variations are more significant than the variation in the work coefficient which is the primary quantitative impeller performance measure. The pressure at the impeller exit and the compressor exit enthalpy are not affected by this parameter. The influence of inlet diameter on compressor performance rapidly diminishes as the flow is throttled with guide vanes. For these reasons, the inlet diameter should be excluded from the eventual impeller design modification.
- The impeller exit diameter greatly affects the magnitude of the flow rate, indicating a large gradient as the flow rate is varied with the size of the impeller. The compressor performance (work coefficient) is a negatively sloped function of the exit impeller diameter. The exit diameter changes should be very limited, since a 10 percent increase in the impeller exit diameter roughly doubles the mass flow rate.

- The impeller discharge area is directly related to the impeller axial width, and affects the flow rate considerably. Impeller performance as a function of the impeller axial width has a small negative gradient, while there is no significant change observed in the impeller exit state pressure. The impeller exit axial width may be altered to change flow rate if necessary for a relatively small change in the compressor performance.

Although the compressor model indicated a reasonable behavior for the variation in the operating input in Chapter 5, the results of the design input variations in this chapter should be taken very cautiously. The intent of the design analysis is to indicate trends in the compressor performance with the design input variations rather then to suggest specific changes in the compressor design parameters. Since the compressor model was found to be sensitive to the refrigerant type, it is reasonable to assume that the model is sensitive to the compressor design modifications. Also, the assumption of constant operating input with design input variations should be regarded with some reservations because of the indicated sensitivity of the compressor model.

Mass flow rate modeling is vital for development of an accurate compressor model, since mass flow rate represents the most sensitive parameter in the compressor model and is significantly affected by the variation in any of the design parameters. The relatively large error obtained in the mass flow rate prediction can be partially explained by this great sensitivity in the mass flow rate suggested by the model. Calculation of the mass flow rate is affected by almost every parameter in the compressor model and, therefore, has the largest error propagation effect. In addition, the flow rate was not measured on the installation, but rather calculated from the chiller heat exchangers' energy balances as explained in Section 4.3. This mass flow rate sensitivity most likely is a major contributor to the mass flow rate estimates within $\pm$ 20 percent of the measured flow rates.

REFERENCES

ASHRAE, 1992, "*System and Equipment Handbook.*" American Society of Heating, Refrigerating and Air-Conditioning Engineers, Inc., Atlanta, Georgia.

Ayder, E., Van de Braembussche, R., and Brasz, J. J., 1993, "*Experimental and Theoretical Analysis of the Flow in a Centrifugal Compressor Volute,*" Journal of Turbomachinery, Vol. 115, July, pp. 583-589.

Braun, J. E., Mitchell, J. W., Klein, S. A., and Beckman, W. A., 1987, " *Models for Variable-Speed Centrifugal Chillers,*" ASHRAE Transactions, Vol. 93, part 1, pp. 1794-1813.

Busemann, A. , 1928, " *Das Forderhohenverhaltniss radialer Kreiselpumpen mit logaritmishspiralegen Schaufeln,*" Zeitschrift fur Angewandte Mathematik und Mechanik, Vol. 8, October, pp. 372-384.

Casey, M. V., 1985, "*The Effects of Reynolds Number on the Efficiency of Centrifugal Compressor Stages,*" Journal of Engineering for Gas Turbines and Power, Vol. 107, April, pp. 541-548.

Dean, R. C., and Senoo, Y., 1960, "*Rotating Wakes in Vaneless Diffusers,*" Journal of Basic Engineering, Transactions of ASME, Series D, Vol. 86, pp. 607-619.

Eckert, B., and Schnell, E., 1980, "*Axial und Radialkompressoren,*" Springer Verlag, Berlin.

Farge, T. Z., and Johnson, M. W., 1992, "*Effect of Flow Rate on Loss Mechanisms in a Backswept Centrifugal Impeller,*" International Journal of Heat and Fluid Flow, Vol. 13, No. 2, June, pp. 189-196.

Hathaway, M. D., Chriss, R. M., Wood, J. R., and Straziar, A. J., 1993, "*Experimental and Computational Investigation of the NASA Low Speed Centrifugal Compressor Flow Field,*" Journal of Turbomachinery, Vol. 115, July, pp. 527-542.

Jansen, W., 1964, "*Steady Fluid Flow in a Radial Vaneless Diffuser,*" ASME Transactions, Series D, Journal of Basic Engineering, Vol. 86, No. 3, September, pp. 607-619.

Jansen, W., 1965, "*Rotating Stall in Radial Vaneless Diffusers,*" ASME Transactions, Series D, Journal of Basic Engineering, Vol. 86, No. 4, December, pp. 750-758.

Johnston, J. P., and Dean R. C., 1966, "*Losses in Vaneless Diffusers of Centrifugal Compressors and Pumps,*" Journal of Engineering for Power, Series A, Vol. 88, pp. 49-62.

Popovic, P., and Shapiro, H. N. , 1995" *A Semi Empirical Method for Modeling a Reciprocating Compressor in Refrigeration Systems,*" ASHRAE Transactions, Vol. 101, part 2.

REFPROP version 4.01, 1994, NIST Thermodynamics Properties of Refrigerants and Refrigerant Mixtures Database, Gaithersburg, Maryland.

Rodgers, C., 1962, "*Typical Performance Characteristics of Gas Turbine Radial Compressor*," ASME Transactions Series A, Journal of Engineering for Power, Vol. 86, No. 2, April, pp. 161-175.

Rodgers, C., 1980, "*Specific Speed and Efficiency of Centrifugal Impellers*," ASME Gas Turbines Conference, New Orleans, March, pp. 191-200.

Senoo, Y., Kinoshita, Y., and Ishida, M., 1977, "*Asymmetric Flow in Vaneless Diffusers of Centrifugal Blowers*," ASME Transactions, Series I, Journal of Fluids Engineering, Vol. 99, No. 1, March, pp. 104-114.

Senoo, Y., Hayami, H., and Ueki, M., 1983, "*Low Solidity Tandem-cascade Diffuser Design for Wide Flow Range Centrifugal Blowers*," ASME Paper 83-GT-3.

Sheets, H. E., 1950, "*The Flow Through Centrifugal Compressors and Pumps*," Transactions of the ASME, Vol. 124, p. 1009.

Shepherd, D. G., 1956, " *Principles of Turbomachinery*," The Macmillan Company, New York.

Stanitz, J. D. , 1952, " *Some Theoretical Aerodynamics Investigations of Impellers in Radial and Mixed Flow in Centrifugal Compressors*," Transactions of the ASME, Vol. 74, p. 473.

Stein, W., and Rautenberg, M., 1988, " *Analysis of Measurements in Vaned Diffusers of Centrifugal Compressors,*" Journal of Turbomachinery, Vol. 110, January, pp. 115-121.

Straub, R. A., Bonciani, L., Borer, C. J., Casey, M. V., Cole, S. L., Cook, B. B., Kotzur, J., Simon, H., and Strite, M. A., 1987, " *Influence of the Reynolds Number on the Performance of Centrifugal Compressors,*" Journal of Turbomachinery, Vol. 109, October, pp. 541-544.

Turton, R. K. 1995, "*Principles of Turbomachinery*," Second Edition, Chapman & Hall, 2-6 Boundary Row, London, SE1 8HN, UK.

Van den Braembusse, R. ,1985, "*Design and Optimization of Centrifugal Compressors,*" Thermodynamics and Fluid Mechanics of Turbomachinery, Volume 2, edited by: Ucer, A. S., Stow, P., and Hirsch, C., NATO ASI Series, Series E: Applied Sciences No. 97B, pp. 829-885.

Wiesner, F. J., and Caswell, H. E., 1959, " *How Refrigerant Properties Affect Impeller Dimensions*," ASHRAE Journal, October, pp. 31-37.

Wiesner, F. J., 1967,"*A Review of Slip Factors for Centrifugal Impellers,*" Journal of Engineering for Power, October, pp. 558-572.

Wiesner, F. J., 1979, "*A New Appraisal of Reynolds Number Effects on Centrifugal Compressor Performance,*" Journal of Engineering for Power, Vol. 101, July, pp. 385-395.

Wisclenius, G., 1965, "*Fluid Mechanics of Turbomachines,*" Dover Press, New York.

APPENDIX A

REFINED MODEL OUTLINE

The new compressor model depicted in Section 5.3 was refined for variable slip factor and a two-dimensional diffuser model. The model is outlined in the following 22 equations.

IMPELLER

The impeller model is identical to the impeller model of the new compressor except for the addition of the variable slip factor. Equations A-1 through A-9 are same as Equations 5-16 through 5-24 given in Section 5.3.1.

$$V_1 = \frac{U_1 \tan\beta_1}{\sin\alpha_1 + \tan\beta_1 \cos\alpha_1} \tag{A-1}$$

$$V_{u1} = V_1 \cos\alpha_1 \tag{A-2}$$

$$h_2 + V_2^2/2 - \left(h_1 + V_1^2/2\right) = U_2\, V_{u2} - U_1\, V_{u1} \tag{A-3}$$

$$\phi_2 = \frac{V_{r2}}{U_2} = \frac{\dot{m}}{A_2\, k_B\, U_2\, \rho_2} \tag{A-4}$$

$$p_2 = f(h_2, \rho_2) \tag{A-5}$$

$$h_{2,is} = f(p_2, s_1) \tag{A-6}$$

$$\eta_{im} = \frac{h_{2,is} - h_1}{h_2 - h_1} \tag{A-7}$$

$$\sigma_{cor} = \frac{V_{u2}}{U_2} + \frac{\phi_2}{\tan\beta_2} \tag{A-8}$$

$$V_2^2 = V_{r2}^2 + V_{u2}^2 = U_2^2\,\phi_2^2 + V_{u2}^2 \tag{A-9}$$

The variable slip factor is introduced in the following expression which was derived in Section 3.14 and given in Equation 3-13.

$$\sigma_{cor} = \frac{1}{1+(1-\varepsilon)\left[1/(\sigma-\phi_2/\tan\beta_2)-1\right]} + \frac{\phi_2}{\tan\beta_2} \tag{A-10}$$

DIFFUSER

The diffuser model applied to the new compressor model in Section 5.3.1 is given by Equations A-11 through A-13.

$$h_3 + V_3^2/2 = h_2 + V_2^2/2 \tag{A-11}$$

$$V_3 = \frac{\dot{m}}{A_3\,\rho_3} \tag{A-12}$$

$$\rho_3 = f(p_3, h_3) \tag{A-13}$$

Additional expressions in the vaneless diffuser model are given in Equations A-14 through A-22. These equations are described in detail in Section 3.3.1.

$$\eta_D + \xi_{fric} + \xi_{mix} = 1 \tag{A-14}$$

$$\eta_D = \frac{p_3 - p_2}{p_{3,id} - p_2} \tag{A-15}$$

$$\frac{p_{3,id}}{\rho_3} - \frac{p_2}{\rho_2} = \left[\frac{V_2^2 - V_3^2}{2}\right]\left[\frac{\kappa - 1}{\kappa}\right] \tag{A-16}$$

$$\xi_{fric} = 1 - C_P - \frac{1}{R^2}\left[\frac{(\gamma_2 \lambda_2)^2 + \left(\frac{b_D}{b_2}\right)^2}{\lambda_2^2 + 1}\right] \tag{A-17}$$

$$C_P = \frac{p_3 - p_2}{1/2\, \rho_2 V_2^2} \tag{A-18}$$

$$\gamma_2 = \frac{1}{1 + \lambda_2^2 \hat{A}(R-1)} \tag{A-19}$$

$$\lambda_2 = 2\pi\left(\frac{b_2}{r_2}\right)\frac{\psi_2}{\phi_2} \tag{A-20}$$

$$\psi_2 = \frac{p_2 - p_1}{\rho_2 U_2^2} \tag{A-21}$$

$$\xi_{mix} = \frac{1}{1 + \lambda_2^2}\left[\frac{(1-\varepsilon) - B}{(1-\varepsilon)}\right]^2 \tag{A-22}$$

These 22 equations were solved using the mass flow rate and the refrigerant state at the compressor exit as known parameters. Determined parameters were matched to find empirical relations. Two empirical relations that generated least errors are listed:

$$\eta_{im} = 1.3 - 5.9434\ \alpha_1^{-0.63847} \tag{A-23}$$

$$\phi_2 = 0.13 + \mathrm{EXP}\left[-34.9681 + 51.9259\left(\frac{h_2 - h_1}{h_3 - h_1}\right)\right] \tag{A-24}$$

Further, these two empirical relations added to the 22 listed analytical expressions comprised the refined model. The set of these equations never yielded a reasonable solution. Errors generated in the model output were found to be functions of the solving orders, and the source of this behavior was never identified. Nevertheless, it is logical to expect that the system of equations can be solved.

Input required for this model is given in the following bulleted section:

- impeller peripheral velocities $U_i = \pi d_i\ RPM$, i = 1,2
- refrigerant state at the compressor inlet,
- refrigerant pressure at the compressor outlet, p_3,
- inlet guide vane setting, α_1,
- impeller nominal blade inlet and outlet tip angles, β_1 and β_2,
- blockage factor, k_B, set to unity,
- constant slip factor from the empirical relation given in Section 3.1.4., $\sigma = 1 - \frac{\sqrt{\sin\beta_2}}{Z^{0.7}}$,
- number of impeller blades, Z,
- nominal discharge areas at the impeller exit, A_2, and the diffuser exit, A_3,
- specific heat ratio for the particular gaseous refrigerant, $\kappa = \frac{c_p}{c_v}$,
- diffuser outlet radius to inlet radius ratio, $R = \frac{r_3}{r_2}$,
- diffuser inlet geometric coefficient, $B = \frac{b_{exp}}{b_2}$,
- diffuser width parameter, $\hat{A} = \frac{\hat{c}_f r_3}{b_3}$,
- friction factor $\hat{c}_f$ (should be set to be between 0.005 and 0.01).

The compressor radial and axial dimensions are denoted on Figure 3.1.

APPENDIX B

ENGLISH TO SI UNIT SYSTEM CONVERSION FACTORS

The English Engineering System of Units was used throughout the project because in the U.S. it is still wide engineering practice to use this unit system; therefore, the results presented in this unit system are more understandable to a reader in the engineering field. Also, the actual data taken by the Navy were in the English Engineering System of Units. In order to easily implement developed compressor models, project analyses were performed in the English Engineering System of Units.

The following units are used throughout the project analysis:

- Pressure

  1 [psia] = 6.8948 [kPa]

- Temperature

  X [F] = [(X-32)*5/9]+273.15 [K]

- Mass

  1 [lbm] = 0.4535 [kg]

- Length

  1 [ft] = 0.3048 [m]

- Density

  1 [lbm/ft^3] = 16.02 [kg/m^3]

- Power

  1 [hp] = 0.746 [kW]

- Specific Energy (Enthalpy)

  1 [Btu/lbm] = 2.3244 [kJ/kg]

- Mass Flow Rate

  1 [lbm/min] = 0.00756 [kg/s]

- Velocity

  1 [ft/sec] = 0.3048 [m/s]

- Refrigeration capacity 1 [ton] = 12,000 [Btu/hr] = 3.52 [kW]

TECHNICAL REPORT DATA
(Please read Instructions on the reverse before completing)

1. REPORT NO.	2.	3. RECIPIENT'S ACCESSION NO.
EPA-600/R-97-038		

4. TITLE AND SUBTITLE	5. REPORT DATE
A Modeling and Design Study Using HFC-236ea as an Alternative Refrigerant in a Centrifugal Compressor	April 1997
	6. PERFORMING ORGANIZATION CODE

7. AUTHOR(S)	8. PERFORMING ORGANIZATION REPORT NO.
Predrag Popovic and Howard N. Shapiro	

9. PERFORMING ORGANIZATION NAME AND ADDRESS	10. PROGRAM ELEMENT NO.
Iowa State University Department of Mechanical Engineering Ames, Iowa 50011	11. CONTRACT/GRANT NO. CR820755-01-4

12. SPONSORING AGENCY NAME AND ADDRESS	13. TYPE OF REPORT AND PERIOD COVERED
EPA, Office of Research and Development **Air Pollution Prevention and Control Division** **Research Triangle Park, NC 27711**	Final; 1/94-9/95 14. SPONSORING AGENCY CODE **EPA/600/13**

15. SUPPLEMENTARY NOTES APPCD project officer is Theodore G. Brna, Mail Drop 63, 919/541-2683.

16. ABSTRACT The report gives results of an investigation of the operation of a centrifugal compressor--part of a chlorofluorocarbon (CFC)-114 chiller installation--with the new refrigerant hydrofluorocarbon (HFC)-236ea, a proposed alternative to CFC-114. A large set of HFC-236ea operating data, as well as a limited number of CFC-114 data, were available for this study. It was determined that the compressor performance can be successfully described by a relatively simple analytical compressor model. Two compressor models, the first of which was obtained from the literature, were developed on the basis of thermodynamic analysis and by utilizing the data base. Two empirical relations were required to predict mass flow rate and the refrigerant state at the compressor exit for each model. The second model is based on empirical relations derived directly from the data base rather than the general empirical relations used in the first model. The literature model had to be optimized for two parameters and corrected for the influence of the inlet guide vanes to yield results comparable to the newly developed model. Both models were based on the HFC-236ea data, and they exhibited systematic errors when used with CFC-114, which indicated the models' dependence on the refrigerant. Both models predicted refrigerant state at the compressor outlet excellently (+/- 2.8 C).

17. KEY WORDS AND DOCUMENT ANALYSIS

a. DESCRIPTORS	b. IDENTIFIERS/OPEN ENDED TERMS	c. COSATI Field/Group
Pollution	Pollution Prevention	13B
Refrigerants	Stationary Sources	13A
Centrifugal Compressors	Hydrofluorocarbons	13G
Halohydrocarbons	Chlorofluorocarbons	07C
Mathematical Models	HFC-236ea	12A
	CFC-114	

18. DISTRIBUTION STATEMENT	19. SECURITY CLASS *(This Report)*	21. NO. OF PAGES
Release to Public	Unclassified	156
	20. SECURITY CLASS *(This page)*	22. PRICE
	Unclassified	

EPA Form 2220-1 (9-73)